Identification and characterization of proteins involved in the cytoskeletal rearrangements caused by bacterial pathogens

by

Michael Dominic Chua

B.Sc. (Hons.), Simon Fraser University, 2012

Thesis Submitted in Partial Fulfillment of the
Requirements for the Degree of
Doctor of Philosophy

in the
Department of Biological Sciences
Faculty of Science

SIMON FRASER UNIVERSITY
Summer 2018

Approval

Name:	**Michael Dominic Chua**
Degree:	**Doctor of Philosophy (Biological Sciences)**
Title:	**Identification and characterization of proteins involved in the cytoskeletal rearrangements caused by bacterial pathogens**
Examining Committee:	**Chair: Tony Williams** Professor
	Julian Guttman Senior Supervisor Professor
	Gordon Rintoul Supervisor Associate Professor
	Wayne Vogl Supervisor Professor Department of Cellular and Physiological Sciences University of British Columbia
	Margo Moore Internal Examiner Professor
	Alfredo Menendez External Examiner Associate Professor Department of Microbiology and Infectious Diseases University of Sherbrooke
Date Defended/Approved:	August 21, 2018

Ethics Statement

The author, whose name appears on the title page of this work, has obtained, for the research described in this work, either:

a. human research ethics approval from the Simon Fraser University Office of Research Ethics

or

b. advance approval of the animal care protocol from the University Animal Care Committee of Simon Fraser University

or has conducted the research

c. as a co-investigator, collaborator, or research assistant in a research project approved in advance.

A copy of the approval letter has been filed with the Theses Office of the University Library at the time of submission of this thesis or project.

The original application for approval and letter of approval are filed with the relevant offices. Inquiries may be directed to those authorities.

Simon Fraser University Library
Burnaby, British Columbia, Canada

Update Spring 2016

Abstract

Bacterial pathogens have evolved to alter the cytoskeleton of their hosts during their respective infection processes. The extracellular bacterium, enteropathogenic *Escherichia coli* (EPEC), generates an actin-rich pedestal to “surf” along the host cell surface. In contrast, *L. monocytogenes* (*L. monocytogenes*) invades its host and polymerizes actin filaments to generate a comet tail for movement within and among host cells of epithelia. *Salmonella enterica* serovar Typhimurium (*S.* Typhimurium) induces actin-rich membrane-ruffles to invade its host cell. These bacteria have evolved to generate their respective actin-rich structures to colonize the intestinal epithelia. To further characterize the actin-rich structures generated by these bacteria, I selected four proteins from a mass spectrometry analysis of EPEC pedestals previously conducted in our laboratory. I found that the known actin-bundling proteins calponin 1 and calponin 2 decorated all the actin-rich structures formed by these three bacteria. Another actin-stabilizing protein transgelin (SM22) also decorated EPEC pedestals and *L. monocytogenes* comet tails. Moreover, the formation of pedestals and comet tails were dependent on SM22 protein levels. Aside from these three members of the calponin family, I found that a ubiquitin conjugating enzyme Ube2N was enriched at the invasion events and at the plasma membrane-bound comet tails formed by *L. monocytogenes.* This novel association of Ube2N with actin structures at the plasma membrane led to my discovering that Ube2N binds directly to actin, and that Ube2N function influences actin-based whole cell motility. Another bacterial pathogen*, Klebsiella pneumoniae* (*K. pneumoniae*), has been shown by others to alter the host actin cytoskeleton. I have found that the disassembly of the host microtubule networks precedes these actin cytoskeletal alterations in lung epithelial cells, and show that the *Klebsiella pneumoniae* gene *ytfL* (Kp *ytfL*) initiates this microtubule disassembly and that the katanin catalytic subunit A like 1 protein (KATNAL1) as well as the katanin regulatory subunit B1 protein (KATNB1) are activated to cause microtubule severing. Through this, I identified the bacterial initiator and the host cell effector proteins responsible for *K. pneumoniae*-induced microtubule disassembly. From these, I identified proteins that are novel to the actin structures of EPEC, *L*. monocytogenes and *S*. Typhimurium as well as effector proteins that are crucial for the novel host microtubule alterations of *K. pneumoniae*.

Keywords: Actin; microtubules; enteropathogenic *Escherichia coli*; *Listeria monocytogenes*; *Salmonella enterica* serovar Typhimurium; *Klebsiella pneumoniae*

To my parents who have always been supportive and loving,

To my sister who always had my back (no matter what),

To my friends who believed in me even when I didn't believe in myself,

To my teachers and mentors who have taught me everything that I know,

To my students who have taught me how to be a better person and teacher,

I am but a collection of all the fantastic memories I share with each one of you and none of this work would be possible without you.

Acknowledgements

This thesis is dedicated to all these people since they have had the most influence on me throughout the past few years. Their support carried me throughout my degree and I would not be able to complete this journey without them.

First and foremost, my family constantly have been supportive all throughout my degree. They fed me, checked up on me, and ensured that I didn't neglect my wellbeing throughout this endeavor. Nothing compares to the love you get from family.

Dr. Julian Guttman has provided me with the opportunity to grow as a scientist. Without all of his help and guidance, none of this work would be possible. He has dealt with the logistical intricacies of making research projects work allowing me to focus on exploring the science.

Dr. Gordon Rintoul and Dr. Wayne Vogl have provided constant guidance and they helped keep me grounded throughout this endeavour. Their counsel has structured my research goals and they helped me explore the key research questions in my project.

Dr. Karen Lo has been the first to identify my knack for science (even when I did not even know I loved research). Karen believed in me and she was the first to get me to do research. From then on, she has mentored me in many ways from teaching me about microbiology and cell culture to her continued support and all the way to encouraging me through all the obstacles in my degree.

Dr. Ann Lin and Dr. HT Law have also taught me various techniques that laid the foundation for the technical skill I have developed throughout my degree.

Karen Lo, Kevin Hipolito, Priya Aggarwal, Avneen Kooner, and Jennifer Shen have been with me through all the ups and downs of my degree. They cheered me on and they gave me counsel when I needed it. Karen was the supportive academic peer that helped me constructively criticize my work and constantly told me to be wary of overworking myself. Kevin was always there to cheer me on and he made sure that I made time for fun throughout my endeavour. Playing pool with him definitely helped me unwind on countless occasions. Priya was there for me when I needed someone to talk to during the stressful times and the countless cups of chai were definitely memorable. Avneen

provided well-grounded advice about the obstacles that came my way. I will never forget those steeped tea-fueled conversations. Jennifer constantly reminded me to take care of myself and she always pushed me to stop staying in lab too late. No one can be a failure who has friends like them.

Kevin Hipolito, Anika Stroman, Avneen Kooner, Gaby Mineva, Alex Bogdan, Brit Walker, Serina Li, Oni Singerr, and Franklin Tam have been instrumental in my research endeavours. Through them, my passion for scientific research and teaching has been constantly invigorated. More importantly, I have learned so much from them throughout the years. Kevin taught me the value of hard work and how you can accomplish a lot from a strong work ethic. Anika taught me about the balancing of research work and life outside the lab. Avneen showed me the value of setting up realistic goals in every endeavour. Gaby constantly ingrained in me the importance of physical wellbeing no matter how the research goes. Similarly, Alex, in many ways, challenged me to reflect on how to take care of myself in order to survive my grad school work. Serina helped me critically reflect on my technical skills and through her influence, I will constantly strive to improve my skills as a researcher. Oni taught me how to “go with the flow” and when things do not work out as you planned, just try again and things will work out in the end. Franklin taught me the value of making time for fun. If you plan things well, you can work hard and still be able to squeeze in enjoyable things in your life.

In terms of funding, in addition to the research grants of Dr. Guttman, I have been fortunate to be supported by the SFU Graduate Fellowship, the President’s PhD scholarship and as well as the private scholarships by Shaughn and Sharon Clements. These unwavering supports have been quite helpful throughout my schooling.

All in all, these people have made a lasting impact on my career. In the book, The Little Prince, there is a quote saying: *It is the time that you spent on your rose that makes your rose so important*. Similarly, it is the time that I spent with these people that make them important to me and I am grateful for meeting them in this phase of my life.

Table of Contents

List of Tables

List of Figures

List of Acronyms

EPEC	Enteropathogenic *Escherichia coli*
CRISPR	Clustered Regularly Interspaced Short Palindromic Repeats
Arp2/3	Actin Related Protein 2/3
N-WASP	Neural-Wiskott Aldrich Protein
Nck	Non-Catalytic region of tyrosine Kinase adaptor protein
ATP	Adenosine Triphosphate
ADP	Adenosine Diphosphate
CH	Calponin Homology domain
CLIK	Calponin Homology-Like repeats
ABS	Actin Binding Site
MTOC	Microtubule Organizing Centre
GTP	Guanosine Triphosphate
GDP	Guanosine Diphosphate
MAPT	Microtubule Associated Protein Tau
DCX	Doublecortin
XMAP215	*Xenopus* Microtubule Associated Protein 215
EB	End Binding Proteins
CLIP170	Cytoplasmic Linker Protein of 170 kDa
AAA-ATPase	ATPases Associated With Many Cellular Activities ATPase
KATNA1	Katanin catalytic protein A1
KATNAL1	Katanin catalytic protein A Like 1
KATNB1	Katanin regulatory protein B1
KATNBL1	Katanin regulatory protein B Like 1
FIGN	Fidgetin
FIGNL1	Fidgetin-Like 1
FIGNL2	Fidgetin-Like 2
GFP	Green Fluorescent Protein
RING	Really Interesting New Gene
HECT	Homologous to the E6-AP Carboxyl Terminus
LEE	Locus of Enterocyte Effacement
BFP	Bundle Forming Pili

CME	Clathrin Mediated Endocytosis
PlcA	Phospholipase A
PlcB	Phospholipase B
LLO	Listeriolysin O
ActA	Actin Assembly Protein A
SUMO	Small Ubiquitin-Like MOdifier
SCV	Salmonella-Containing Vacuole
VAP	Vacuole-associated Actin Polymerization
SIF	Salmonella-Induced Filaments
SM22	Smooth Muscle 22 kDa Protein
BDM	2,3-Butanedione Monoxime
FL	Fosmid Library Clone
FLP	Fosmid Library Pool
AMP	Adenosine Monophosphate

Preface

Humans encounter a variety of microbes and while not all bacteria cause disease, several bacteria can colonize specific organs and their resulting infections can lead to varying symptoms. The most common routes of infection include ingestion or inhalation of the bacteria and consequently the lungs and intestines become the primary sites of infection. Upon encountering the host cell epithelia, particular bacteria have evolved to manipulate the host cytoskeleton. My research primarily focuses on identifying proteins that have yet to be associated with these bacterial infections and through my research, I aim to add to our current understanding of the proteins involved in host cytoskeletal rearrangements.

In Chapter 2, Chapter 3, and Chapter 4, I focused on the epithelial infections of enteropathogenic *Escherichia coli*, *Listeria monocytogenes* and/or *S.* Typhimurium. These bacteria generate actin-rich structures, but the complete protein makeup of these structures has not been elucidated. In each of these chapters, I explored the role of calponin 1, calponin 2, SM22 and Ube2N in the generation of these bacterially-induced actin-rich structures.

In Chapter 5, I examined a different bacterial pathogen, *Klebsiella pneumoniae*. Our laboratory has discovered that this bacterium can cause microtubule severing and ultimately, the microtubule networks of entire monolayers of lung cells are disassembled. This is the first instance in which a bacterium can affect the microtubules of an entire cell monolayer. Therefore, I aimed to characterize this event by quantifying the degree of microtubule disassembly, then identified a bacterial effector that can activate the host proteins to trigger the observed microtubule severing.

In the work I have presented, most of my experiments utilize 2-dimensional cell cultures. In a biological setting, organs are complex structures that cannot be mimicked by my 2-dimensional models. As such, further experiments using 3-dimensional systems should be examined to supplement my findings.

Chapter 1.

Introduction

1.1. Actin

The actin cytoskeleton is a filamentous network which plays important roles in many cellular processes such as cell shape maintenance, membrane curvature and scission, and cellular motility[1–5]. The basic unit of this cytoskeletal system is monomeric actin, also known as globular actin (G-actin) and its polymerization into double-stranded helical actin filaments (F-actin) (Fig. 1.1A) that form the building blocks of various actin-based structures within cells[6–8]. Due to their abundance and their structural integrity, these filaments lay the foundation of many structures within the cell.

Actin filaments largely contribute to the structural integrity of the cell. Short branches of actin typically line the plasma membrane of most cell types and these provide the necessary scaffold to maintain the shape of the cell[9–11]. Within adherent cells, parallel bundles of actin stress fibres stretch across the base of the cell to tether it to the substratum[12]. The structural rigidity of stress fibres relies heavily on the tensile strength of thick parallel bundles of actin filaments that affix two attachment points, called focal adhesions, at the base of a cultured cell. Moreover, in epithelial cells, parallel actin bundles also act as tension wires at the junctional complex to enhance the tight structural integrity of the epithelia[13,14]. These stabilized actin filaments provide the durable, but still flexible material necessary to support the shape of the cell.

Actin structures can be quite dynamic due to the myriad of regulatory proteins that maintain actin filaments and thus, the other main function of actin is in the formation of protrusions along the cell periphery during cell movement. At the cell cortex and especially at the leading edge of migrating cells, actin is organized in branched arrays and provide the force necessary to push the plasma membrane forward[5,15,16]. Protrusions called lamellipodia extend the cell membrane causing sufficient membrane tension to pull the entire cell in the direction of actin polymerization[17–20]. To continue this movement, older actin filaments are disassembled to replenish the pool of actin and actin-associated proteins required to continue building new branches at the growing

ends of the actin array abutting the plasma membrane at the leading edge of the lamellipodia[21,22]. Within the lamellipodia, parallel actin bundles are generated, called filopodia, that guide the direction of cellular movement[23,24].

1.1.1. Polymerization of actin filaments

Within the cytosol, adenosine triphosphate (ATP)-bound actin monomers are stabilized by the actin-binding protein, profilin. When two actin monomers come in contact, profilin dissociates from the actin monomer and this allows the rapid binding of the actin monomers in a head-to-tail manner[7,25]. Addition of another actin monomer to the bulky head of the dimer creates a trimer that is essential for actin filament nucleation[26,27]. A polar filament is then created such that actin monomers are rapidly added to the barbed end (plus end) of the filament and actin monomers slowly dissociate at the pointed end (minus end)[28]. When the amount of cytosolic actin surpasses the critical concentration, actin monomers spontaneously polymerize to form actin filaments. After actin monomers bind, actin eventually starts to hydrolyze its associated ATP into adenosine diphosphate (ADP)[29,30]. In the ADP-bound state, the actin monomer has a reduced binding affinity to other monomers[31] and so, ADP-bound monomers at the pointed end can dissociate. Thus, shortening of the filament occurs when the rate of actin dissociation from the filaments is greater than the rate of incorporation at the barbed end. As a result, the rate of actin polymerization is dependent on the kinetics of actin addition at the barbed end[8,21,32].

To overcome the thermodynamic barriers of actin polymerization, actin-nucleating proteins facilitate actin polymerization by serving as templates for ATP-bound actin monomers to bind and initiate the formation of a filament. Actin polymerization typically occurs through two well-studied mechanisms – one requires the actin-related protein-2/3 (Arp2/3) complex[33] and the other utilizes the formin family of dimeric actin-binding proteins[34]. Another process utilizes tandem protein complexes such as the Spire-mediated actin polymerization[35].

1.1.1.1 Arp2/3-dependent actin polymerization

In most cells, the Arp2/3 complex in tandem with the Neural Wiskott-Aldrich Syndrome protein (N-WASp) acts as the primary actin-nucleating machinery for polymerizing filaments[36]. The Arp2/3 complex comprises of 7 protein subunits in which

the Arp2 and Arp3 subunits are structurally similar to actin monomers[33]. N-WASp, on the other hand, contains both an Arp2/3 complex binding domain and an ATP-actin binding domain[37,38]. By binding to both ATP-actin and the Arp2/3 complex, N-WASp forms the crucial trimer needed for actin filament nucleation[36,39,40].

Alternatively, the Arp2/3 complex can also initiate branching of actin filaments. In this process, the binding of N-WASp and the Arp2/3 complex allows for a conformational change within the Arp2/3 complex to allow its docking on the side of an existing actin filament[38,41]. As this occurs, N-WASp can prime the Arp2/3 complex with ATP-actin monomers to initiate the growth of a daughter filament at the characteristic 70° angles seen *in vivo* from the mother filament[42,43]. Through this mechanism, a branched array of actin filaments can be formed.

1.1.1.2 Formin-dependent actin polymerization

Parallel arrays of actin can also be made within the cytosol and this actin nucleation often occurs through the formin protein family. Depending on the cell type, various formins can initiate actin polymerization as long as they have functional formin homology 1 and 2 (FH1 and FH2) domains[34]. In contrast to Arp2/3-dependent actin polymerization, formin-dependent polymerization requires a short actin filament (actin nucleus) as a template for actin polymerization[44,45]. The ring-shaped formin dimer can bind to the barbed end of this actin nucleus and the ATP-actin that is bound to the FH1 domain can then be incorporated into the growing filament[46,47]. Through step-wise incorporation of ATP-actin at the barbed end of both strands of the actin filament, the formin dimer elongates the double stranded filament[48].

1.1.1.3 Spire-mediated actin polymerization

Unlike the Arp2/3 complex and the formins, Spire nucleates actin polymerization by forming a single strand of actin monomers. To do this, Spire utilizes its four actin-binding domains to bring 4 ATP-actin monomers in close proximity to one another[49]. The complex of Spire and a single-stranded actin tetramer becomes the template for the growing actin filament such that ATP-actin monomers can integrate into this newly-formed filament[49]. Interestingly, the efficiency of actin nucleation for Spire relies on stabilizing the pointed end of the actin filament while other proteins can assist in the

incorporation of actin at the barbed end. Recent studies have shown that Spire-mediated actin nucleation is commonly used to promote formin-mediated polymerization[50].

1.1.2. Maintenance of actin filaments

Aside from the critical concentration of actin monomers in the cytosol, the stability of actin filaments also depends on a team of actin-binding proteins that work collaboratively to stabilize or destabilize actin filaments[51,52]. Several key proteins or protein families have been well-studied in both aspects of actin maintenance and their functions play crucial roles in actin dynamics.

1.1.2.1. Actin-stabilizing proteins

The length of actin filaments can be stabilized in many ways such as binding, bundling, and crosslinking filaments. Protein families such as fascin, calponin, α-actinin, and plastin all have characteristic actin-binding domains, which interact with the sides of an actin filament. Through the interactions of these proteins with actin, they can organize actin filaments into more stable arrays or protect actin filaments from disassembly by actin severing enzymes. Notably, there are many more actin-stabilizing proteins that have been studied, but this section will focus only on several families of proteins that are related to my research projects.

Fascin

Fascin contains two actin binding domains situated on opposite ends of the protein, enabling fascin to link two actin filaments to form parallel arrays[53]. As a result, the role of fascin has primarily been associated with bundling actin filaments within the filopodia in various cell types and the microvilli in intestinal epithelial cells[53]. At these structures, fascin confers the proper packing and stability for the filopodia to protrude from the cell surface. Without fascin, the actin filaments within the filopodia are more loosely packed and these filopodia protruded in a parallel direction to the leading edge of the cell[53]. As such, the force generation of loosely packed actin bundles were dampened without fascin.

Calponin

The calponins are calcium-sensitive proteins characterized by a unique actin-binding domain that is found in over a dozen proteins and since this actin-binding motif was first discovered in calponins, it was called the calponin homology domain (CH domain)[54]. Interestingly, at least two CH domains are necessary for functional actin-binding of these peptide domains[55,56]. The CH1 domain typically has all the binding affinity for F-actin while the CH2 domain contributes to the stability of actin-binding. Proteins with only one CH domain do not necessarily utilize the actin-binding function of their CH domain.

The most ubiquitous calponins are calponin 1 (CNN1), calponin 2 (CNN2) and transgelin (SM22)[55,57]. Ironically, these calponins only have one CH domain, but these proteins have calponin homology-like repeats (CLIK repeats) that compensate for the lack of a second CH domain[54,58]. SM22 only has one CLIK repeat while CNN1 and CNN2 each have three CLIK repeats[55]. Although the CH domain of these calponins do not have actin-binding affinity[54,56], many studies have shown that these proteins may function as docking sites for other signalling or actin-binding proteins[59–61]. Instead, the two functional actin-binding sites (ABS) are found in between the CH domain and the first CLIK repeat (ABS1) as well as in the first CLIK repeat (ABS2)[57,62].

Although the calponins share similar structural components, these three proteins have markedly different functions in actin dynamics. CNN1 is more abundant in skeletal muscle cells[63,64] and as such, its main role in non-muscle cells have yet to be elucidated. Currently, only *in vitro* experiments have suggested that CNN1 functions to provide structural flexibility to individual filaments by stabilizing the pocket between alternating actin monomers within the filament[65,66]. Unlike CNN1, both CNN2 and SM22 are abundant in many cell types[57,61,64,67]. Instead of bundling actin filaments in stress fibers, CNN2 function has been associated with regulating highly dynamic actin structures within podosomes and the leading edge of motile cells[62]. Interestingly, the C-terminal tail of CNN2 has been shown to inhibit the actin-binding site within its CLIK repeat [68] and mutants lacking the C-terminal tail reverted to acting as actin bundling proteins at stress fibers[62]. This suggests that full-length CNN2 is not an actin bundling protein, but rather it functions either to stabilize actin filaments or as previously mentioned, to provide scaffolding for the regulation of actin filaments. On the other hand, SM22 has both

functional actin binding domains[57,62], but its actin binding affinity is weaker than CNN1 and CNN2[62]. SM22 experiments have shown that SM22 loosely bundles actin filaments in an ionic-sensitive manner *in vitro*[69]. Within cells SM22 decorates actin filaments at podosomes and membrane ruffles[62]. SM22 knock-downs lead to the reorganization of stress fibers and the reduction of cell movement [70]. Taken together, the cytoskeletal role of SM22 may be in promoting actin polymerization within highly dynamic actin structures[57,70]. Although these three calponins have distinct functions, these proteins all contribute to regulating actin stability.

α-actinin

The actin crosslinker α-actinin has two CH domains that are situated at the N-terminus of the protein and this forms its actin-binding domain[71]. The functional form of the protein requires a homodimer such that each of the actin-binding domains are used for binding to two filaments[72]. Notably, the known role of α-actinin has been to stabilize stress fibers and loss of α-actinin led to stress fiber collapse[73,74].

Plastin

The plastins/fimbrins is another family of actin-bundling proteins and members of this family each have four CH domains embedded within two actin binding domains (ABD1 and ABD2)[55]. When the ABD2 domain of plastin binds to an actin filament, a conformational change in the ABD1 increases its actin binding affinity resulting in the bundling of multiple actin filaments[75]. The function of plastins has been especially associated with parallel bundles within microvilli and stereocilia[76], but in general, plastins contribute to actin bundling in focal adhesions, lamellipodia, filopodia and membrane ruffles of motile cells as well as stress fibers[76].

1.1.2.2 Actin-destabilizing proteins

Most actin-destabilizing proteins are severing enzymes that splice actin filaments into multiple shorter filaments. The most notable severing proteins are gelsolin and the cofilin protein family.

Gelsolin

The actin-binding protein gelsolin is composed of multiple calcium binding domains and increasing calcium ion concentrations are important in activating the

severing activity of gelsolin[77]. In its inactive state, the C-terminal tail blocks the N-terminal actin-binding domains[78]. As calcium ions bind to gelsolin, the N-terminal actin domain is exposed allowing its binding to actin filaments[78]. This region of gelsolin binds between two adjacent actin monomers on the same strand [77,79] and this breaks the hydrophobic interactions of those adjacent actin monomers leading to severing of the actin filament. Afterwards, gelsolin remains on the barbed-end of the severed filament where it functions as a capping protein[79].

Cofilin

Cofilin destabilizes the actin filament by binding to the ADP-bound pointed end[43]. At this region, cofilin can bind onto the actin monomer at a 1:1 ratio[80] and induce conformational changes that bends the actin filament[81]. The induced stress enhances the dissociation of actin monomers or short actin fragments causing the replenishment of the monomeric actin pool in the cytosol[82]. Interestingly, crosslinking proteins such as fascin cannot protect actin filaments from cofilin-induced severing[83].

1.1.3. Bacterial manipulation of actin

Several bacterial pathogens have evolved to manipulate their host by hijacking the actin machinery[84,85]. In most cases, these bacteria use the actin machinery to generate actin-rich structures for motility along the apical surface or within their host cell while others induce actin-dependent cellular processes to cause internalization into the host. To do this, these bacterial pathogens express protein effectors that mimic or induce the recruitment of actin-nucleating proteins to the vicinity of the bacteria[84,85]. For example, enteropathogenic *Escherichia coli* and enterohemorrhagic *Escherichia coli* secrete effectors, particularly Tir, to recruit the actin-nucleating machinery beneath the bacteria and this generates protrusions to allow the bacteria to move along the host cell surface[86]. *Shigella flexneri* and certain *Salmonella enterica* bacteria secrete many bacterial effectors (IpaA, IpgB1, IpgB2, IpgD for *Shigella* and SipA, SopB, SopE, SopE2 for *Salmonella*) into the host cytosol to initiate actin-based host cell membrane ruffling for internalization into their host k[87,88]. *Listeria monocytogenes* triggers actin-dependent clathrin-mediated endocytosis using bacterial surface internalin proteins InlA and InlB[89]. Then, the internalized *Shigella flexneri* and *Listeria monocytogenes*, through IcsA (which activates N-WASp) and ActA (which mimics N-WASp) respectively, both recruit the

Arp2/3 complex to generate comet tails and move around the host cytosol or protrude to neighboring cells[90,91]. In all of these situations, commandeering the actin cytoskeleton is essential for bacterial spread and dissemination within host tissues[92,93].

1.2. Microtubules

In animals, the microtubule network is an array of long hollow tubes that spans the entire cell. In proliferating cells, microtubules emanate from the microtubule organizing centre (MTOC) and grow outwards to the cell periphery[94]. In contrast, differentiated epithelial cells have a meshwork of microtubules at the apical side of the cell, but they also have a subset of microtubules that are tethered to this meshwork and encompass the length of the polarized epithelial cell[95]. These microtubule arrays provide scaffolding for protein motors to transport various cargos such as protein complexes, vesicles, organelles, and even condensed chromosomes. As a result, microtubules are implicated in many different cellular processes such as vesicular trafficking, organellar transport, cell division, and cell motility[2,96]. Because microtubules are essential to many cellular functions, control of the microtubule network can affect the function of tissues and organs. Stabilizing or destabilizing microtubules can alter proliferation rates of cells as well as the transport of vesicles in and out of tissues[2,97]. As such, several classes of anti-cancer drugs target microtubule function[98–100].

Microtubules are also enriched in specialized cellular structures such as the cilia in differentiated epithelial cells and the flagella of sperm cells[101]. Disassembling microtubules alters the morphology of these specialized microtubule-rich structures[102]. Therefore, the manipulation of microtubule arrays has deleterious consequences at the cellular level.

1.2.1. Growth

The centerpiece of the microtubule network is the microtubule organizing centre (MTOC) and as the name implies, it governs the arrangement of the entire array[103]. In non-polar animal cells the MTOC is composed of a pair of centrioles surrounded by many ring-like structures called the γ-tubulin ring complex (γ-TuRC)[103–105]. The γ-TuRC is an offset ring arrangement of 13 γ-tubulin subunits and this provides the nucleation template for the binding of α/β-tubulin heterodimers[106]. The growth of a microtubule

starts when guanosine triphosphate (GTP)-bound α/β-tubulin heterodimers are added onto any of the available 13 binding sites on the γ-TuRC (Fig. 1.1B). In the presence of high GTP and magnesium ions, tubulin heterodimers are spontaneously added in a head-to-tail fashion onto this nucleating complex[107]. Soon, short protofilaments are formed and these short filaments bind laterally together such that α-tubulin subunits on adjacent protofilaments are side-by-side and similarly, β-tubulin subunits are next to the β-tubulin of the next protofilament. The sheet-like intermediate form of these arranged protofilaments quickly assemble into the characteristic hollow tube of a microtubule[106], but due to the offsetting of the γ-TuRC, there is a seam in the microtubule making it asymmetrical[106]. Nonetheless, each microtubule has a directionality (polarity) wherein the β-tubulin subunits are exposed on the growing end (plus end) of the microtubule and the α-tubulin subunits are facing the γ-TuRC-tethered end (minus end) of the microtubule[108,109]. Lastly, elongation of the microtubule occurs as more tubulin heterodimers are added at the plus end of the microtubule[105,110].

In polarized columnar or cuboidal epithelial cells, microtubules do not emanate from the MTOC located near the nucleus, but rather the γ-TuRCs are tethered at the apex of the cell and microtubules grow towards the cell base[111]. This results in the minus ends of the microtubules at the apical side of the cell while the plus ends are at the basal area. Microtubule containing axonemes also make up the cores of cilia and flagella. In these structures, microtubules grow from the basal body near the surface of the cell and their plus ends are oriented towards the tip of the structures[112].

1.2.2. Stabilization of microtubules

Similar to actin filaments, microtubules undergo constant rearrangement within the cell. Without stabilizing proteins, a single microtubule can undergo rapid growth and shrinkage depending on the incorporation rate of tubulin heterodimers[110]. Both α-tubulin and β-tubulin bind to GTP, but only β-tubulin has hydrolytic activity that turns GTP to guanosine diphosphate (GDP)[113]. GTP hydrolysis causes the GDP-bound tubulin heterodimers to dissociate from an exposed end. When the incorporation rate of GTP-bound tubulin heterodimers lags or the end of a microtubule is uncapped, GTP hydrolysis leads to the collapse of microtubules[114]. This phenomenon is called dynamic instability and as such, microtubules rely on stabilizing proteins that protect the microtubule from catastrophe.

1.2.2.1. Protective microtubule associated proteins

Protecting the length and plus ends of the growing microtubule is crucial for preventing catastrophe. Several proteins have been known to bind to particular regions of the microtubule to structural stabilize the microtubule or to cap the plus ends to prevent the dissociation of tubulin heterodimers from the microtubule.

MAP family of proteins

The most ubiquitous microtubule associated proteins belong to the class of MAP2, MAP4, and MAPT (Tau)[115] and all of these proteins share similar C-terminal repeating microtubule binding motifs[116]. MAP2 and MAPT are predominantly enriched in neuronal cells[117,118], while MAP4 is enriched in other cell types[119]. These proteins utilize their microtubule binding motifs to bind to adjacent tubulin heterodimers on the same protofilament[120] and this prevents the binding of destabilizing enzymes onto the microtubule. In addition, when these MAPs are bound to adjacent microtubules, they can form complexes to create bundles of microtubules[121]. In contrast, phosphorylation of these microtubule binding proteins typically increases microtubule catastrophe rates as they leave the length of the microtubule exposed for protein binding[122,123].

DCX

Doublecortin (DCX) has two tandem microtubule binding domains that bind between two tubulin heterodimers on adjacent protofilaments[124]. DCX binding to microtubules inhibits GTP hydrolysis by β-tubulin and it also provides the structural stability in between the protofilaments of the microtubule[124]. Both of these roles have been shown to contribute to microtubule nucleation and elongation.

XMAP215

The *Xenopus* microtubule associated protein 215 (XMAP215) is a microtubule polymerase that promotes the addition of tubulin heterodimers to the plus end of microtubules[125]. This enriches the amount of GTP-bound tubulin heterodimers at the plus end forming the characteristic GTP-bound tubulin cap of stable microtubules[126]. Through this mechanism, XMAP215 prevents the dynamic instability of the microtubule[110,126].

EB Proteins

Three end binding proteins (EB1, EB2, EB3) are found in animal cells, but EB1 is the most ubiquitous[127]. EB1 is trafficked by motors to the plus end of microtubules[128], where it serves as an adaptor protein to two contrasting functions, depending on its binding partner. The EB1-XMAP215 complex can promote the addition of tubulin heterodimers to elongate the microtubules[129], but EB1 complexing with the cytoplasmic linker protein of 170 kDa (CLIP-170) can cause catastrophe by enhancing GTP-hydrolysis at the plus end[130]. Nevertheless, end binding proteins are generally thought to contribute to microtubule integrity.

1.2.2.2. Microtubule Severing proteins

Microtubule catastrophe can be catalyzed by microtubule severing proteins when these enzymes cause distinct breaks within the length of microtubules[131]. The severing of microtubules generates multiple microtubule fragments which can rapidly depolymerize on both the new plus and minus ends of each fragment.

Katanin

The katanin family of proteins are thought to induce microtubule severing in a synergistic manner. Within this family, the katanin catalytic subunit A1 protein (KATNA1) and the katanin catalytic subunit A like 1 protein (KATNAL1) have been shown to mechanically cause the severing of microtubules[132,133] whereas the katanin regulatory subunit B1 protein (KATNB1) and the katanin regulatory subunit like 1 protein (KATNBL1) bind to the catalytic subunits and enhance microtubule severing activities[133,134]. Another catalytic protein the katanin catalytic subunit A like 2 protein (KATNAL2) has also been identified but its function is poorly understood[133,135].

Of the four characterized katanins, KATNA1 and KATNAL1 have similar domains each containing an N-terminal microtubule interacting domain and an ATPases Associated with many cellular Activities (AAA)-ATPase domain[132]. In contrast, KATNB1 and KATNBL1 only share a common C-terminal domain that can bind with either KATNA1 or KATNAL1[134]. Notably, unique to KATNB1 is a WD40 microtubule binding domain that allows this regulatory protein to bind to microtubules[134]. Regulation of these katanins relies on several known kinases such as the Aurora kinase A, Aurora kinase B, and the Polo-like kinase 1[136,137]. These kinases can regulate the lengths of microtubules

by activating the katanins at the edge of non-mitotic cells and these kinases also control microtubules during mitosis by recruiting the katanins to the MTOC or the interface of the condensed chromosome and microtubules[137,138].

From these structural findings, the functions of each protein have been characterized. In their hexameric ring complex conformation, KATNA1 and KATNAL1 can both hydrolyze ATP[132,139]. The hydrolysis of ATP generates a conformational change in the protein complex allowing the pulling of the exposed tubulin C-terminal tails on a microtubule[140]. This critical step removes the tubulin heterodimer from the microtubule and creates a gap in the microtubule[139]. Further binding and catalysis of the katanin complex can generate mechanical torsion on the microtubule to accomplish complete severing of all the protofilaments. Interestingly, KATNA1 or KATNAL1 alone has low microtubule severing activity and only in the presence of KATNB1 or KATNBL1 does microtubule severing activity increase[141]. Since KATNB1 has its WD40 domain, KATNB1 has been shown to enhance microtubule severing by recruiting the KATNA1 complex to the microtubule[133,134]. Interestingly, KATNBL1 does not have the same domain, but addition of this subunit to KATNA1 produced similar microtubule severing activity to KATNB1-KATNA1 complexes[133]. Although the mechanism is still undetermined, it seems that the way KATNBL1 binds to KATNA1 in a similar fashion as KATNB1-KATNA1 binding also enhances microtubule severing[133]. As a result, the microtubule severing activity of these protein complexes contribute to the maintenance of microtubules.

Spastin

Spastin is another microtubule severing protein and its severing mechanism is similar to that of the katanins. Monomeric spastin also has an AAA-ATPase domain[142] and upon complexing into the characteristic hexameric ring[143], spastin can remove the α-tubulin subunit from the microtubule[140,143]. Through similar mechanisms as katanin, spastin also severs microtubules in an ATP hydrolysis-dependent manner and they differ only in the lengths of the resulting microtubule fragments. Katanin produces microtubule fragments of various lengths whereas spastin produces equal-length microtubule fragments[144].

Fidgetin

Fidgetin (FIGN) is a recently discovered microtubule severing protein alongside Fidgetin-like 1 (FIGNL1) and Fidgetin-like 2 (FIGNL2). Subcellular localization of green fluorescent protein (GFP)-tagged constructs for the three fidgetins showed that FIGN and FIGNL2 were restricted within the nucleus whereas FIGNL1 was found within the nucleus and the cytoplasm[145]. Microtubule severing through fidgetin is similar to the severing activity of katanins and spastin[146,147], but fidgetin-induced severing has been primarily shown to contribute to microtubule shortening at anaphase[148].

1.2.3. Bacterial manipulation of microtubules

Similar to manipulating the actin cytoskeleton, the integrity of the microtubule network within host cells during bacterial infection has been studied in a few cases. To date, most microtubule alterations focus on the localized destruction of microtubules within its host cell. *Escherichia coli* EspG[149] and *Shigella flexneri* VirA[150] are both secreted protein effectors that bind to microtubules and these cause the instability and collapse of microtubules in the immediate vicinity of the bacterium. *Edwardsiella tarda* also has a similar bacterial effector, EseG, to that of *Escherichia coli* EspG[151], but its mechanism of microtubule destabilization remains poorly understood. Similarly, internalized *Listeria monocytogenes* can recruit the host protein stathmin through its surface protein ActA and the resulting tubulin sequestration around the bacteria leads to the collapse of the surrounding microtubules[152–155]. Another bacterium, *Pseudomonas aeruginosa* can upregulate cyclic nucleotide signals through ExoY and this induces the shortening of host microtubules within the cell[156,157].

1.3. The Ubiquitylation System

The ubiquitylation system is one of the many posttranslational modifications utilized by animal cells in its signalling repertoire (Fig.1.2). Ubiquitylation involves the tagging of a protein substrate with a small ubiquitin protein and repetitive ubiquitylation of the same substrate creates a polyubiquitin tag on the protein[158]. Addition of ubiquitin monomers onto monoubiquitylated proteins can occur on either lysine 48 (K48) or lysine 63 (K63) of the monoubiquitin tag[159]. As a result, the polyubiquitylated protein can be directed towards protein degradation or towards further cellular signalling cascades

respectively[160]. Ubiquitylation signalling ultimately has two main functions within a cell – to target proteins for degradation, or to tag proteins for further signalling pathways. Notably, in non-protein degradation ubiquitylation, this posttranslational modification has been implicated in cellular processes such as organellar trafficking, DNA damage repair, and immune response activation[160].

1.3.1. Mechanism

Ubiquitylation involves three enzyme families that relay cytosolic ubiquitin monomers onto the protein substrate. The first enzyme family is called the ubiquitin activating protein (E1) family and consists of only 2 known proteins in humans[161]. The second enzyme family is called the ubiquitin conjugating protein (E2) family and consists of over 40 known E2 proteins[162]. Ubiquitin ligating proteins (E3) make up the last enzyme family and they consist of over 600 proteins and more are continuously being discovered[163].

Cytosolic ubiquitin is typically activated in an ATP-dependent mechanism by an E1 protein[164]. Once activated, the ubiquitin monomer is passed onto the cysteine catalytic domain of an E2 conjugating protein[164]. The thioester bond formed between the E2 protein and the ubiquitin monomer allows the E2 protein to position ubiquitin for ligation to the substrate. Binding of the substrate is dependent on the substrate-specific E3 ligase protein and the E3 protein catalyzes the transfer of ubiquitin to the protein substrate[163]. Simplistically, ubiquitylation occurs through this step-wise transfer of ubiquitin onto the substrate.

Complexity occurs through which E2 and E3 combination is involved in the ubiquitylation event. The choice of E2 protein dictates K48- or K63- polyubiquitylation since most E2 proteins can do one or the other[165]. Moreover, for some K63-polyubiquitylation-specific E2 proteins such as the ubiquitin conjugating enzyme 2N (Ube2N), accessory proteins are required to facilitate ubiquitylation for specific signalling cascades[166,167]. In addition, aside from E3 proteins dictating substrate specificity, two main types of E3 ligase proteins are responsible for how ubiquitin is added onto the substrate. The really interesting new gene (RING)-type ligase facilitate the direct transfer of ubiquitin from the E2 protein to the substrate whereas the homologous to the E6-AP carboxyl terminus (HECT)-type ligase forms a thioester bond with the ubiquitin on the E2

protein prior to the transfer of the ubiquitin to the substrate[163]. Still, the functions of the E2 proteins focus on positioning of the ubiquitin for ligating while the E3 protein binds the substrate and transfers the ubiquitin onto the substrate.

1.3.2. Bacterial manipulation of ubiquitylation

Ubiquitylation affects multiple cellular signalling pathways. Consequently, several bacteria have learned to use ubiquitylation to their benefit. Bacterial hijacking of the ubiquitylation pathway involves either inhibiting the ubiquitylation of certain substrates or commandeering E2 proteins to tag novel substrates during infection. Enteropathogenic *Escherichia coli* uses several secreted effectors to target the E1 proteins to globally reduce host cell ubiquitylation pathways [168] whereas enterohemorrhagic *Escherichia coli* uses OspG to target specific E2 proteins to block the ubiquitylation pathway[169] and using the bacterial proteins, NleL and NleG, that mimic host E3 proteins, subvert ubiquitylation to only its desired substrates[170]. *Shigella flexneri* also targets E2 proteins using OspG[171] and using IpaH, ubiquitylates proteins involved in immune response signalling[172]. In addition, *Shigella flexneri* also uses OspI to prevent Ube2N induction of the immune response[173,174]. *Salmonella enterica* and *Legionella pneumophila* also possess proteins (SopA, NleG, SspH for *Salmonella* and LubX, SidC/SdcA for *Legionella*) that mimic host E3 proteins which allows the bacteria to ubiquitylate its own set of novel substrates and downregulate the immune response[175]. As a result, these bacterial pathogens have benefited from altering host ubiquitylation mechanisms.

1.4. Enteropathogenic *Escherichia coli* (EPEC)

Escherichia coli (*E. coli*) are Gram-negative rod-shaped bacteria that are ubiquitious in many environments and host organisms[176]. In particular, the microbiomes of many mammalian gastrointestinal tracts have many strains of commensal *E. coli* and they contribute to the metabolism of nutrients for both the microbiome and the host[177]. Through horizontal gene transfer with other bacteria, a subset of *E. coli* strains have acquired various gene plasmids that have allowed them to trigger host cell responses that benefit their survival. Several categories of *E. coli* have evolved to cause mild to severe diarrhea during their infections and these include enteropathogenic *E. coli* (EPEC), enterohemorrhagic *E. coli* (EHEC), enteroinvasive *E. coli* (EIEC),

enterotoxigenic *E. coli* (ETEC), enteroaggregative *E. coli* (EAEC), and diffuse-adhering *E. coli* (DAEC)[178].

Among these strains of *E. coli*, EPEC is primarily detrimental to infants under the age of five years old[179]. Fecal-oral contact[178,179], or the ingestion of the bacteria through contaminated hands or food, allows the bacteria to be transmitted among individuals. After ingestion, the bacteria reach the intestines where attachment to the epithelium promotes colonization of the intestines. As the bacteria accumulate on the host cell surface, they secrete a number of bacterial protein effectors encoded by the locus of enterocyte effacement (LEE) and non-LEE gene clusters[180,181]. Eventually, the amount of secreted bacterial effectors overwhelms the host cells and causes drastic epithelial alterations. Aside from these bacterial effectors, lipopolysaccharide on the bacterial surface can also elicit innate immune responses from the host. The secretion of effectors and the resulting changes in the host's epithelium lead to the infected individual experiencing persistent watery diarrhea[178,182,183]. Through this diarrhea, the bacteria can often be cleared over time, but the characteristic loss of water and electrolytes becomes the main concern if the infection persists more than several days. Infantile death results from diarrhea-related dehydration rather than as a direct consequence of bacterial infection[184,185]. As such, the onset of these symptoms are typically managed with constant rehydration to recover water and electrolyte levels[185]. Antibiotic treatment is reserved for severe cases where the inflammation of the gastrointestinal tract becomes life-threatening since unnecessary treatment with antibiotics have caused the rampant development of antibiotic-resistant EPEC strains. To date, multi-drug resistant EPEC are still prevalent and these continue to cause treatment-challenging disease in developing countries[184].

1.4.1. Colonization

The attachment of the bacteria to the surface of epithelial cells is crucial for colonization of the intestines[186]. As the bacteria approach the intestinal epithelia, rope-like appendages on the bacterial surface allow the bacteria to anchor onto their host cell surface. Two types of these appendages, the flagella and the bundle forming pili, have been shown to be important for bacterial attachment[187,188]. Typically, the flagellum is used for bacterial motility, but during the colonization, EPEC use their flagella for the initial attachment. Previous studies have shown that flagella-deficient EPEC mutants

were unable to adhere onto cells and conversely, non-pathogenic *E. coli* that were transformed with a plasmid carrying the EPEC flagellar gene *fliC* were able to attach onto host cells[188]. Aside from the flagella, the bundle forming pili (BFP) can tether the bacteria onto the host cell surface, but EPEC can also grasp onto other EPEC bacteria through the interactions of their BFP[187]. As a result, EPEC can aggregate into "microcolonies" that help these bacteria adhere to the host cell surface. Interestingly, a plasmid-cured strain of EPEC, JPN15, that does not have flagella, BFP and some effector proteins, can still attach to host cells[189]; however, the ability of the JPN15 strain to cause diarrheal disease appears diminished since, in one study, only two out of nine volunteers experienced diarrhea compared to nine out of ten volunteers who ingested wildtype EPEC (E2348/69)[190]. This supports the conclusion that EPEC adherence is important for the progression of the disease.

Once an EPEC bacterium docks onto the host cell surface, a bacterial needle-like apparatus is formed to inject bacterial protein effectors into the host cell cytosol (Fig.1.3). This apparatus, called the type-three secretion system (T3SS), is a common bacterial structure used for secreting protein effectors onto host cells[180]. EspA proteins form the shaft of the needle that spans from the bacterial outer membrane to the host cell membrane[190]. EscC, EscD, EscF, and the other Esc lipoproteins make up the basal body embedded on the bacterial membrane[190] while secretion of protein effectors requires the ATPase EscN to facilitate the shuttling of proteins through the apparatus[190]. Notably, deletion of the ATPase EscN prevents the secretion of any bacterial effectors into the host cytosol[190]. With a fully functional T3SS, the first effectors secreted by the bacteria are the pore forming proteins EspB and EspD which create a pore on the host cell membrane and secure the T3SS on the host cell surface[191]. Once this is established, many LEE and non-LEE encoded bacterial effectors are injected into the host cytosol, but the first of these effectors is the translocated intimin receptor (Tir)[192]. The secretion of Tir is crucial since it gets translocated into the host cell membrane and performs two crucial functions at the bacterial attachment site. The first function is to bind to the bacterial surface protein intimin and this enhances the attachment of EPEC on the host cell surface[86,193]. The other function is that the clustering of multiple Tir proteins underneath the bacterial attachment site initiates the polymerization of actin filaments[193]. The accumulation of actin raises the bacteria from the host cell surface and this actin-rich protrusion called a pedestal, is a hallmark of EPEC infections[194].

1.4.2. Formation of actin-rich pedestals

The integration of Tir into the host cell membrane marks the initiation of a bacteria-induced manipulation of the host actin cytoskeleton. This signalling cascade starts with the accumulation of Tir on the host cell cytosol underneath the bacterial attachment site[193]. In this region of the host cell plasma membrane, host cell kinases such as c-Fyn and Abl phosphorylate several residues on Tir[194,195], but the turning point of this signalling regimen is the phosphorylation of the tyrosine at position 474 (Y474) of Tir[192]. The phosphorylation of Y474 allows the host cell protein nck (non-catalytic region of tyrosine kinase adaptor protein) to bind to Tir[194] and in turn, nck ultimately recruits the actin-nucleating proteins N-WASp and the Arp2/3 complex to the site of bacterial attachment[195]. N-WASp recruitment has been shown to be indispensable for EPEC-induced actin polymerization and the complexing of nck and Tir is sufficient to activate N-WASp-mediated actin polymerization[195]. Consequently, N-WASp activates the Arp2/3 complex similar to its classical role in actin polymerization and actin filaments are then formed within the host cell at the bacterial attachment site. The abundance of the intimin-Tir complex underneath the bacteria concentrates the polymerization of actin filaments at the cytosolic side of the host plasma membrane and these push both the host plasma membrane and the attached bacteria away from the host cell surface. The resulting actin-rich structure is a dynamic EPEC-induced pedestal which allow the bacteria to "surf" along the host cell surface[196].

Although these proteins are the minimal components necessary to form EPEC-induced pedestals, a variety of host cell proteins regulate the generation of these actin-rich structures. Endocytic proteins such as clathrin, CD2AP, epsin, and Eps15 are recruited to the apical tip of pedestals where these proteins contribute to the scaffolding of the actin polymerizing machinery[197,198]. In addition, cortactin is a known actin-associated protein that enhance the binding of N-WASp and the Arp2/3 complex to actin filaments. In EPEC pedestals, cortactin is believed to contribute to the linking of the N-WASp and Arp2/3 complex to the Tir-nck assembly at the host cell membrane[199]. Aside from these proteins, recent work has shown that the cytoskeletal protein spectrin formed a lattice along the membrane that encases the EPEC pedestal[200]. This spectrin lattice is believed to provide structural integrity to the EPEC pedestal and that abolishment of the spectrin cytoskeleton impaired the formation of EPEC pedestals *in situ*[201]. In addition, two intermediate filament proteins cytokeratin 8 and cytokeratin 18 have also been found

at the base of EPEC pedestals where they may have a role in regulating cytoskeletal rearrangements during pedestal formation[202,203]. Taken together, the generation of EPEC pedestals relies on the balance between several host protein complexes.

1.4.3. Disease progression

After the establishment of intimate attachment to host cell epithelia, EPEC continues to secrete additional effectors that cause various alterations including microvilli effacement, cytoskeletal rearrangement, immune response suppression, and collapse of intestinal epithelial barrier integrity.

One of the hallmarks of EPEC infection is the ability of bacteria to efface microvilli on intestinal epithelial cells. To do this, EPEC secretes the effector EspF, which can bind to monomeric actin as well as the actin nucleating factors N-WASp and the Arp2/3 complex and this binding allows EspF to shorten microvilli within the vicinity of the EPEC pedestal[204]. The mitochondria associated protein (Map) also contributes to the shortening of microvilli by interacting with the known actin dynamics regulatory protein Cdc42[205]. Through this mechanism, EPEC can control the terrain of the host cell surface. Intracellularly, the bacteria also control the cytoskeleton. EspF can also bind to cytokeratin 18[202]; EspG is believed to be able to regulate the depletion of microtubules[149]; and EspH can suppress the formation of filopodial protrusions[205]. By secreting these effectors, EPEC can efficiently generate pedestals and move along the host cell surface.

Because EPEC remains extracellular, it also relies on its effectors to impede the host's immune signalling mechanisms. To do so, EspF binds to the phosphatidylinositol-3-kinase and impedes macrophage uptake[206]. The non-LEE proteins (NleB, NleC, NleD, NleE, and NleH) target the inhibition of the NFκB cytokine activation pathway[205]. Through these effectors, the host's immune response is dampened during EPEC infection.

Epithelial alterations caused by EPEC infection largely contribute to the symptoms of profuse watery diarrhea. As EPEC colonizes the intestines, many effectors target cellular junctional proteins as well as plasma membrane ion and water channels. EspF, EspG, Map and NleA alter tight junction proteins causing a leakiness at the

intercellular junctions[206]. In addition, EspF and EspG cause the cytosolic sequestering of the aquaporin water channels and consequently, this reduces water reabsorption from the lumen of the colon into the cell cytoplasm[207]. Lastly, gap junction proteins which typically serve as intercellular water and ion channels are relocalized to the apical surface of the epithelia causing the flux of water and ions into the intestinal lumen[208]. All these alterations nullify the barrier function of the intestinal epithelia and lead to the accumulation of ions and consequently water in the intestinal lumen.

1.5. Listeria monocytogenes

Listeria are Gram-positive rod-shaped bacteria that can withstand cold temperatures, low pH and high salt environments[209] and as such, they can proliferate in various water or soil environments as well as in the gastrointestinal tract of animals. Of the 17 *Listeria* species, only *Listeria monocytogenes* (*L. monocytogenes*) and *Listeria ivanovii* are pathogenic where humans and ruminating animals are their respective hosts[210]. *L. monocytogenes* pose a severe threat to humans because they can proliferate in our water system and food. Even refrigerated, (low temperature), pickled (low pH) and salted (high salt concentration)[209] food can harbor the bacteria. Although intensive monitoring of food production has vastly reduced the number of infectious cases, *Listeria* outbreaks can still occur due to the low dose necessary to cause disease. Immunocompetent individuals can experience gastroenteritis from consuming food containing ~10^9 bacteria; however, elderly individuals, children and pregnant women are susceptible to infection with as few as 100 bacteria[211,212]. In these individuals, bacterial infections can extend from gastroenteritis to bacterial sepsis and 'metastatic infections' of the liver, spleen, and in severe cases, the brain. During pregnancy, the fetus can also be infected due to the ability of *L. monocytogenes* to cross through the placental barrier. resulting in complications and even miscarriages[212].

Similar to EPEC, the main site of infection after ingestion is the intestine. When the bacteria reach the intestine, environmental factors trigger various bacterial mechanisms such as riboswitches and RNA expression to upregulate the expression of specific protein effectors[213]. Unlike EPEC, *L. monocytogenes* invades intestinal cells through clathrin-mediated endocytosis. Once inside host vacuoles, the bacteria can either get transcytosed through the epithelia into the lamina propria or can escape the vacuoles and enter the cytoplasm[89]. In the lamina propria, the bacteria can make their

way into the blood vessels. Ultimately, reaching the blood allows the bacteria to disseminate to various organs and the colonization of the liver, spleen, brain, and fetus can lead to inflammation and mortality rates of up to 30% if left untreated [212]. If the bacteria stay inside the epithelial cells, they can hijack host cytoskeletal elements and use these elements to spread into neighboring epithelial cells.

If *Listeria* infections are detected early, β-lactam-based antibiotics such as amoxicillin and gentamicin are the most effective in halting the spread of bacterial infection [212].

1.5.1. Internalization

Once in the intestines, phagocytic cells can easily internalize *L. monocytogenes* [214]. To subvert neutralization by phagocytes, the bacteria invade the intestinal epithelia through clathrin-mediated endocytosis (CME). CME internalization requires the accumulation of ligand-receptor signals on the host plasma membrane (Fig. 1.4). Internalins are expressed on the surface of *L. monocytogenes* and during the internalization event, *L. monocytogenes* engages the endocytic mechanism through binding internalin A (InlA) and internalin B (InlB) to the E-cadherin and c-Met receptors respectively on the host cell membrane[215,216]. This initiates the signalling cascades that recruit the clathrin endocytic machinery (clathrin, Eps15, epsin, Grb2, dynamin, and CD2AP) to create the classical clathrin-based membrane invagination and dynamin-based scission together with actin forces at the membrane complete the internalization of *L. monocytogenes* into a vacuole [89,217,218]. From this vacuole, the bacteria can either be transported to the basal membrane where it is exocytosed into the basal tissue or the bacteria can escape into the cytosol by secreting phospholipase A (PlcA), phospholipase B (PlcB), and listeriolysin O (LLO)[214,219]. All of these lipases contribute to the disintegration of the vacuole. Then, *L. monocytogenes* can replicate and commandeer host cell actin machinery to move around within the cytosol.

1.5.2. Comet tail formation

When *L. monocytogenes* enters the host cytosol, several bacterial factors are upregulated. The actin assembly protein A (ActA) is crucial for the formation of the branched network of actin filaments called a comet tail[220]. As its name suggests, ActA

initiates actin polymerization by recruiting the actin nucleating Arp2/3 complex. ActA functionally mimics N-WASp[91] and as such, ActA facilitates the addition of monomeric actin onto the Arp2/3 complex to initiate actin polymerization. Notably, this process creates branched actin arrays and initially, the short actin strands accumulate around the bacteria[221]. The immunolocalization of this stage of the infection shows prominent rings of F-actin staining around the bacteria and thus, this stage of actin polymerization is referred to as *L. monocytogenes* actin cloud formation[221]. ActA then concentrates to one pole of the bacterium where branched filamentous actin forms the comet tail[222].

As elongation of the branched actin array occurs, actin-associated proteins are recruited and contribute to the regulation of the growing comet tail. Actin stabilizing proteins have been shown to have a crucial role in comet tail elongation. In *in vitro* studies, fascin, α-actinin, and plastin can elongate comet tails when the Arp2/3 complex was removed after the initial comet tail formation[223]. Moreover, the complex roles of actin stabilizing proteins have been studied at the scale of single actin filaments[224]. The degree of compacting actin filaments within the comet tails is similar to that of stress fibres and filopodial protrusions[224]. This suggested that actin stabilizing proteins could influence the stiffness required for the functionality of comet tails.

The resulting comet tail provides the propulsive force to push the bacterium in a unilateral direction enabling the bacteria to gather nutrients or to use the propulsive force of the comet tail to protrude the host plasma membrane and force internalization into the neighboring host cell[92,225–227]. In both cases, the comet tail is crucial for the survival and dissemination of the bacteria within host tissues.

1.5.3. Disease progression

Aside from hijacking the host actin cytoskeleton and acquiring nutrients from the host cytosol, *L. monocytogenes* also alters various cellular processes. The affinity of LLO for host cell membranes generally also causes the protein to bind to mitochondria, the endoplasmic reticulum (ER), lysosomes, and the nucleus[219]. Although the mechanism is unknown, LLO was found to cause rounding and fission of mitochondria[228]. LLO also induces ER stress[229] which leads to blocking protein translation and increased protein degradation of ER-sequestered proteins. LLO also breaks the membrane envelope of lysosomes causing the release of oxidative agents

into the host cytosol[219]. Lastly, LLO can cause DNA damage in the nucleus by altering histone modifications and inducing the degradation of the human telomerase reverse transcriptase [230]. To exacerbate this, *L. monocytogenes* also affects post-translational modification systems that control oxidative stress responses. *L. monocytogenes* affects the tagging of proteins with small ubiquitin-like modifiers (SUMO) by inducing the degradation of SUMO-conjugating protein Ubc9[231]. This signalling is crucial for cytokine production and cellular responses to pathogenic toxins.

In summary, *L. monocytogenes* causes a variety of cellular stresses in infected cells. Together with the inflammatory responses during infection, *L. monocytogenes* spread causes deleterious damage to colonized organs.

1.6. *Salmonella enterica* serovar Typhimurium

The *Salmonella* genus is a group of Gram-negative rod-shaped bacteria that belong to the same *Enterobacteriaceae* family as *E. coli*. In this genus, there are two main species, *Salmonella enterica* (*S. enterica*) and *Salmonella bongori,* which survive primarily within warm-blooded and cold-blooded vertebrates respectively[232]. Focusing on the 2557 strains (or serovars) of *S. enterica*, only the Typhi, Paratyphi, Typhimurium and Enteritidis serovars cause disease in humans, usually through the ingestion of contaminated food containing at least 50,000 bacteria[233]. *S. enterica* serovar Typhi and *S. enterica* serovar Paratyphi cause typhoid fever which is brought on by inflammatory symptoms from bacterial spread[234]. Severe damage to the lungs, liver, spleen and brain cause mortality rates of up to 20%. In contrast, the more clinically common serovars, *S. enterica* serovar Typhimurium (*S.* Typhimurium) in North America and Oceania and *S. enterica* serovar Enteritidis (*S.* Enteritidis) in other parts of the world, cause inflammatory diarrhea[235,236]. As diagnosis is difficult to differentiate from other diarrheagenic bacterial pathogens, those who are immunocompromised, especially children, suffer the most and poor treatment leads to mortality rates of up to 24% in developing countries[233].

S. Typhimurium infections are similar to EPEC and *L. monocytogenes* wherein colonization occurs in the intestines[233]. *S.* Typhimurium also needs to evade the host inflammatory response, and thus, the bacteria invade the host cells to survive. *S.* Typhimurium can invade the intestinal epithelia by secreting bacterial effectors into the host cytosol and that causes actin rearrangements at the host membrane forming

membranous ruffles[87]. These ruffles engulf the bacteria and the microbes reside in vacuoles called the *Salmonella*-containing vacuoles (SCVs) where they can manipulate host processes for nutrient acquisition and replication[237]. Phagocytic cells can also use general phagocytosis to internalize *S.* Typhimurium, but upon internalization, *S.* Typhimurium employs specific bacterial effectors to inhibit their neutralization[238]. The intracellular life of the bacteria eventually ends with dissemination to the surrounding tissue upon rupture of the host cell[233]. If the infection cannot be controlled by the host immune system, the eventual spread to the blood and other organs will cause more severe symptoms.

1.6.1. Internalization into intestinal epithelial cells

Upon arriving into the intestinal lumen, *S.* Typhimurium attaches to the host epithelial cell by using strand-like surface molecules called adhesive fimbrae[239]. As the bacteria approaches the host cell membrane, the bacteria generate a similar T3SS to EPEC[240], and then delivers its own concoction of bacterial protein effectors into the host cytosol (Fig. 1.5). To induce membrane ruffling, the bacterial proteins SopB, SopE, and SopE2 activate the host Rho-associated proteins such as RhoG, Rac1 and Cdc42[241,242]. These Rho-associated proteins control the signalling mechanisms for actin rearrangement and as a result, this creates plasma membrane-encased actin-rich ruffles[243]. SopE and SopE2 activation of Rac1 and Cdc42 are sufficient for the formation of these ruffles[241] while SopB supplements actin rearrangement by enhancing upstream phosphoinositidylphosphate-based activation of RhoG and Cdc42[242]. The absence of any one of these effectors does not diminish actin rearrangement at the host membrane. Rather, mutating all three are required to prevent membrane ruffling[244]. Another bacterial protein effector SipA then causes the stabilization of actin filaments formed near the bacterial attachment point[245]. SipA is thought to target the host actin stabilizing protein plastin[246] and this improves the stability of actin filaments during the membrane ruffle-based internalization of *S.* Typhimurium[243]. Although *sipA* mutants can still induce membrane ruffling, their internalization is attenuated[247]. Together, SopB, SopE, SopE2, and SipA work in concert to allow the internalization of the bacteria into SCVs.

Closure of the SCV is dependent on SopB regulation of actin around the internalization site. As the SCV matures, SopB still regulates phosphoinositidylphosphate-based signaling and prevents the fusion of the SCV with

lysosomes[242]. At this point, S. Typhimurium generates a secondary T3SS that secretes another combination of bacterial effectors that govern the acquisition of nutrients and the endurance of the SCV within the host cell.

1.6.2. Disease progression

As *S.* Typhimurium replicates within its host, it further recruits actin and microtubule components to generate vacuole-associated actin polymerization (VAP)[248] and microtubule-based *Salmonella*-induced filaments (SIFs) around the SCV[237,249]. In addition to enhancing nutrient acquisition, VAP formation and SIFs inhibit the fusion of the SCV with lysosomes or the Golgi apparatus[250]. This allows the bacteria to proliferate within its host. After proliferation, the bacteria induce cell death through multiple mechanisms. The secreted effector SpvB, through unknown mechanisms, has been shown to induce cell death in two epithelial cell lines[251]. Another secreted effector SlrP has been shown to interact with thioredoxin-1 and a heat shock protein ERdj3 to initiate apoptosis in epithelial cells[252]. Rupturing of the host cell after induced cell death allows the bacteria to disseminate within the intestines and to other organs[251,252].

Intestinal barrier integrity is also lost due to the effect of actin rearrangement on cellular junctions, the programmed cell death of infected cells, and the consequences of the inflammatory response. Aside from causing actin rearrangement at the bacterial attachment site, SopB, SopE, SopE2 and SipA contribute to overall actin rearrangement within the cell. In turn, this affects the localization of tight junction proteins and consequently, the ion-gating integrity of the epithelia[253]. Also, the previously mentioned induced cell death caused by proliferating intracellular bacteria also compromises the epithelia[251]. Lastly, the inflammatory response caused by *S.* Typhimurium can also exacerbate the symptoms. The recruitment of neutrophils induces leakiness of the intestinal epithelia causing a flux of chloride ions into the intestinal lumen[254]. Together, these events cause massive damage to the homeostasis of the host intestines.

1.7. *Klebsiella pneumoniae*

The *Klebsiella* genus also consists of Gram-negative rod-shape bacteria from the *Enterobacteriaceae* family. Many of the *Klebsiella* species are found in soil environments and are natural members of the mammalian gastrointestinal microbiome[255]. As such,

many humans are carriers of various strains of *Klebsiella* species. Pathogenicity is typically associated with the *Klebsiella pneumoniae* (*K. pneumoniae*) species which consist of *K. pneumoniae* subspecies *pneumoniae*, *K. pneumoniae* subspecies *ozaenae*, and *K. pneumoniae* subspecies *rhinoscleromatis*[255]. Human infections with *Klebsiella oxytoca* have also been reported, but *K. pneumoniae* are most prevalent from both community- and hospital-acquired infections[256].

1.7.1. Prevalence of infection

The categorization of *K. pneumoniae* strains are based primarily on the expression of the capsular polysaccharide. To date, the most virulent of these strains are the K1 and K2 strains which express excessive amounts of capsular polysaccharide[257]. Culturing of these strains results in biofilm-forming mucoid-like colony forming units and this has given these strains the unique characteristic of being hypermucoviscous[258,259]. Since there has been a correlation between virulence and capsule expression, the K1 and K2 strains have also been described as hypervirulent strains of *K. pneumoniae*[260]. Community-acquired infections with these bacteria typically manifest as urinary tract infections, pneumonia, endophthalmitis, and/or liver abscesses in both immunocompetent and immunocompromised individuals[256]. Notably, infections with these hypervirulent strains have been linked more with Asian populations as these populations have a higher intestinal carriage rate as compared to people from other countries[257].

A growing concern is the spread of hospital-acquired hypervirulent *K. pneumoniae* infections. Because these bacteria can form biofilms and capsular expression increases the bacterial survival in environments with lower water activity[255], contamination of medical equipment has become a significant issue in the hospital setting[260]. In the United States, *Klebsiella spp*. have become the third most common bacterial pathogen in infections associated with central lines, catheters, ventilators, and surgical equipment[256,261]. The resulting symptoms include bacteremia, pneumonia, and inflammation at the surgical incision site[259]. Unfortunately, diagnosis and identification of *K. pneumoniae* can be difficult as most symptoms are similar to other common hospital-acquired bacterial infections. If left untreated, *K. pneumoniae* can spread throughout the body including the brain and consequently, mortality rates can reach up to 44%[262].

1.7.2. Pathogenesis in host cells

Aside from the clinical symptoms of the infection, the life cycle and cellular mechanism of *K. pneumoniae* is still poorly understood. *In vivo* mouse studies focused on correlating capsular expression with survival from the host immune response[263,264]. Consequently, infections of cultured macrophages showed that *K. pneumoniae* prevents phagosome maturation and induces programmed cell death to evade the host immune response[265]. Still, the interactions with epithelial cells need further study. Cell culture models have shown that *K. pneumoniae* can invade bladder epithelial cells[266] whereas invasion rates in intestinal cells are minimal compared to a known invading pathogen such as *Salmonella typhi*[267]. Aside from studying invasion rates, only one study examined the subcellular alterations that *K. pneumoniae* induces in lung epithelial cells[268]. In this study, *K. pneumoniae* caused cell rounding as seen in the arrangement of the actin cytoskeleton and cell cytotoxicity was also observed[268]. Again, this cytotoxicity was correlated to capsular polysaccharide expression of *K. pneumoniae* suggesting that capsular polysaccharide is crucial for bacterial pathogenicity.

Instead of further examining the host cells during infection, researchers have focused on identifying virulence factors of *K. pneumoniae* (Fig. 1.6). As mentioned previously, extensive work has shown that the highly virulent strains of *K. pneumoniae* express excessive amounts of capsular polysaccharide[257,263,268,269]. This aids in the masking of the highly immunogenic lipopolysaccharide on the bacterial surface. Loss of capsule polysaccharide makes *K. pneumoniae* more susceptible to C3 complement-mediated phagocytosis and lung clearance[270,271]. Recent studies have shown that in addition to the masking effect of the capsular polysaccharide, *K. pneumoniae* actively modifies the structure of its lipopolysaccharide upon entering the lungs[272]. Moreover, *K. pneumoniae* also possesses outer membrane proteins such as OmpK35 and OmpK36 that limit the flux of antimicrobials into the bacterial cytoplasm[273]. As a result, *K. pneumoniae* can evade the host immune responses using these mechanisms. *K. pneumoniae* also utilizes its type II secretion system and type VI secretion system, however their roles in pathogenicity have only been recently studied[274]. Furthermore, the roles of many proteins on the outer membrane of *K. pneumoniae* are currently being explored[275] while unique inner membrane proteins such as ytfL have yet to be studied in the context of *K. pneumoniae* infection.

1.7.3. Disease treatment

Previously, treatment of most bacterial infections involved broad spectrum antibiotics which target a wide variety of bacterial pathogens. Over the years, many bacteria have developed resistance to these antibiotics, and specifically, *K. pneumoniae* have developed β-lactamases and carbapenemases[276,277]. These proteins can cleave the β-lactam ring[276] which is the core structure of common antibiotics such as penicillin, cephalosporins such as ampicillin, and carbapenems. As a result, special attention has been given to *K. pneumoniae* as multi-drug resistant hypervirulent strains have become rampant in the hospital setting. Nowadays, treatment of *K. pneumoniae* infections use fluoroquinolones such as ciprofloxacin[257] and these are combined with aminoglycosides to combat aggressive spread of bacteria in severe cases[276]. Extreme cases of multi-drug resistant bacteria can also be treated with the polymyxin, also known as colistin[278].

1.8. Rationale and Research Hypothesis

Enteropathogenic *Escherichia coli*, *Listeria monocytogenes*, and *Salmonella enterica* serovar Typhimurium have all been shown to generate actin-rich structures that are crucial to their respective infections. Although the minimal components required to generate these structures have been elucidated, our understanding of the mechanism that regulate these structures are unclear. Previously, our laboratory conducted a mass-spectrometry based analysis of the protein composition of EPEC-induced pedestals. Because several proteins have yet to be associated with bacteria-induced actin structures, **I hypothesize that there are novel proteins from the mass spectrometry analysis that are important for the formation of EPEC pedestals, *L. monocytogenes* comet tails, and *S.* Typhimurium membrane ruffles**. I aim to elucidate proteins that have novel functions in general actin dynamics.

In parallel to the actin rearrangement induced by EPEC, *L. monocytogenes* and *S.* Typhimurium, recent work in our laboratory has discovered that the microtubules of an entire monolayer of lung epithelial cells are disassembled during *Klebsiella pneumoniae* infections. This phenotype is preceded by microtubule severing events that are induced even when there were no bacteria attached on the host cells. Moreover, infection with known avirulent mutants of *K. pneumoniae* still induced the phenotype. Because none of the known *K. pneumoniae* virulence factors are responsible for the

microtubule disassembly phenotype, **I hypothesize that *K. pneumoniae* induces microtubule disassembly through a novel mechanism and this ultimately triggers host cell microtubule severing enzymes**. Through my research, I aim to identify novel bacterially-derived factor(s) that ultimately cause microtubule disassembly.

1.9. Figures

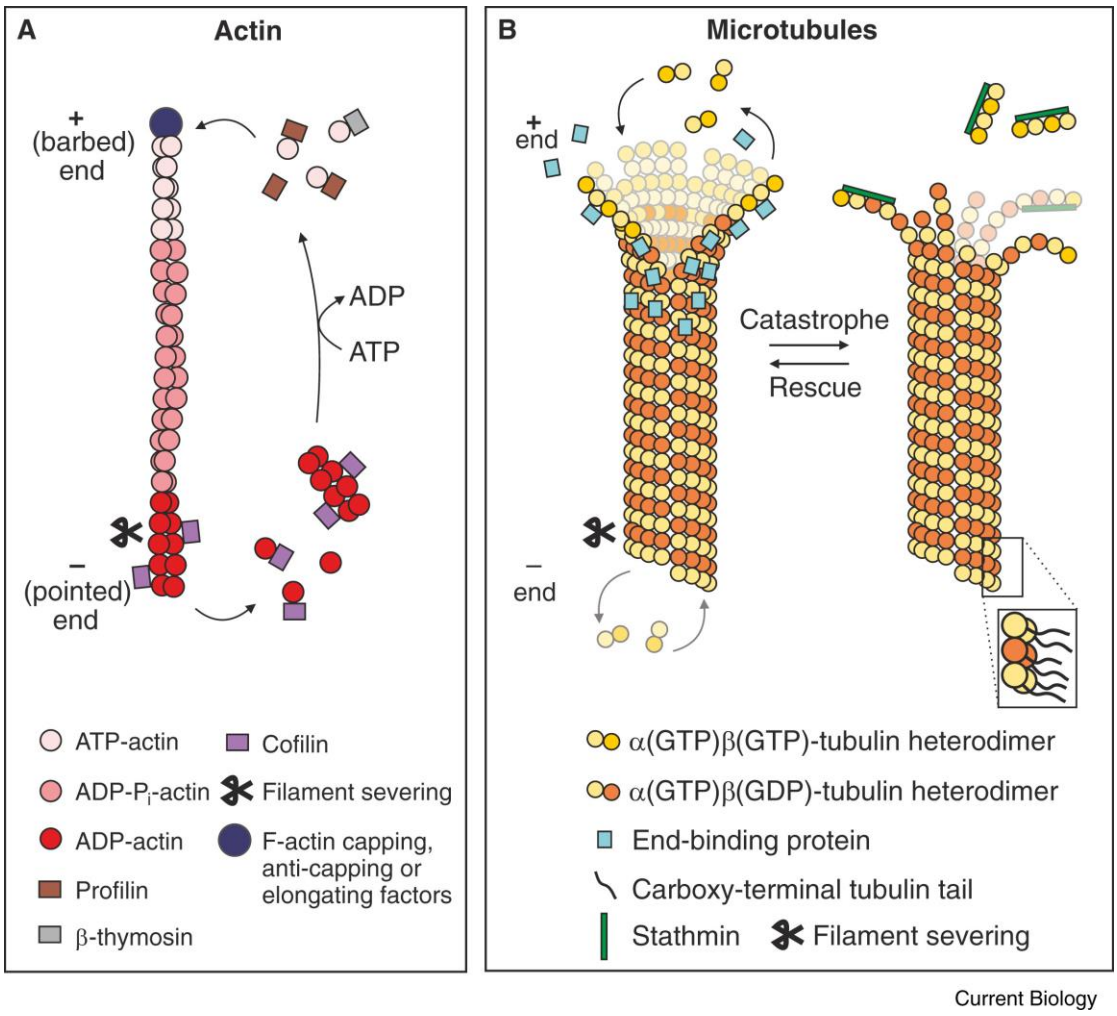

Figure 1.1: Maintenance of actin filaments and microtubules.
(A) ATP-actin monomers are added onto the barbed end of the actin filament while severing of monomers occurs at the pointed end. (B) α/β-heterodimers bind to the plus end of the microtubule. Catastrophe occurs when these heterodimers dissociate from either end of the microtubule tubule. Reprinted by permission from Elsevier Ltd: Current Biology [279], copyright 2015.

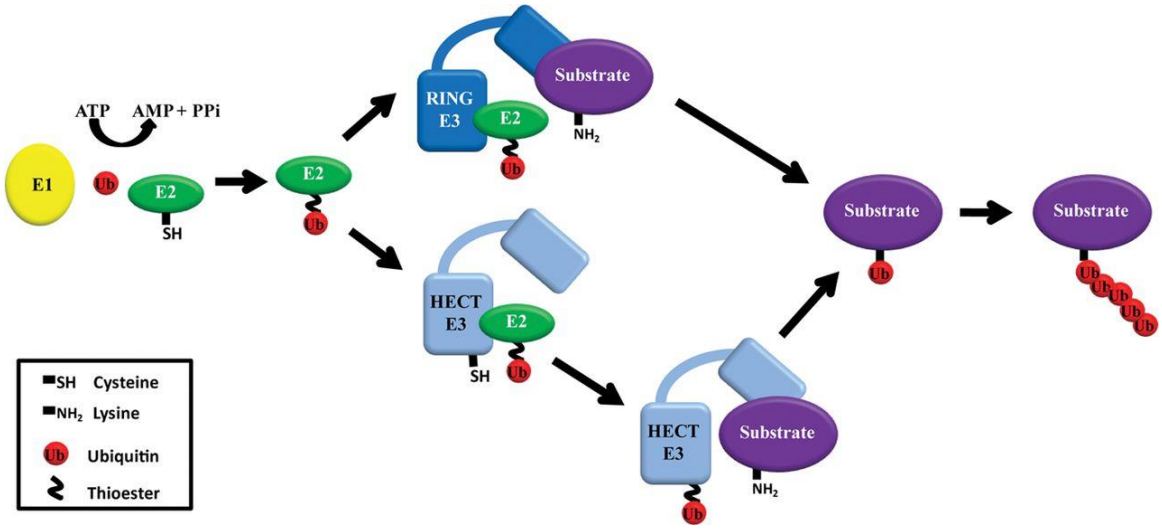

Figure 1.2: Mechanism of ubiquitylation.
Ubiquitylation is initiated by the transfer of a ubiquitin monomer from the cytosol to a target substrate. The ubiquitin monomer is activated by the E1 enzyme and then transferred to the E2 enzyme. The ubiquitin-carrying E2 enzyme binds to either a RING-type or HECT-type E3 enzyme. The E3 enzyme catalyzes the transfer of the ubiquitin monomer to its specific substrate. Repeating this mechanism produces a polyubiquitylated substrate. Reuse permission granted by Portland Press: Biochemical Journal [280], copyright 2011.

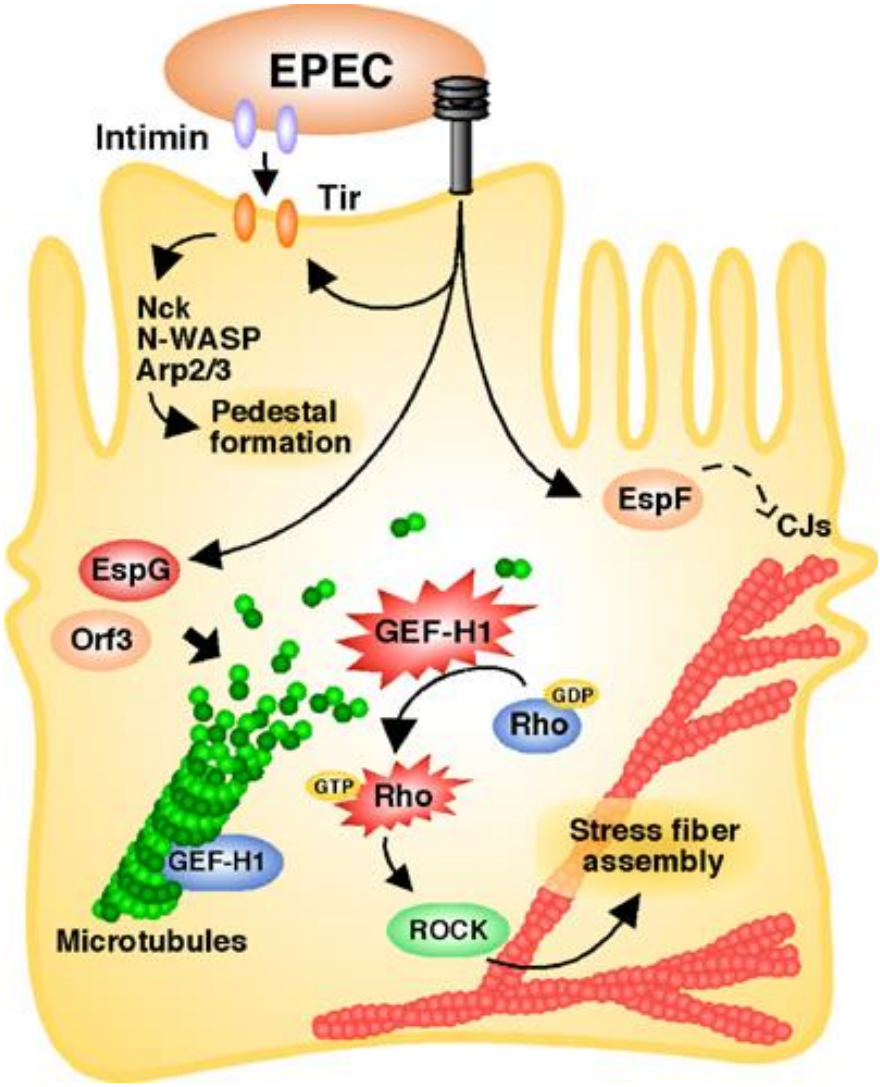

Figure 1.3: Cytoskeletal rearrangements of EPEC during its infection
EPEC secretes Tir to initiate pedestal formation through a N-WASP and Arp2/3-dependent actin polymerization. EPEC also secretes other effectors such as EspF and EspG to rearrange the cytoskeleton of its host. Reprinted by permission from John Wiley and Sons: The EMBO Journal [281], copyright 2004.

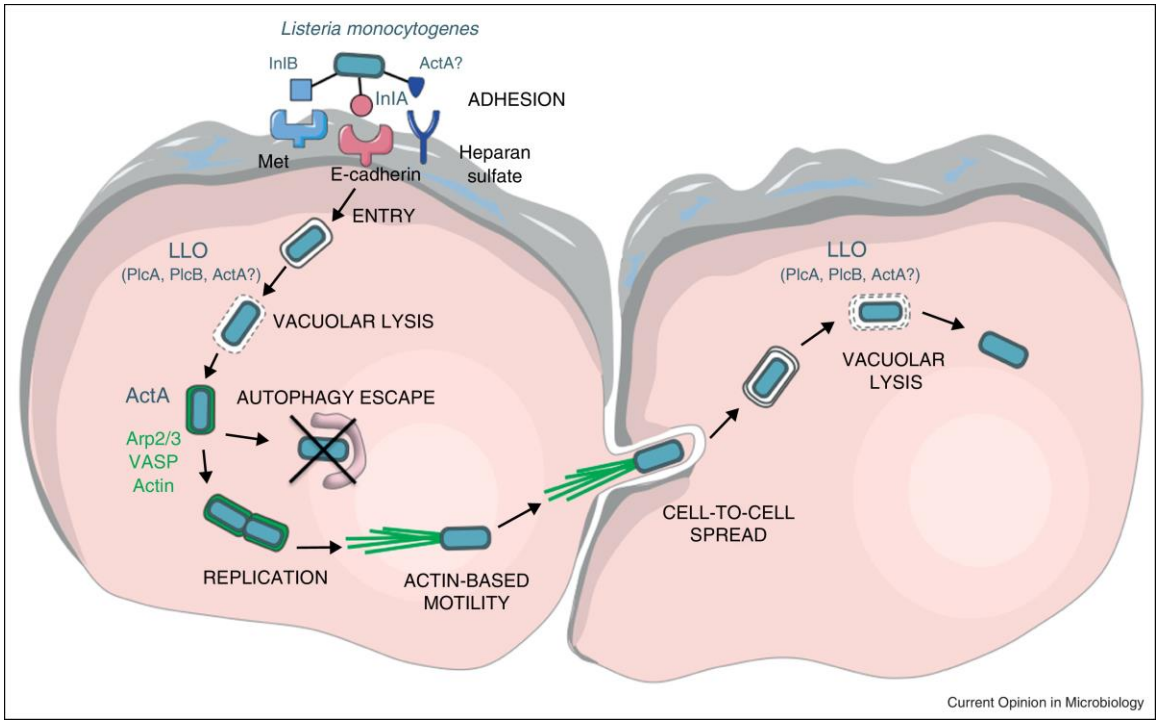

Figure 1.4: Intracellular life cycle of *Listeria monocytogenes* within its host. Internalization occurs through receptor-mediated endocytosis. Upon internalization into the host, *L. monocytogenes* utilizes its LLO protein effector to escape into the cytosol. After escaping into the cytosol, the bacterium uses its surface protein ActA to recruit the host Arp2/3 complex and actin polymerizing machinery. Extensive polymerization of actin filaments generates a comet tail for propulsion within its host or onto neighboring cells. Reprinted by permission from Elsevier Ltd: Current Opinion in Microbiology [282], copyright 2013.

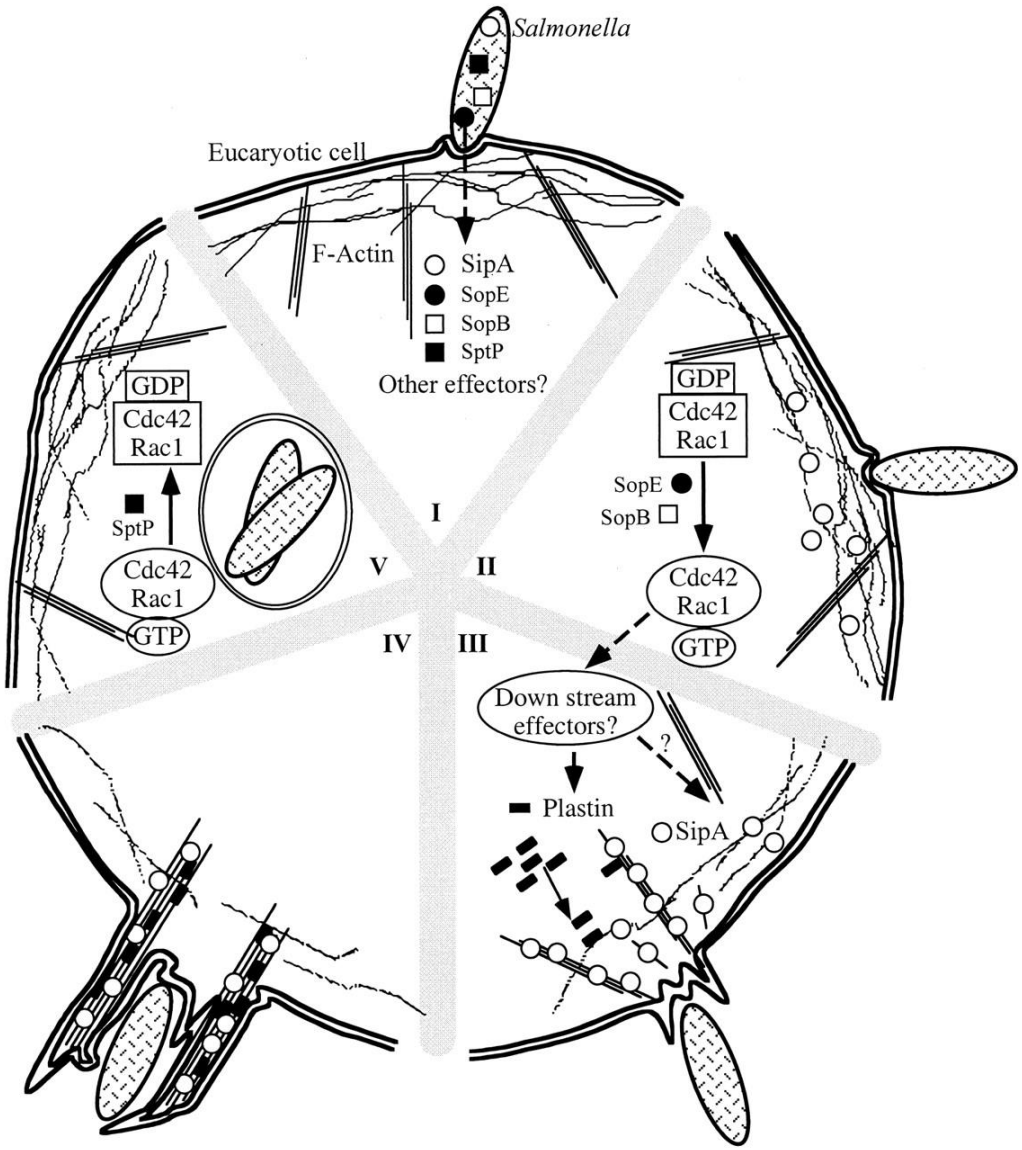

Figure 1.5: *S.* Typhimurium internalization into its host.
(I) Bacterial effectors are secreted into the host. (II). SopB, SopE and SopE2 cause actin rearrangements along the host cell surface. (III) SipA enhances the polymerization and stability of the actin filaments generated. (IV) The bacterium is internalized through the actin-rich membrane ruffles. (V) The bacterium resides in a *Salmonella*-containing vacuole to acquire nutrients and replicate. Reuse permission granted by the National Academy of Sciences of the United States of America [243] copyright 2000 National Academy of Sciences.

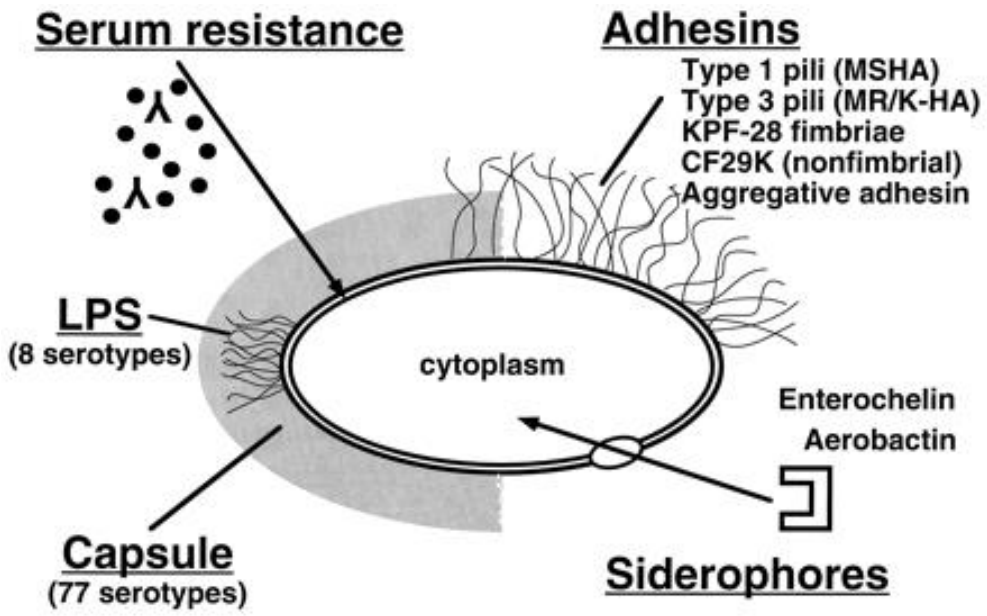

Figure 1.6: Known bacterial effectors of *Klebsiella pneumoniae*.
Most of the research on *K. pneumoniae* have focused on the adhesive fimbrae, lipopolysaccharide (LPS), siderophores, and the capsule polysaccharide. These bacterial effectors have been correlated with the ability of *K. pneumoniae* to colonize its host. Reprinted by permission from the American Society of Microbiology: Clinical Microbiology Reviews [283], copyright 1998.

Chapter 2.

Calponins Are Recruited to Actin-rich Structures Generated by Pathogenic *E. coli*, *Listeria* and *Salmonella*

The content of this chapter is in revision for publication.

Chua MD, Walker BD, Jin JP, Guttman JA. (2017). Calponins Are Recruited to Actin-rich Structures Generated by Pathogenic *E. coli*, *Listeria* and *Salmonella*. *Anat Rec* (Hoboken). (*In revision*).

MDC designed the project, performed and supervised the experiments, analysed the data and prepared the manuscript. BDW performed experiments and reviewed the manuscript. JPJ generated the antibodies used for the experiments and reviewed the manuscript. JAG directed the project by contributing to the project design, data analysis and the writing of the manuscript.

2.1. Abstract

The ingestion of enteropathogenic *Escherichia coli* (EPEC), *Listeria monocytogenes* or *Salmonella enterica* serovar Typhimurium leads to their colonization of the intestinal lumen, which ultimately causes an array of ailments ranging from diarrhea to bacteremia. Once in the intestines, these microbes generate various actin-rich structures to attach, invade or move within the host intestinal epithelial cells. Although an assortment of actin-associated proteins has been identified to varying degrees at these structures, the localization of many actin stabilizing proteins have yet to be analyzed. Here, we examined the recruitment of the actin-associated proteins, calponin 1 and 2 at EPEC pedestals, *L. monocytogenes* actin clouds, comet tails and listeriopods, and *S.* Typhimurium membrane ruffles. In other systems, calponins are known to bind to and stabilize actin filaments. In EPEC pedestals, calponin 1 was recruited uniformly throughout the structures while calponin 2 was enriched at the apical tip. During *L. monocytogenes* infections, calponin 1 was found through all the actin-rich structures generated by the bacteria, while calponin 2 was only present within actin-rich structures formed by *L. monocytogenes* near the host cell membrane. Finally, both calponins were found within *S.* Typhimurium-generated membrane ruffles. Taken together, we have shown that although calponin 1 is recruited to actin-rich structures formed by the three bacteria, calponin 2 is specifically recruited to only membrane-bound actin-rich structures formed by the bacteria. Thus, our findings suggest that calponin 2 is a novel marker for membrane-bound actin structures formed by pathogenic bacteria.

2.2. Introduction

Enteropathogenic *Escherichia coli* (EPEC), *Listeria monocytogenes* (*L. monocytogenes*), and *Salmonella enterica* serovar Typhimurium (*S.* Typhimurium) are food-borne pathogens that cause a wide variety of symptoms from mild diarrhea to death [179,180,213,284–286]. Although these bacteria use different strategies to colonize their host's intestines, they all usurp the actin cytoskeleton of their hosts[87,287–289].

During EPEC infections, the bacteria remain extracellular. The microbes attach onto their host cell and secrete protein effectors through a needle-like type three-secretion system (T3SS)[180,290]. Among the first set of effectors secreted into the host cell

cytosol is the translocated intimin receptor (Tir)[291]. Tir is inserted into the host cell membrane and it has the dual function of engaging in the docking of the bacteria to the host cell surface while simultaneously recruiting actin polymerizing proteins such as the Neural Wiskott-Aldrich Syndrome protein (N-WASp) and the actin related protein Arp2/3 complex to the site of bacterial attachment[193,195,287,292]. The resulting structures form protrusions (pedestals) consisting of a dendritic actin-rich core surrounded by the host cell plasma membrane beneath the attached bacteria[194,293].

L. monocytogenes invade their host cells through clathrin-mediated actin-dependent endocytosis[216–218,294]. Once inside their host cells these microbes rapidly escape from their endocytic vacuoles and generate a variety of actin structures during their infectious cycle. Key to their actin-recruitment is the bacterial surface protein ActA [220,295]. Using this effector, short actin filaments are initially recruited around each bacterium forming an “actin cloud.” These actin filaments eventually elongate and polarize to one end of the bacterium to generate an actin-rich comet tail[227] that propels each microbe within the host cell. These comet tails are also used for bacterial translocation from cell-to-cell within membrane structures called listeriopods[92,296,297].

S. Typhimurium also invades its host, but the mechanism of entry is dependent on utilizing its T3SS to inject several crucial protein effectors SopB, SopE and SopE2 into the host cytosol[87,241–243]. SopB, SopE, and SopE2 target the activation of host Rho GTPases that regulate the reorganization of actin at the bacterial attachment site[241,244]. Another effector, SipA, is also used in the internalization event to elongate the actin filaments at the region of *S*. Typhimurium invasion[245,247]. Through this concerted targeting of actin regulating proteins, *S.* Typhimurium generated membrane ruffles that eventually engulf the bacteria into newly formed host vacuoles[87,243].

In regulating the actin cytoskeleton, a subset of actin-associated proteins is dedicated to binding and stabilizing actin filaments. Many of these actin-stabilizing proteins such as plastins and formins, act as bundling agents that protect actin filaments from depolymerization[15,76,223]. As a result, plastins and formins have both played crucial roles in stabilizing the actin-rich structures formed by EPEC, *L. monocytogenes*, and *S.* Typhimurium[226,246,298]. The identification of actin-associated proteins at these structures is continuously expanding and through a mass spectrometry-based analysis of concentrated EPEC pedestals our laboratory identified calponin[299]. Because calponins

promote the stability of the actin cytoskeleton[63,300], we investigated whether the two structurally similar calponins, calponin 1 and calponin 2, were recruited to EPEC, *L. monocytogenes*, and *S.* Typhimurium actin-rich structures. Through the immunolocalization of these proteins, we found that calponin 1 was recruited within the entire structure of the EPEC pedestals while calponin 2 was enriched at the apical tip of the pedestals. In *L. monocytogenes* infections, calponin 1 immunolocalized to actin clouds, comet tails and listeriopods while calponin 2 was found exclusively when *L. monocytogenes* formed actin-rich structures near the host cell membrane. Lastly, both calponin 1 and 2 uniformly colocalized with the actin filaments in *S.* Typhimurium membrane ruffles. Taken together, our findings show that calponin 1 ubiquitously decorates all actin-rich structures formed by these three bacterial pathogens, while calponin 2 is only present at membrane-associated actin-based bacterial structures, suggesting that calponin 2 can be used as a novel marker of the membrane-bound phases of these bacterial infections.

2.3. Materials and Methods

2.3.1. Cell growth and maintenance

Caco2 colon epithelial cells (ATCC, Cat. No HTB-37) were grown in the well of tissue-culture plates using GE HyClone Dulbecco's Modified Eagle Medium (DMEM) with 10% Gibco Fetal Bovine Serum (FBS) and 1% GE HyClone non-essential amino acids (NEAA). The cells were incubated at 37°C with 5% CO_2.

2.3.2. Bacterial growth

Enteropathogenic *Escherichia coli* (wild-type EPEC [strain E2348/69], EPEC [strain JPN15] (a naturally occurring plasmid cured strain that lacks the bundle forming pilus, bfp), JPN15 Δ*escN*, and JPN15 Δ*tir*[190,192] and *Salmonella enterica* serovar Typhimurium (SL1344, Δ*sipA* and Δ*sopB/E/E2*)[253,301,302] were cultured in Luria-Bertani (LB) broth while *Listeria monocytogenes* (EGD600 and Δ*actA*)[303,304] were cultured in Brain Heart Infusion (BHI) broth. Bacterial stocks were streaked on agar plates and grown at 37°C for approximately 24 hours. Single colonies were then grown in their respective broth at 37°C for 16 hours. EPEC cultures were incubated as standing

cultures while *S*. Typhimurium and *L. monocytogenes* were incubated as shaking cultures.

2.3.3. EPEC infections

Caco2 cells were seeded onto coverslips in 24 well plates at least 5 days prior to infection. On the day of the infection, 1 mL of fresh DMEM with 10% FBS and 1% NEAA were added to the Caco2 cells. Then, the overnight cultures of all four EPEC strains were diluted 100-fold in LB broth. Next, 2 µL of the diluted bacterial stock was added to the host cells. The infection was incubated at 37°C for 3 hours and then, to remove unattached bacteria, the media was replaced with 1 mL of fresh DMEM with 10% FBS and 1% NEAA. Afterwards, the infection was incubated for another 3 hours for a total of 6 hours of infection time. The cells were then fixed for immunofluorescence staining or lysed for immunoblotting.

2.3.4. *L. monocytogenes* infections

Similar to EPEC infections, Caco2 cells were grown on coverslips in 24 well plates. On the day of the infection, 1 mL of the overnight cultures of EGD600 or Δ*actA* was diluted in 9 mL of BHI broth and grown for at least 2 hours. When the optical density (OD_{600}) of the bacterial culture reached approximately 1.00, 1 mL of each bacterial stock was pelleted and washed repeatedly with warm phosphate buffered saline (PBS). Following the last PBS wash, the bacteria were resuspended in 1 mL warm serum-free DMEM and then diluted 10-fold. Next, the Caco2 cells were washed at least 6 times with serum-free DMEM and then, 1 mL of serum-free DMEM was added to each well. 30 µL of the diluted bacterial stock was then added to the Caco2 cells and then the well plate was spun at 215 g for 2 minutes. The cells were incubated at 37°C for 2 hours and then the cells were washed three times with warm PBS. Afterwards, fresh DMEM with 10% FBS, 1% NEAA, and 50 µg/mL gentamicin was added to kill extracellular bacteria. The infection was incubated at 37°C for another 4 hours to have a total infection time of 6 hours. After the infections, the cells were fixed for immunofluorescence staining or lysed for immunoblotting.

2.3.5. *S.* Typhimurium infections

Similar to the other bacterial infections, Caco2 cells were seeded onto coverslips in 24 well plates. On the day of the infection, 300 µL of each overnight culture of *S.* Typhimurium was subcultured in 10 mL of LB broth. After 3 hours, bacteria were pelleted from 1 mL of each stock and resuspended in 1 mL serum-free DMEM. Next, the Caco2 cells were washed repeatedly with serum-free DMEM and then 1 mL of serum-free DMEM was added to each well. 7.5 µL of the resuspended bacteria was then added on the cells and the well plate was centrifuged at 215 g for 2 minutes. The infection was then incubated at 37°C for 20 minutes before the cells were fixed for immunofluorescence staining or lysed for immunoblotting.

2.3.6. Immunolocalization of calponin in infected cells

After the infections the cells were washed three times with warm PBS and then fixed in warm 3% paraformaldehyde diluted in PBS at room temperature for 15 minutes. Following the fixations, the cell membranes were permeabilized using either -20°C acetone or room temperature PBS containing 0.2% Triton-X100. To permeabilize cells with acetone, the coverslips were washed twice with PBS, submerged in -20°C acetone for 8 minutes, and then air-dried for 10 minutes. To permeabilize cells with Triton-X100, the coverslips were washed with PBS once, incubated with PBS with 0.2% Triton-X100 for 5 minutes, and then washed three times with PBS. After permeabilization, the coverslips were blocked using 5% normal goat serum (NGS) in PBS with 0.05% Tween-20 and 0.1% bovine serum albumin (TPBS/BSA). Afterwards, the coverslips were incubated with calponin-specific antibodies [300,305] at 4°C overnight. The CP1 antibody was generated using purified calponin 1 from chicken gizzard tissue and had been shown to detect human calponin 1 expressed from *E. coli*,[306] while the 1D11 antibody was generated using purified calponin 2 from mouse tissue [306] and had been shown to detect calponin 2 in mouse skin fibroblasts [300]. On the day prior to incubating the coverslips, the antibodies were incubated with fixed bacteria to remove non-specific cross-reacting immunoglobulins. To immunolocalize calponin 1, the coverslips were incubated with mouse monoclonal antibody CP1 diluted 1.46 µg/µL in TPBS/BSA. To immunolocalize calponin 2, the coverslips were incubated with mouse monoclonal antibody 1D11 diluted 0.90 µg/µL in TPBS/BSA. Separate coverslips were incubated with normal mouse IgG prepared at equivalent concentrations as the CP1 and 1D11

antibodies respectively. The next day, the coverslips were washed three times with TPBS/BSA to remove excess antibodies and then incubated with Alexa 488-conjugated goat anti-mouse secondary antibody (Invitrogen, Cat. No A11001) diluted 2.00 µg/µL in TPBS/BSA at room temperature for 2 hours. Afterwards, excess antibodies were removed through three TPBS/BSA washes, then the coverslips were incubated with Alexa 594-conjugated phalloidin (Molecular Probes, Cat. No A12381) at room temperature for 15 minutes. Excess phalloidin was washed using TPBS/BSA and then the coverslips were mounted on Prolong Diamond Antifade with DAPI (Molecular Probes, Cat. No P36962). Fluorescence microscopy analysis was conducted using a Leica DMI4000B inverted microscope with a Hamamatsu Orca R2 CCD camera.

2.3.7. Immunoblotting of calponin in infected cells

After the infections, the cells were washed three times with warm PBS and then lysed using RIPA lysis buffer (150 mM sodium chloride, 50 mM Tris pH 7.5, 5 mM ethylenediaminetetraacetic acid (EDTA), 1% Nonidet P-40, 1% deoxychloic acid, 0.1% sodium dodecyl sulfate) supplemented with cOmplete Mini protease inhibitors (Roche, Cat. No 11836153001). Afterwards, protein lysates from uninfected and infected samples were equalized by quantifying protein concentrations using a bincinchoninic acid assay. The normalized protein samples were then loaded onto a 10% sodium dodecyl sulfate polyacrylamide gel electrophoresis (SDS-PAGE) gel. After electrophoresis, the resolved proteins were transferred onto a nitrocellulose membrane and then blocked using 4% BLOTTO in Tris-buffered saline with 0.1% Tween-20 (TBST). The membranes were then incubated with monoclonal antibody CP1 (0.074 µg/µL) or 1D11 (0.046 µg/µL) diluted in TBST with 1% BSA (TBST/BSA) at 4°C overnight. A separate immunoblot was incubated with normal mouse IgG prepared to the same concentration of the 1D11 antibody. Next, the membranes were washed successively with TBST before incubating with horseradish peroxidase-conjugated goat anti-mouse secondary antibody (Invitrogen, Cat. No G21040) diluted 0.0002 µg/µL in TBST/BSA. The membranes were incubated in the secondary antibodies at room temperature for 2 hours and then washed successively with TBST and TBS. Chemiluminescence was detected using the Millipore Luminata Crescendo HRP substrate and the blots were imaged using a Fujifilm LAS4000 chemiluminescent scanner. To ensure that the uninfected and infected cell lysates were loaded evenly, the

blots were stripped using a mild stripping buffer (0.2 M glycine, 3.5 mM sodium dodecyl sulfate, 1% Tween-20, pH 2.2), washed repeatedly and then incubated in mouse anti-α-tubulin antibodies (Developmental Studies Hybridoma Bank, Cat. No 12G10) diluted to 0.01 µg/µL in TBST/BSA and HRP-conjugated goat anti-mouse secondary antibody. The blots were then analyzed through chemiluminescence as described above.

2.4. Results

2.4.1. Calponin 1 and 2 are present at EPEC pedestals, with calponin 2 enriched at the apical tip

WT EPEC (strain E2348/69) generate microcolonies and very short pedestals that are difficult to resolve. In contrast, the JPN15 strain, which does not have a functional plasmid within it that is responsible for the formation of bundle forming pili (bfp) does not generate microcolonies and thus forms distinct pedestals that are easily identified. To determine if calponin 1 and/or calponin 2 were recruited to EPEC pedestals, we immunolocalized those proteins in Caco2 human intestinal cells infected with either EPEC strain (Fig. 2.1A). Within the short pedestals formed by wild-type EPEC [strain E2348/69], the calponin 1 antibody detected an enrichment of calponin 1 within EPEC pedestals. Similarly, calponin 2 accumulated at those sites (Fig. 2.1A'). To further examine of the presence of these proteins at EPEC pedestals we examined pedestals formed by EPEC (JPN15). Noticeably, calponin 1 decorated the length of the pedestal (Fig. 2.1B), whereas calponin 2 was enriched at the apical pedestal tips and this accumulation declined towards the pedestal base (Fig. 2.1B').

The recruitment of calponin 1 and calponin 2 beneath the bacteria could be the result of simply bacterial attachment or the actin dynamics within the induced pedestal. To test this, we infected host cells with an JPN15 Δ*escN* mutant, which does not have a functional T3SS and an JPN15 Δ*tir* mutant which does not express functional Tir protein; both of these mutants do not form pedestals. We found that calponin 1, and calponin 2 were not recruited to sites of JPN15 Δ*escN* (Fig. 2.1C, 2.1C') or JPN15 Δ*tir* attachment (Fig. 2.1D, 2.1D'). In addition, normal mouse IgG did not colocalize with the actin-rich pedestal (Fig. 2.1E, 2.1E'). From this, we surmised that calponin accumulation is dependent on the formation of actin pedestals.

2.4.2. Calponin 1 and calponin 2 differed in their recruitment to *L. monocytogenes* actin-rich structures

L. monocytogenes generate three distinct actin-rich structures in the host cell cytosol – the cytoplasmic actin cloud and comet tail, and the membrane-associated listeriopod. Because we found that the calponins had differential recruitment patterns within EPEC pedestals, we examined if calponin 1 and calponin 2 accumulated within actin structures formed by *L. monocytogenes*. Calponin 1 uniformly decorated all three structures formed by *L. monocytogenes* (Fig. 2.2A). In contrast, calponin 2 was not prominent in actin clouds or comet tails that were away from the host cell membrane, but rather calponin 2 decorated actin clouds, comet tails, and listeriopods located near the host cell membrane (Fig. 2.2A'). Thus, calponin 2 recruitment was transient within actin clouds and comet tails, but calponin 2 was enriched in all membrane protruding listeriopods observed. In addition, the Δ*actA* mutant *L. monocytogenes* does not recruit actin and as expected, neither calponin 1 nor calponin 2 were observed around the bacteria (Fig. 2.2B, 2.2B'). Normal mouse IgG were also absent from the actin structures formed by *L. monocytogenes* (Fig. 2.2C, 2.2C'). Taken together, our findings imply that calponin 1 is ubiquitously recruited to all *L. monocytogenes* actin-rich structures, while calponin 2 may be temporally recruited to *L. monocytogenes*-generated actin-structures at the host plasma-membrane.

2.4.3. Both calponins are enriched in *S.* Typhimurium membrane ruffles

Unlike *L. monocytogenes*, *S.* Typhimurium only generates actin-rich structures during the internalization into its host cell. Once *S.* Typhimurium attaches onto its host cell surface, it forces the host membrane to generate large ruffles for its internalization into its host. To determine if the calponins were recruited to *S.* Typhimurium-generated membrane ruffles, we infected Caco2 cells with wildtype *S*. Typhimurium (SL1344 strain). Both calponin 1 and calponin 2 localized with the actin filaments within the ruffles (Fig. 2.3A, 2.3A').

Actin rearrangement caused by *S.* Typhimurium is regulated by several secreted bacterial effectors (SopB, SopE, and SopE2). Another effector, SipA, contributes to the stabilization of membrane ruffles. To determine if calponin 1 and calponin 2 recruitment

in the membrane ruffles were targeted by these effectors, we infected Caco2 cells with Δ*sipA* and Δ*sopB/E/E2* mutant strains of *S.* Typhimurium. Of these mutants, the Δ*sipA* mutant could still induce membrane ruffling. Both calponin 1 and calponin 2 were still prominent in membrane ruffles formed by the Δ*sipA* mutant. (Fig. 2.3B, 2.3B'). The Δ*sopB/E/E2* mutant is unable to generate membrane ruffles and did not recruit calponin 1 nor calponin 2 to the site of bacterial attachment (Fig. 2.3C, 2.3C'). In addition, normal mouse IgG did not label *S.* Typhimurium membrane ruffles (Fig. 2.3D, 2.3D').

2.4.4. Bacterial infection does not alter calponin 2 protein levels

Aside from protein recruitment, bacterial pathogens can also alter the expression levels of protein targets. To determine if there were changes to the protein expression levels of both calponins we immunoblotted infected and uninfected Caco2 lysates then probed them with the Calponin 1 and 2 antibodies. Positive reactivity on Western blots with the anti-calponin 1 antibody was not seen (data not shown). Thus, we were unable to determine if there were any changes in calponin 1 levels. However, we were able to show an unchanged level of expression of calponin 2 for all of the infections (EPEC, *L. monocytogenes* and *S*. Typhimurium) (Fig. 2.4A, 2.4B, 2.4C). Normal mouse IgG did not show prominent bands at the molecular weight of calponin 2 (Fig. 2.4A', 2.4B', 2.4C').

2.5. Discussion

Calponin 1 and calponin 2 are homologous proteins and share many structural similarities and contain similar actin binding domains[58,64]. However, despite these similarities, these two proteins have markedly different functions. Several studies indicate that calponin 1 utilizes both of its actin binding sites, ABS1 and ABS2, in stabilizing actin filaments in stress fibres within the cell[54]. In contrast, the C-terminal tail of calponin 2 has been implicated in inhibiting its ABS2 actin-binding domain, which limits the binding affinity of calponin 2 to stress fibres[62,68]. As a result, the transient stability conferred by calponin 2 is suggested to be crucial for more dynamic actin networks and consequently, the function of calponin 2 has been demonstrated to be vital for cellular processes such as cell motility and cell division[64]. Our study showed different localization patterns for calponin 1 and calponin 2 which allude to different functional roles of these calponin isoforms within the bacterially-generated actin structures.

Because calponin 1 is primarily found in smooth muscle cells, the function of calponin 1 in non-muscle cells is still poorly understood. Previously, *in situ* analysis of calponin 1 localization during actin rearrangement suggested that calponin 1 may confer conformational stability to individual actin filaments[66] and functions to cross-linked actin networks[65]. In addition, *in vitro* studies also showed that calponin 1-saturated actin filaments were more flexible than sub-saturated filaments[66]. In our study, calponin 1 decorated EPEC pedestals, *L. monocytogenes* comet tails and *S*. Typhimurium ruffles to varying degrees. Perhaps, calponin 1 enrichment within these actin-rich structures contributes to the balance required to maintain the flexibility of individual actin filaments and actin networks. Other cytoskeletal actin structures rely on actin binding proteins for filament elasticity[10,108] and these bacteria-generated structures may therefore need the same properties for their functions. During actin-based bead motility (which is used to study *L. monocytogenes* comet tail motility *in vitro*), high concentrations of actin cross-linkers such as α-actinin and fascin can limit bead velocity, but another actin cross-linking protein (filamin) can increase that velocity[307]. From these findings, abundance and selection of actin binding proteins at the structures may dictate the elasticity of the actin arrays. Similarly, the levels of bound calponin 1 may be essential in balancing the necessary conformational stability and flexibility of actin filaments within these bacterially-generated structures.

On the other hand, the enrichment of calponin 2 at EPEC pedestals, *L. monocytogenes* membrane-abutting actin-rich structures, and *S*. Typhimurium membrane ruffles is consistent with several studies that have indicated that calponin 2 is important in actin-rich protrusions at the plasma membrane. Calponin 2 has been shown to stabilize the actin filaments within the protrusions at the leading edge of motile cells [61]. The introduction of calponin 2 in cultured cells lacking endogenous calponin 2 protected actin filaments from cytochalasin B-mediated destabilization[308], while calponin 2 mRNA transcripts and protein levels were abundant within the protrusions at the leading edge of migratory neural crest cells[61]. In another study, calponin 2 enrichment was suggested to be dependent on the mechanical tension exerted on the actin filaments and this enrichment was vital for actin stability[308]. From this, the projection of bacterially-generated actin structures through the plasma membrane could explain the recruitment of calponin 2 at the bacteria-induced actin structures we examined, suggesting that calponin 2 may contribute to the structural stability of bacterial actin-rich structures at the

host cell plasma membrane. Notably, the recruitment of both calponins into *S.* Typhimurium-induced membrane ruffles were independent of sipA secretion and this suggests that the localization of these calponins into actin-rich structures at the plasma membrane does not require bacterial induction. Further studies can focus on the signalling cascade that recruits calponin 1 and calponin 2 during these membrane-bound actin structures.

In summary, our study revealed that calponin 1 and calponin 2 are actin-associated proteins that are newly identified in the actin-rich structures formed by EPEC, *L. monocytogenes*, and *S*. Typhimurium. In addition, our findings propose that calponin 2 may be a novel marker for the actin-rich structures generated by these bacteria at the host cell plasma membrane.

2.6. Figures

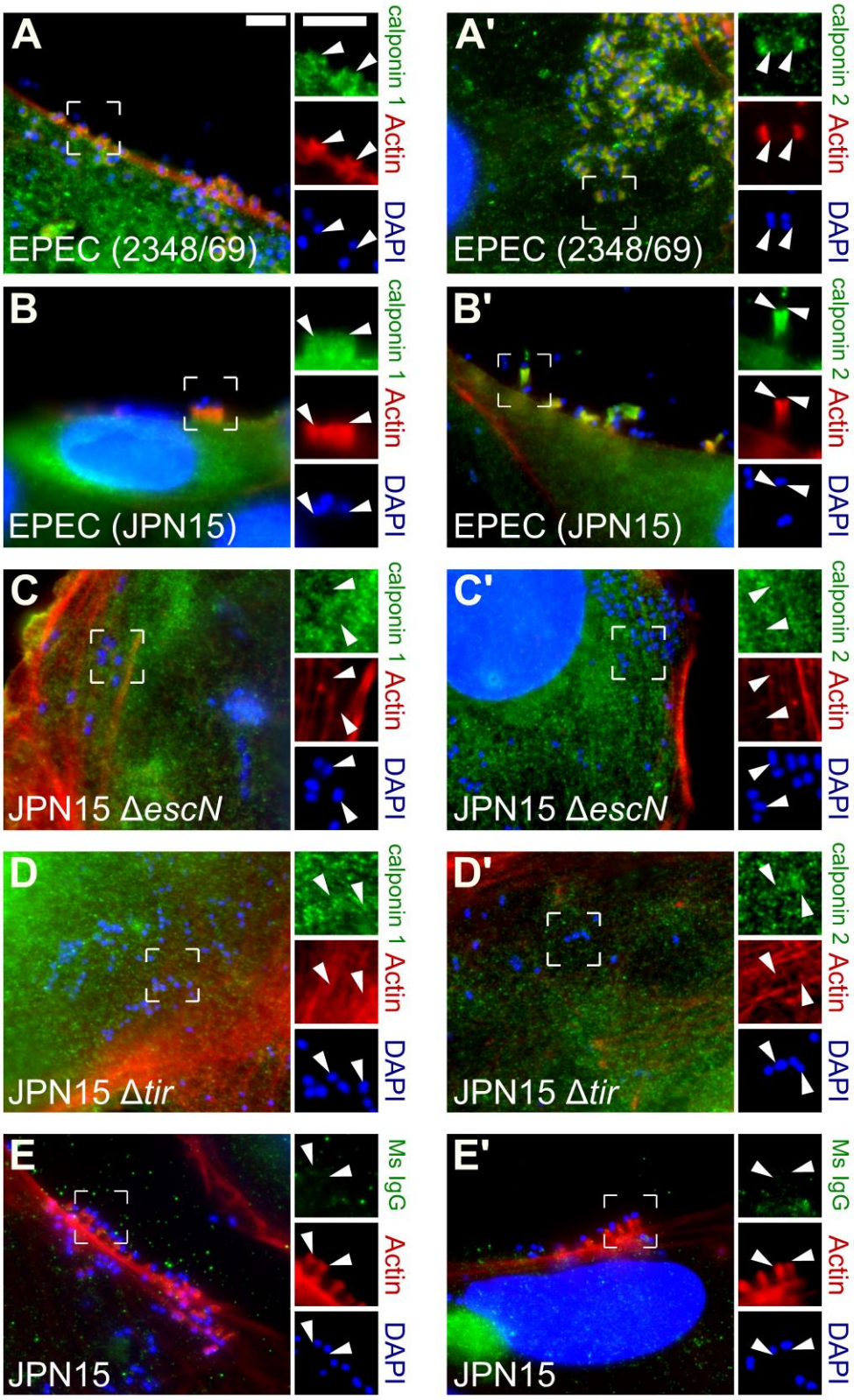
A
EPEC (2348/69)
calponin 1
Actin
DAPI
A'
EPEC (2348/69)
calponin 2
Actin
DAPI
B
EPEC (JPN15)
calponin 1
Actin
DAPI
B'
EPEC (JPN15)
calponin 2
Actin
DAPI
C
JPN15 ΔescN
calponin 1
Actin
DAPI
C'
JPN15 ΔescN
calponin 2
Actin
DAPI
D
JPN15 Δtir
calponin 1
Actin
DAPI
D'
JPN15 Δtir
calponin 2
Actin
DAPI
E
JPN15
Ms IgG
Actin
DAPI
E'
JPN15
Ms IgG
Actin
DAPI

Figure 2.1: Calponin 1 was found uniformly throughout an EPEC pedestal while calponin 2 was enriched at the tip of the pedestal.

(A) Calponin 1 colocalized with the actin in wildtype EPEC pedestals. (A') Calponin 2 was also recruited to the sites of actin enrichment within wildtype EPEC pedestals. (B) Calponin 1 was found throughout the longer pedestals of EPEC (JPN15 strain) while (B') calponin 2 enrichment was found at the tip of EPEC (JPN15 strain) pedestals. (C, C') Neither calponin 1 nor calponin 2 were enriched around JPN15 Δ*escN* bacteria that were unable to form pedestals. (D, D') Similarly, JPN15 Δ*tir* bacteria did not form pedestals and both calponins were not recruited to the site of bacterial attachment. (E, E') Normal mouse IgG did not accumulate at EPEC pedestals. Arrowheads denote site of bacterial attachment. Scale bar = 5 μm.

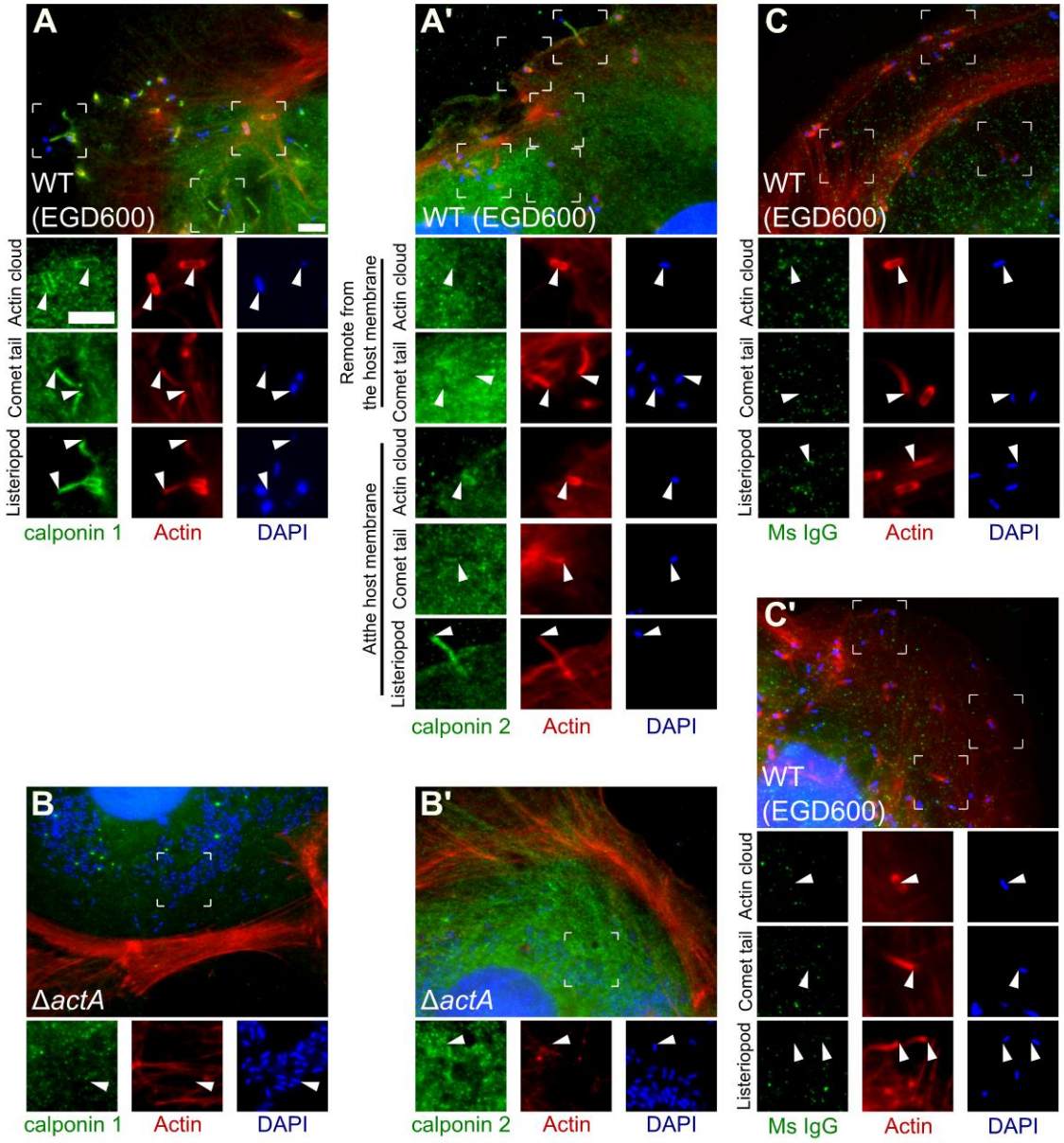

Figure 2.2: Calponin 1 immunolocalized to all actin-rich structures formed by *L. monocytogenes* while calponin 2 was only recruited to these structures at the host cell membrane.

(A) Calponin 1 had a uniform staining pattern in actin clouds, comet tails, and listeriopods. (A') Calponin 2 was only enriched at actin clouds, comet tails, and listeriopods near the host membrane. (B, B') Both calponins were not enriched around the non-actin polymerizing Δ*actA* bacteria. (C, C') Normal mouse IgG was not enriched at the actin structures formed by *L. monocytogenes*. Arrowheads denote internalized bacteria. Scale bar = 5 μm.

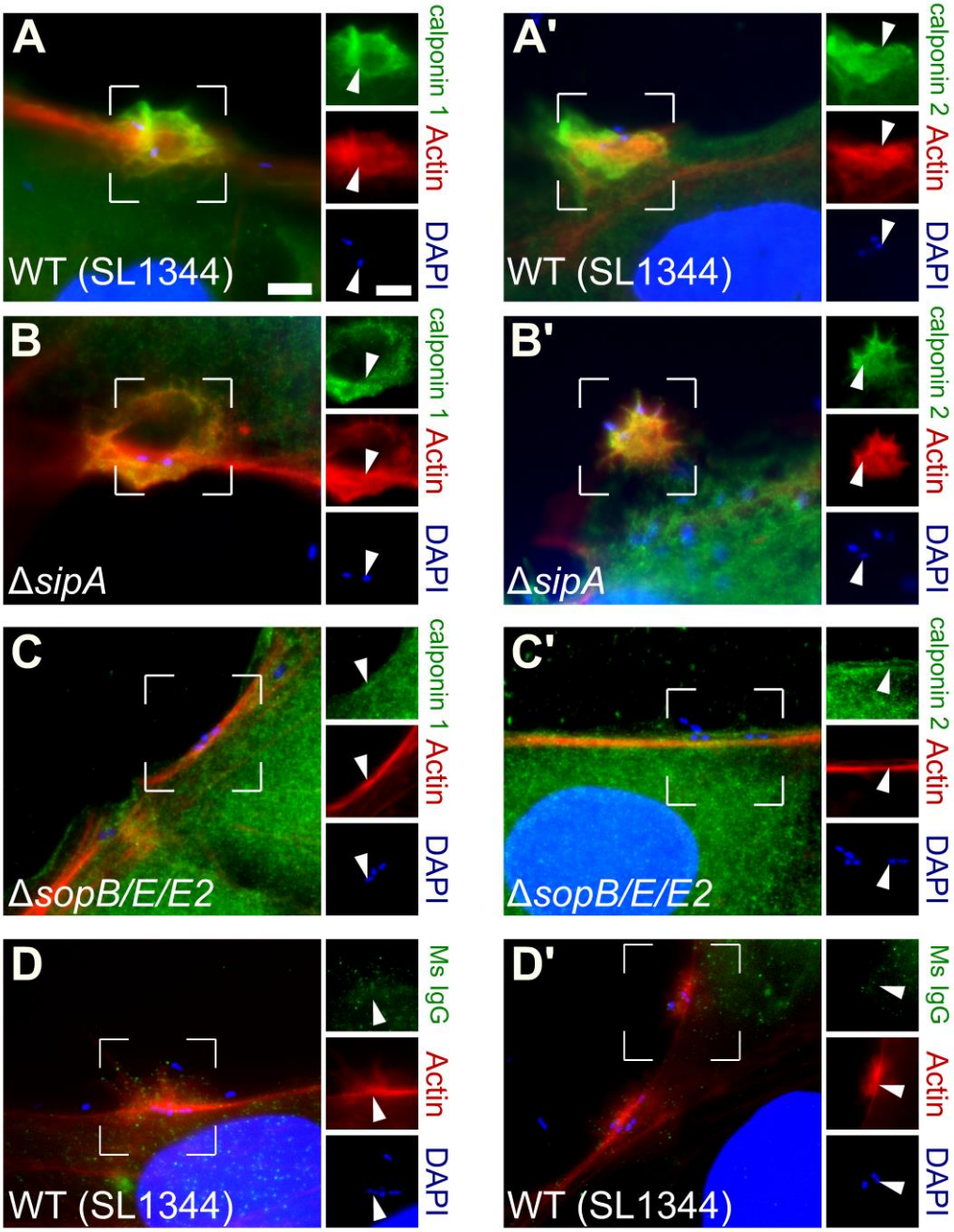

Figure 2.3: Both calponins were enriched within *S.* Typhimurium membrane ruffles.

(A) Wildtype *S.* Typhimurium generated membrane ruffling that were enriched with calponin 1. (A') Calponin 2 was also enriched within the *S.* Typhimurium-induced membrane ruffles. (B, B') The Δ*sipA* bacteria could still form membrane ruffles and both calponin 1 and calponin 2 were still colocalized with the actin filaments in the membrane ruffles. (C, C') When membrane ruffles were not induced by Δ*sopB/E/E2* bacteria, both calponin 1 and calponin 2 were not enriched underneath the bacterial attachment site. (D, D') Normal mouse IgG did not accumulate at *S.* Typhimurium membrane ruffles. Arrowheads denote attached bacteria on the host cell surface. Scale bar = 5 µm.

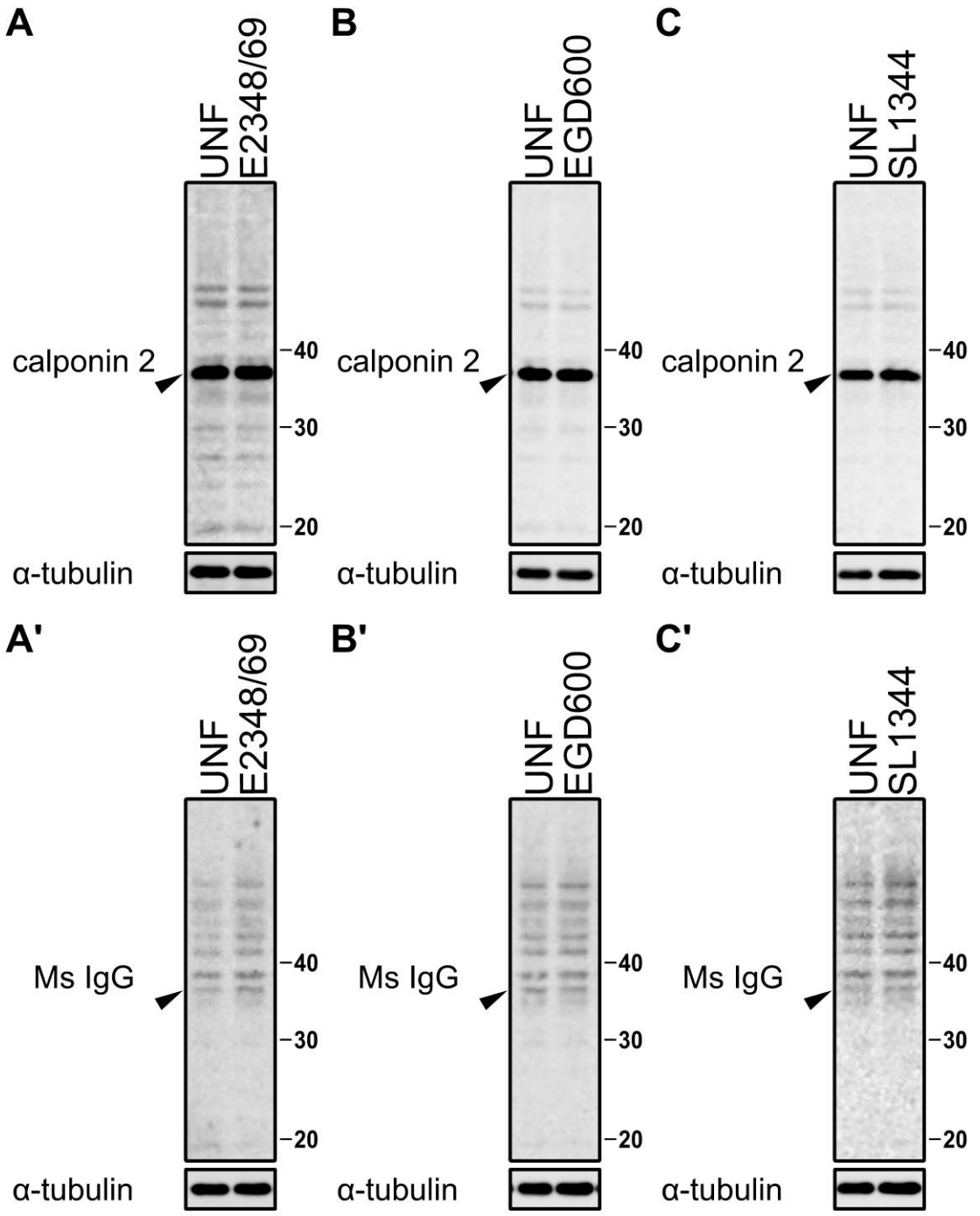

Figure 2.4: Calponin 2 were not altered during EPEC, *L. monocytogenes*, and *S.* Typhimurium infections.

Anti-α-tubulin was used as a loading control for each immunoblot. Arrowhead indicates the band of interest. (A) Calponin 2 expression was unaltered during WT EPEC (E2348/69) infection. (B) Calponin 2 levels were unchanged during WT *L. monocytogenes* (EGD600) infection. (C) WT *S.* Typhimurium (SL1344) infection did not alter calponin 2 protein levels. (A', B', C') Normal mouse IgG did not show a prominent band at the molecular weight of calponin 2. UNF indicates uninfected cells.

Chapter 3.

SM22 is required for the maintenance of actin-rich structures generated during bacterial infections

The content of this chapter has been published in Experimental Cell Research.

Chua MD, Hipolito KJ, Singerr OB, Solway J, Guttman JA. (2018). SM22 is required for the maintenance of actin-rich structures generated during bacterial infections. Exp Cell Res. 369(1): 139-146. (Ahead of print.) doi:10.1016/j.yexcr.2018.05.015.

MDC designed the experiments with JAG. MDC, KJH, and OBS conducted the experiments and analysed the data. JS generated the EGFP-SM22 plasmid and reviewed the manuscript. MDC and JAG wrote and reviewed the manuscript.

3.1. Abstract

The host actin cytoskeleton is utilized by an assortment of pathogenic bacteria to colonize and cause disease in their hosts. Two prominently studied actin-hijacking bacteria are enteropathogenic *Escherichia coli* (EPEC) and *Listeria monocytogenes*. EPEC form actin-rich pedestals atop its host cells to move across the intestinal epithelia, while *Listeria monocytogenes* generate branched actin networks arranged as actin clouds around the bacteria and as comet tails for propulsion within and amongst their host cells. Previous mass spectrometry analysis revealed that a member of the calponin family of actin-bundling proteins, transgelin/SM22 was enriched in EPEC pedestals. To validate that finding and examine the role of SM22 during infections, we initially immunolocalized SM22 in EPEC and *L. monocytogenes* infected cells, used siRNA to deplete SM22 and EGFP-SM22 to overexpress SM22, then quantified the alterations to the bacterially generated actin structures. SM22 concentrated at all bacterially-generated actin structures. Depletion of SM22 resulted in fewer pedestals and comet tails and caused comet tails to shorten. The decrease in comet tail abundance caused a proportional increase in actin clouds whereas overexpression of SM22 reversed the actin cloud to comet tail proportions and increased comet tail length, while not influencing EPEC pedestal abundance. Thus, we demonstrate that SM22 plays a role in regulating the transitions and morphological appearance of bacterially generated actin-rich structures during infections.

3.2. Introduction

Microbes commonly control the host cytoskeleton as part of their pathogenesis processes[309,310]. Bacteria and viruses use this cytoskeletal system for their entry, intracellular life cycle and movement from cell-to-cell. Two well-studied bacteria that use the actin cytoskeleton are Enteropathogenic *Escherichia coli* (EPEC) and *Listeria monocytogenes*. During EPEC infections, these extracellular bacteria attach to the apical surface of intestinal epithelial cells where they use a type III secretion system to deliver an assortment of bacterial effectors directly into the host cells. One of these effectors is Tir, the translocated intimin receptor[204,291,311]. Once in the cytosol, Tir inserts into the host cell plasma membrane to enable firm docking with the bacterial surface protein intimin and the subsequent triggering of branched actin nucleation beneath the bacterial

attachment site. The accumulation of branched actin protrudes the host plasma membrane, forming a pedestal with EPEC atop it[195,205,290,312].

Unlike EPEC, *L. monocytogenes* invades its host cells using clathrin-mediated endocytosis[217,313]. When in the cytoplasm of those cells, the bacteria rapidly lyse their plasma membrane-based vacuoles that surround the microbes and initiate the recruitment of branched actin filaments using its surface protein ActA. Actin polymerizes around the bacterium and forms a ring of filamentous actin that surrounds the microbe and is referred to as an actin cloud[314,315]. As the infections progress, ActA moves to one pole of *L. monocytogenes* where it continues to nucleate host actin into actin-rich comet tails[315]. These comet tails are used by the bacteria to move throughout the cytosol and for protrusion into neighboring host cells[227,316].

A subset of actin-associated proteins maintains polymerized parallel actin filaments by bundling and stabilizing the structures[23,51]. Although the calponin family of proteins are categorized as actin bundling proteins known to recruit to parallel actin structures, one of its members, SM22, appeared in a proteomics screen of EPEC pedestals components[62,299]. Here we demonstrate SM22 at all actin-rich structures generated by both EPEC and *L. monocytogenes*. When SM22 is depleted using small interfering (siRNA), EPEC pedestal formation is reduced and fewer *L. monocytogenes* actin clouds progress to form comet tails. In contrast, overexpressing SM22 did not significantly alter EPEC pedestal formation, but did revert the *L. monocytogenes* actin cloud to comet tail distribution. Through this work, we uncover a novel function of SM22 at bacterially induced actin structures and suggest that a host protein may control the maturation of *L. monocytogenes* during their pathogenesis.

3.3. Materials and Methods

3.3.1. Cell culture and bacterial growth

Human cervical cells (HeLa) were grown in GE HyClone Dulbecco's Modified Eagle Media (DMEM) with 10% Gibco Fetal Bovine Serum (FBS). Human colon cells (Caco2) were grown in GE HyClone Dulbecco's Modified Eagle Media (DMEM) with 1% HyClone non-essential amino acids and 10% Gibco Fetal Bovine Serum (FBS). Caco2 cells were polarized using the Corning BioCoat HTS Caco-2 Assay System and the cells

were cultured based on the manufacturer's protocols. *Potorous tridactylus* kidney cells (PtK2) were cultured with GE Hyclone DMEM/F-12 (1:1 ratio) with 10% Gibco Fetal Bovine Serum (FBS). All cultured cells were grown in a 37˚C incubator maintained with 5% CO2. For the growth of the bacteria, frozen stocks of EPEC (JPN15 and JPN15 Δ*tir* and JPN15 Δ*tir*+*tir*)[189,192] or *L. monocytogenes* (EGD600 and EGD600 Δ*actA*)[303,304,317] were streaked onto Luria-Bertani (LB) agar plates or brain heart infusion (BHI) agar plates and these plates were incubated at 37˚C. Afterwards, one EPEC colony was inoculated into 4 mL of LB broth and grown as a standing culture at 37˚C for 16 hours prior to infection. All cultures of the EPEC Δ*tir*+*tir* strain was grown in media supplemented with 12.5 µg/mL chloramphenicol. Similarly, single colonies of *L. monocytogenes* were inoculated into 2 mL of BHI broth and grown in a shaking incubator at 37˚C for 16 hours.

3.3.2. EPEC infection

Cultured HeLa or Caco2 cells were seeded onto round coverslips in 24-well plates and allowed to grow for 2 days. On the day of the infection, the bacterial culture was diluted 100-fold in LB broth. Then, cell culture media was replaced with 1 mL of fresh DMEM with 10% FBS and 2 µL of the diluted bacterial culture was added onto the cultured cells to infect at a multiplicity of infection (MOI) of 10. The well plate was then incubated at 37˚C for 3 hours and afterwards, the media was replaced with fresh DMEM with 10% FBS to remove unattached bacteria. The well plates were then incubated for another 3 hours at 37˚C before the cells were fixed in paraformaldehyde for immunofluorescence staining (See Immunofluorescence Staining below). To generate elongated pedestals, PtK2 cells in DMEM/F12 with 10% FBS were infected similar to HeLa cells. Three hours post infection, the media was then replaced with 40 mM 2,3-butanedione monoxime (BDM) in DMEM/F12 with 10% FBS and the cells were incubated for 30 minutes. This media change was repeated five times. After a total of 6 hours of infection, the cells were similarly fixed in paraformaldehyde for immunofluorescence staining (See Immunofluorescence Staining below).

3.3.3. *L. monocytogenes* infection

HeLa cells were prepared on round coverslips in 24-well plates and grown for 2 days. On the day of the infection, the 16-hour culture of *L. monocytogenes* was diluted

10-fold in BHI broth and allowed to grow as a shaking culture at 37˚C for approximately 2.5 hours. Once an optical density (OD600) of 1.00 was reached, the bacteria were pelleted and washed three times with warm phosphate buffered saline (PBS). After the three PBS washes, the bacteria were resuspended in 1 mL DMEM without FBS and diluted 100-fold. To infect the prepared HeLa cells at an MOI of 10, the cells were washed 6 times with DMEM then 300 µL of the diluted bacteria was added onto each well of HeLa cells and then an additional 700 µL of DMEM is added to each well. Next, the well plates were centrifuged at 215 g for 2 minutes to synchronize the infections and enhance bacterial attachment on the host cells. The well plates were incubated at 37˚C. After two hours, the wells were washed twice with warm PBS and fresh DMEM with 10% FBS containing 50 µg/mL gentamicin. The cells were then incubated at 37˚C for another 4-5 hours prior to fixation for immunofluorescence staining (See Immunofluorescence Staining below).

3.3.4. RNA interference of SM22 and detection of SM22 through Western blotting

HeLa cells were seeded on 24-well plates and allowed to grow for 1 day at 37˚C. GE Dharmacon ON-TARGETplus SMARTpool siRNA was obtained for the human SM22α and SM22β genes (Cat No: L-003714-00-0005 and L-011468-00-0005). GE Dharmacon ON-TARGETplus Non-targeting siRNA (Cat No: D-001810-10-05) was used as the control siRNA. Before transfections, non-targeting siRNA, SM22α siRNA, SM22β siRNA, or both SM22α and SM22β siRNA were resuspended in DMEM. The siRNA were transfected into the HeLa cells using the InterferIN transfection reagent (Polyplus Transfections; Cat No: 409-10) based on the manufacturer's procedure. After 72 hours, cells were lysed with cold RIPA lysis buffer (150 mM NaCl, 50 mM Tris pH 7.5, 5 mM EDTA, 1% Nonidet P-40, 1% Deoxychloic acid, 0.1% SDS) supplemented with the Roche cOmplete protease inhibitors cocktail (Cat No: 11836170001). Cell debris was then separated by centrifugation. Protein supernatants were then normalized using the protein concentrations obtained from a bicinchoninic acid assay, mixed in 1x sample buffer (0.0625M Tris pH 6.8, 2% SDS, 10% glycerol, 0.1M DTT, 0.01% bromophenol blue), boiled at 100°C, and then run on a 10% acrylamide gel. After gel electrophoresis, proteins were transferred to a Bio-Rad nitrocellulose membrane and then blocked with 4% BLOTTO for 30 minutes. The membrane was then washed with tris buffered saline with 0.1% Tween-20 (TBST) and then incubated with rabbit anti-SM22 antibodies

(Abcam; Cat No: ab14106) diluted to a concentration of 0.0009 µg/µL in TBST with 0.1% BSA (TBST/BSA). After overnight incubation at 4˚C, the membrane was washed with TBST, then incubated with goat anti-rabbit conjugated with HRP diluted to a concentration of 0.0002 µg/µL in TBST/BSA for 2 hours at room temperature. Afterwards, the membrane was washed with TBST and TBS prior to ECL detection. To visualize the chemiluminescence on the membrane, the membrane was incubated in Perkin-Elmer ECL Lightning Plus reagent (Cat No: NEL104001EA) and then imaged using the Fujifilm LAS4000 chemiluminescent imager. To determine protein loading, blots were incubated in a mild stripping buffer (0.15% glycine, 0.1% SDS, 1% Tween-20, and HCl to adjust to pH 2.2) for 20 minutes and then washed with PBS and TBST prior to blocking with 4% BLOTTO. The blots were then incubated in mouse anti-αtubulin antibodies (Developmental Studies Hybridoma Bank, University of Iowa; Cat No: 12G10) diluted to a concentration of 0.01 µg/µL in TBST/BSA. ECL detection was conducted as mentioned above.

Following the confirmation of the depletion of SM22 via western blotting, fresh HeLa cells were depleted of SM22 using siRNA and after 72 hours, EPEC or *L. monocytogenes* infections were conducted as mentioned above.

3.3.5. Overexpression of SM22

For the transfections, HeLa cells were seeded on round coverslips in a 24-well plate. After one day, EGFP (Clontech) or EGFP-SM22^{318} was transfected into the HeLa cells using the jetPEI transfection reagent using the manufacturer's protocol (Polyplus Transfections; Cat No: 101-10N). Bacterial infections were conducted on the transfected cells on the day after transfection.

3.3.6. Immunofluorescence Staining and Microscopy

After infection, the cells were washed three times with warm phosphate buffered saline (PBS). The cells were then fixed with warm 3% paraformaldehyde for 15 minutes at room temperature. Next, the cells were washed once with PBS and then, permeabilized using PBS with 0.2% Triton-X100. The coverslips were washed three times and then incubated in 5% normal goat serum (NGS) in PBS with 0.05% Tween-20 and 0.1% bovine serum albumin (TPBS/BSA). Rabbit anti-SM22 antibodies (Abcam; Cat

No: ab14106) were diluted to a concentration of 0.018 µg/µL in TPBS/BSA, and then the coverslips were incubated in the anti-SM22 antibodies overnight at 4°C. Afterwards, the coverslips were washed with TPBS/BSA and then incubated with Alexa-488 anti-rabbit antibodies (Invitrogen; Cat No: A11008) diluted to a concentration of 2 µg/µL in TPBS/BSA for 2 hours at room temperature. Excess antibodies were removed by washing three times with TPBS/BSA and then, the coverslips were incubated in 0.66 µM Alexa-594 phalloidin (Invitrogen; Cat No: A12381) diluted in TPBS/BSA for 15 minutes at room temperature. The coverslips were then washed and mounted in Prolong Gold antifade with DAPI (Invitrogen; Cat No: P36930). The mounted slides were imaged at 1000x total magnification using a Leica DMI4000B inverted microscope with a Hamamatsu Orca R2 CCD camera.

3.3.7. Statistical Analysis

Fluorescent images of at least 30 cells were taken from three independent trials. These images were analyzed using the measure tool and Cell Counter plugin of ImageJ [319]. Statistical significance was determined at $P<0.05$ using the Student's *t*-test on GraphPad Prism.

3.4. Results

3.4.1. SM22 colocalizes with branched actin in the host cell structures formed by EPEC and *L. monocytogenes*

A proteomics screen of EPEC pedestals identified SM22 as a highly abundant component of the structures[299]. SM22 is known to bundle actin at parallel actin structures[67,320] and in our study, SM22 also colocalized to stress fibres (Fig. 1A). To determine if SM22 is recruited to pedestals during EPEC infections, we infected cultured HeLa cells with EPEC (JPN15 strain), a *tir*-deficient mutant (JPN15 Δ*tir*), and the *tir* mutant with a complement with *tir* (JPN15 Δ*tir*+*tir*). The JPN15 strain is a bundle-forming pilus mutant that does not aggregate like other wild type EPEC strains, thus generating clearly defined individual pedestals as opposed to clustered microcolonies of bacteria atop groups of pedestals. The JPN15 and Δ*tir*+*tir* strain generate pedestals after the insertion of Tir into the host cell plasma membrane while the *tir*-deficient bacteria weakly bind onto the host cell membrane and do not form pedestals as they cannot recruit actin.

We found that SM22 colocalized with actin in pedestals formed by JPN15 and Δ*tir+tir* bacteria (Fig. 3.1A) and was not present at the sites of bacterial attachment of tir-deficient bacteria. Using the small molecule 2,3-butanedione monoxime (BDM) on EPEC-infected PtK2 cells[299], we generated elongated pedestals and SM22 was uniformly found through the full length of all pedestals formed (Fig. 3.5). This elongation procedure and cell type was identical to the samples that initially identified transgelin/SM22 at pedestals in the proteomics screen[299].

To determine if SM22 was recruited to branched actin structures formed by other bacteria, we exploited *L. monocytogenes*. We infected cultured cells with a wildtype strain of *L. monocytogenes* (EGD600 strain) and an *actA*-deficient mutant (Δ*actA*) as the bacterial protein ActA is required to induce actin polymerization. We observed that SM22 co-localized with filamentous actin at both the actin clouds and comet tails formed by the bacteria (Fig. 3.1B). Neither actin nor SM22 were recruited to *actA*-deficient bacteria.

Proteomics database entries for SM22 show abundant levels in intestinal cells[321,322]. Based on this, we determined if SM22 was recruited to EPEC pedestals and *L. monocytogenes* comet tails in human intestinal epithelial cells. Infection of unpolarized and polarized Caco2 cells showed that SM22 was indeed recruited to both of these actin-rich structures (Fig. 3.6A, 3.6B). Western blotting showed that SM22 was present in Caco2 cells and that both bacterial types did not alter the SM22 protein levels during the infections (Fig. 3.6C).

3.4.2. Knockdown of SM22 reduces the number of pedestals formed by EPEC

To determine if SM22 plays a functional role in pedestal formation, we transfected non-targeting small interfering RNA (siRNA) as a control and siRNA for SM22α and/or SM22β to deplete the amount of SM22 present in our cultured cells. SM22α and SM22β share 68% sequence homology and high structural similarity[323]. These proteins primarily differ in their abundance in various cell types[321]. Once treated with the siRNA, we infected control and SM22-depleted cells with EPEC (JPN15 strain).

In the SM22α siRNA-treated cells, the bacteria were still able to form pedestals as evidenced by immunofluorescence labeling of SM22 colocalized with actin at the pedestals (albeit to a lesser degree) (Fig. 3.2A). When both siRNAs for SM22 were used

together, pedestals were still formed, but SM22 was undetectable at the structures. Fewer pedestals formed in the SM22α or SM22α/β siRNA transfected cells as 60% of attached EPEC formed pedestals on non-targeting siRNA (control) transfected cells, while only 16% and 20% of the bacteria formed pedestals in SM22α or SM22α/β siRNA transfected cells, respectively (Fig. 3.2B). Depletion of SM22β alone slightly reduced pedestal formation, but not to the same degree as SM22α depletion (Fig. 3.7A). Pedestal formation dropped slightly from 64% in control transfected cells to 46% in SM22β-depleted cells (Fig. 3.7B).

Western blot analysis of uninfected cells showed a doublet band (Fig, 3.2C) corresponding to the full-length and C-terminally cleaved variants of SM22 similar to those shown in SM22 previous studies[320]. Depletion using only the SM22α siRNA resulted in the reduction of full-length SM22 compared to non-targeting siRNA-treated cells (higher band of the doublet), while transfection of both SM22α and SM22β siRNA reduced the levels of both the full-length and C-terminally cleaved derivative of SM22 (lower band of the doublet) found in our immunoblotting (Fig. 3.2C). The transfection of only SM22β siRNA depleted the lower band of the SM22α doublet and SM22β protein to undetectable levels (Fig. 3.7C).

3.4.3. Fewer comet tails are formed during *L. monocytogenes* infections when SM22 is depleted in host cells

To determine the effect SM22 has on actin clouds and comet tails formed by *L. monocytogenes*, we infected control or SM22-depleted HeLa cells with wildtype *L. monocytogenes*. Similar to EPEC induced pedestals, SM22 dimly colocalized with actin clouds in SM22α siRNA-treated cells. However, comet tails that formed in these host cells did not have SM22 present (Fig. 3.3A). When both siRNA for SM22 were transfected, SM22 was absent from all actin-rich structures formed by *L. monocytogenes*. This depletion of SM22 decreased the numbers of comet tail in the infections and changed the proportions of actin clouds to comet tails in the samples. In cells with endogenous levels of SM22, 41% of actin-recruiting bacteria formed actin clouds and 59% formed comet tails (Fig. 3.3A, 3.3B). Whereas in SM22α siRNA treated cells, 71% of the bacteria formed actin clouds and 29% formed comet tails. When both SM22α and SM22β siRNAs were transfected, 63% of the bacteria formed actin clouds while 36% formed comet tails. Following the measurement of comet tail lengths, we

found that the average length of comet tails was reduced in SM22-depleted host cells from 5.2 μm in control cells to 2.7 μm and 3.2 μm in SM22α and SM22α/β siRNA treated cells, respectively. Transfection of only the SM22β siRNA however did not have any apparent effect on the ratio of actin clouds and comet tails or the length of comet tails (Fig. 3.7D, 3.7E, 3.7F).

3.4.4. Overexpression of SM22 does not affect EPEC pedestal formation, but *L. monocytogenes* comet tail formation is increased

If depleting SM22 reduced the number of EPEC pedestals formed, we then hypothesized that overexpression of SM22 would increase their abundance. To test this, we transfected HeLa cells with either EGFP or EGFP-SM22 and infected these cells with EPEC bacteria. We identified cells that had green fluorescence and had a discernible amount of attached bacteria (Fig. 3.4A). From these, there were no significant differences in the proportion of attached bacteria that formed pedestals between the EGFP and the EGFP-SM22 transfected cells (Fig. 3.4A, 3.4C).

Similarly, because depleting SM22 reduced the number of comet tails formed and the length of comet tails, we determined if overexpressing SM22 would increase the number of comet tails formed and the length of those comet tails (Fig. 3.4B). In EGFP-transfected cells, 56% formed actin clouds while 44% formed comet tails; while in EGFP-SM22-transfected cells, 38% formed actin clouds while 62% formed comet tails (Fig. 3.4D). Although transfection of the EGFP vector alone altered the proportion of comet tails that formed, overexpression of SM22 increased the proportion of comet tail forming bacteria to all the bacteria that formed actin structures. Moreover, the average comet tail length was also increased when SM22 was overexpressed; increasing from 3.4 μm in EGFP-expressing cells to 4.7 μm in EGFP-SM22-expressing cells (Fig. 3.4E).

3.5. Discussion

SM22 is a known actin bundling protein that stabilizes parallel actin filaments through its multiple calponin-like (CLIK) domains[58,68,320]. Using bacterial pathogens, we found that SM22 decorated branched actin-generated structures formed by both EPEC and *L. monocytogenes* and controlled the proportion of actin clouds to comet tails as

well as comet tail length in infected cells. Our findings of SM22 homogeneously staining throughout the structures suggest that the function of this protein maintains the structure of EPEC pedestals and *L. monocytogenes* comet tails rather than just affecting the actin polymerization region.

Unlike other calponin proteins which exclusively bind to parallel bundles of actin, SM22 is found in highly branched actin structures such as podosomes and membrane ruffles in macrophages and the recruitment rate of SM22 is similar to the recruitment rate of cytoplasmic actin monomers within these structures[62,322]. Moreover, calponins have previously been shown to provide conformational stability to actin filaments[324] and this has been hypothesized to impede the severing of those filaments[62]. Because we have shown that depleting SM22 reduced both pedestal and comet tail formation, SM22 may be acting to protect these actin filaments from severing enzymes as hypothesized previously[62]. SM22α and SM22β are isoforms of the SM22 protein both of which seem to be abundant in human epithelial cells. Our data showed that depleting either SM22α or SM22β had deleterious effects on EPEC pedestals and *L. monocytogenes* comet tails, but depleting both did not have compounding effects. This further confirms that these proteins may have redundant roles in actin binding. In addition, we observed longer comet tails when SM22 was overexpressed in *L. monocytogenes*-infected cells. Perhaps, SM22 provides the necessary stability to nascent branched actin filaments and this function of SM22 is vital for the development of branched actin arrays at bacterially-generated actin-rich structures.

Arguably the most interesting finding of our study was the altered proportions of actin clouds to comet tails during *L. monocytogenes* infections. Admittedly, altering protein levels using siRNA or EGFP-tagged constructs generated varying proportions between actin clouds and comet tails in our control samples. Different transfection reagents were used to optimize siRNA-based depletion of SM22 and vector-based overexpression. Although we did not observe any apparent deleterious effects on host cell morphology, the transfection procedure alone could have affected some of the proportions of actin clouds and comet tails. Additionally, constitutive expression of EGFP altered the amount of protein within the host cytosol which could invariably affect the kinetics of comet tail formation. Amidst these possible factors that could have affected comet tail formation, we observed drastic alterations to the proportion of comet tails in the SM22 depleted cells and the SM22 overexpressing cells compared to the

corresponding transfection controls for each experiment. Nonetheless, how can a host actin-associated protein regulate those stages of the infections? Actin clouds are generated through the actions of the bacterial protein ActA that surround the microbes. Actin filament stability through SM22 may contribute to the concentration of ActA-tethered actin filaments within the *L. monocytogenes* actin cloud. When we depleted SM22, movement of actin filaments to one pole of the bacterium may have been impeded, thus stalling bacteria at the actin cloud phase. Taken together, we have shown that SM22 contributes to the formation of bacterially generated actin structures and likely controls the transition of those structures during infections when multiple phases of actin organization are hijacked by microbes.

3.6. Figures

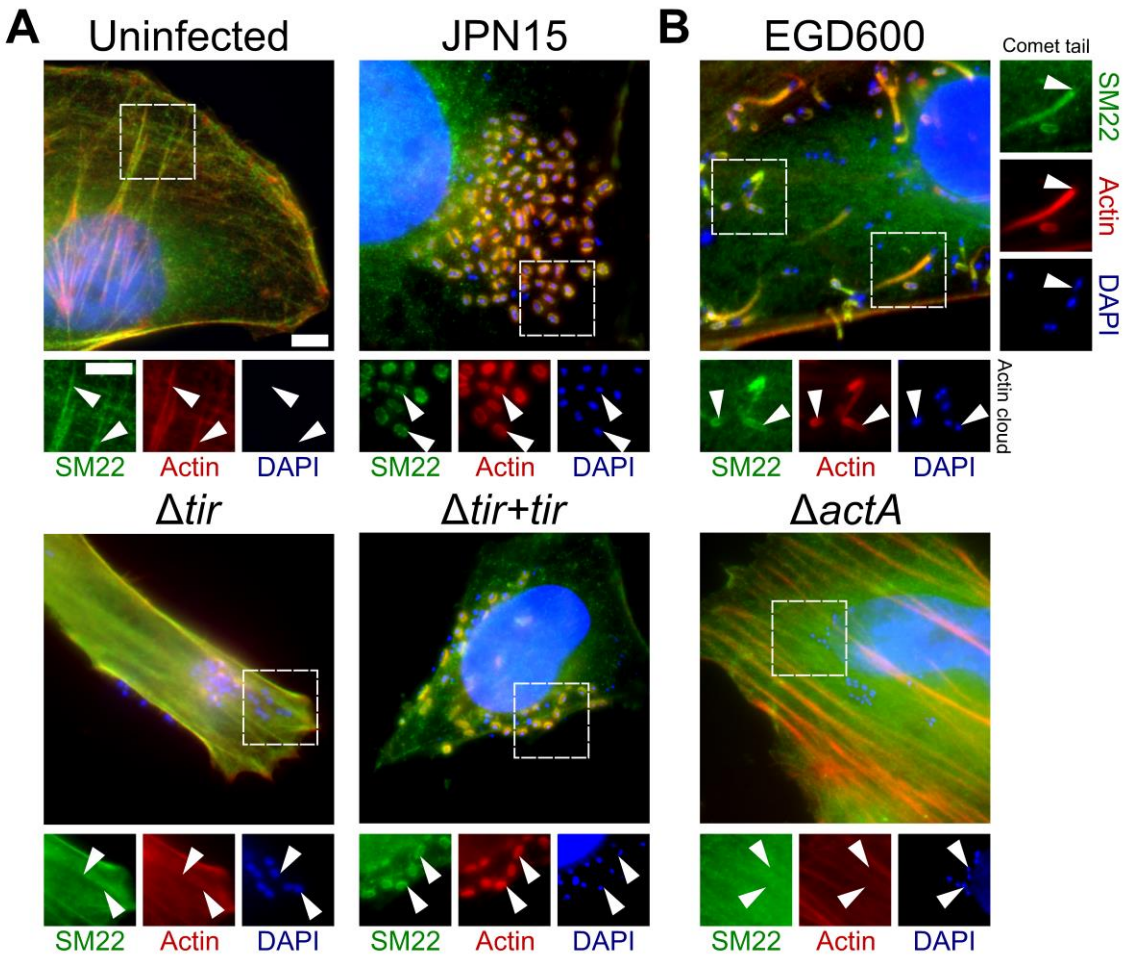

Figure 3.1: SM22 is enriched at all actin structures in uninfected, EPEC-infected, and *L. monocytogenes* infected cells.

(A) SM22 is only recruited to pedestals formed by wild-type EPEC (JPN15) and JPN15 Δ*tir+tir*. SM22 is not recruited by the JPN15 Δ*tir* bacteria that are unable to form pedestals. Arrows indicate the sites of bacterial attachment. Scale bar = 5 μm. (B) In *L. monocytogenes* infections, SM22 colocalizes with actin in actin clouds and comet tails. The Δ*actA* bacteria are unable to induce actin polymerization and thus, SM22 is not recruited to its surroundings. Arrows indicate the internalized bacteria.

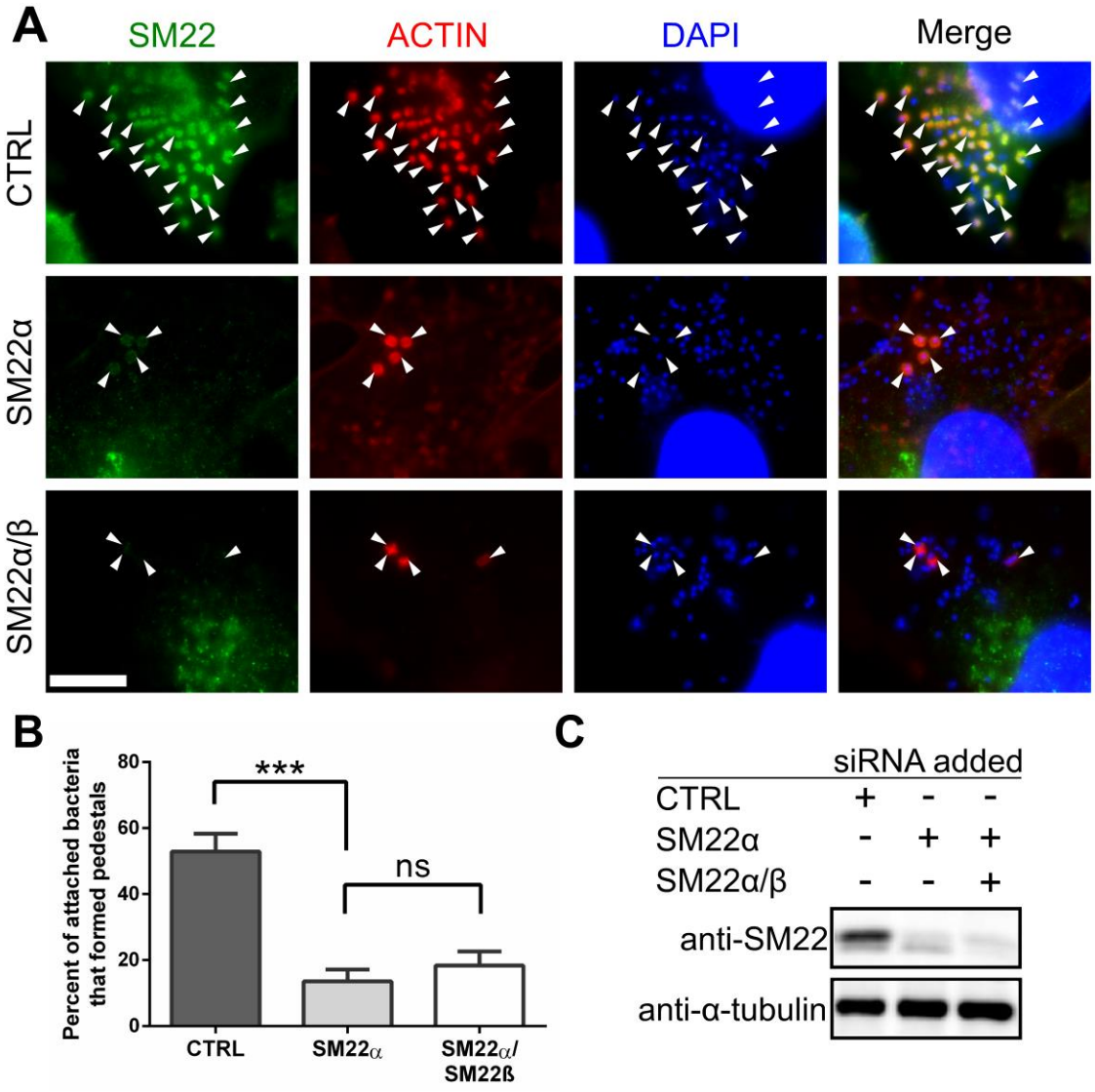

Figure 3.2: Depletion of SM22 reduces EPEC pedestal formation.
(A) Fewer EPEC pedestals are formed when SM22 levels are reduced. Arrows indicate pedestals formed by the bacteria. Scale bar = 10 µm. (B) Quantification of attached bacteria shows a decrease in the number of pedestals formed when host cells are treated with either SM22α or SM22α/β siRNA. Error bars indicate standard error of mean among quantified host cells. ***P<0.0001 using Student's *t* test with Welch's correction. (C) Treatment with the SM22α siRNA reduced the dominant band detected by the SM22 antibody while treatment with the SM22β siRNA reduced the fainter lower band detected by the SM22 antibody.

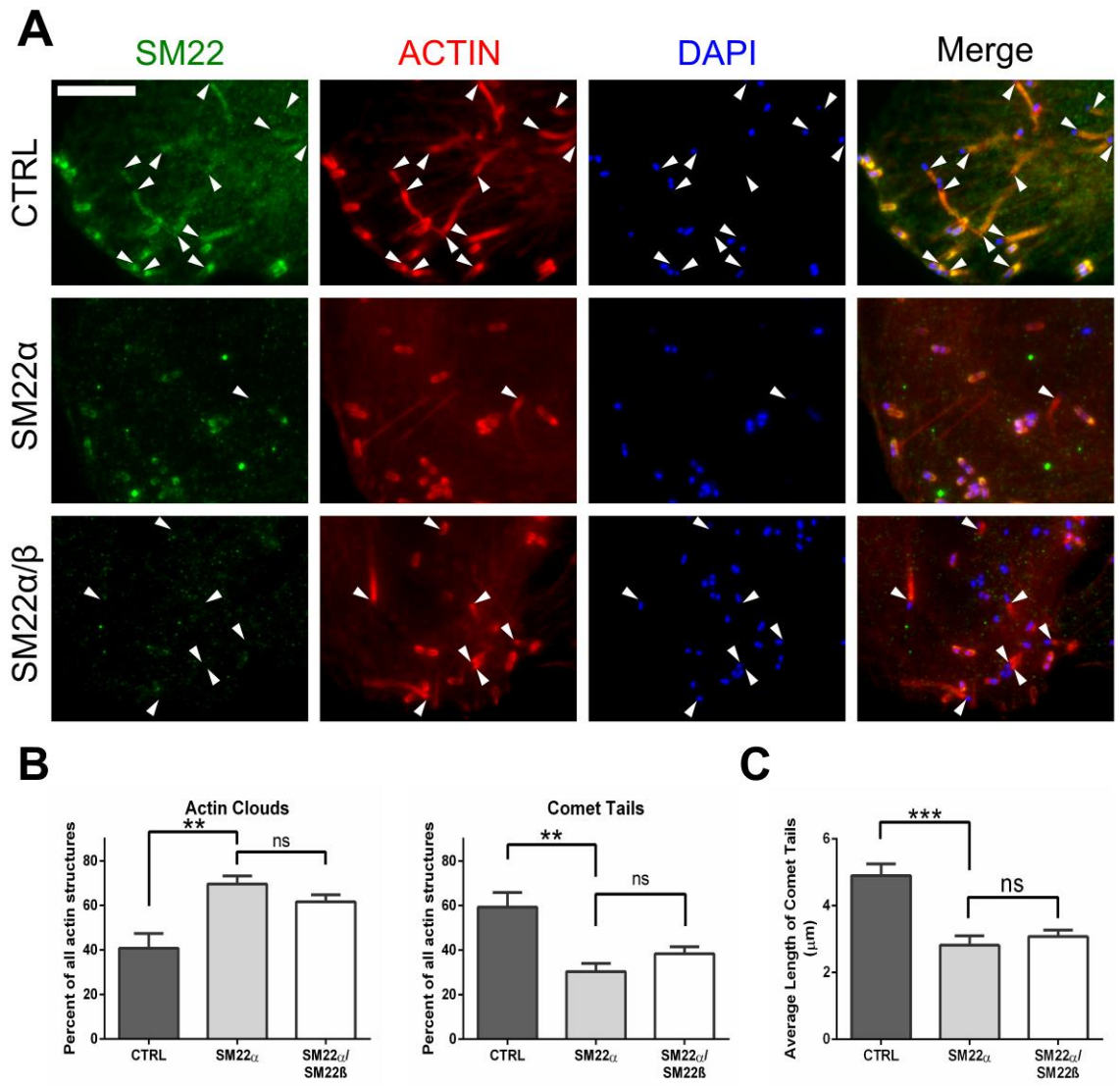

Figure 3.3: Comet tail formation and length declines when SM22 is reduced.
(A) Fewer comet tails were observed in SM22 siRNA treated cells. These comet tails were shorter than those in the control siRNA treated cells. Arrows indicate comet tails formed by *L. monocytogenes*. Scale bar = 10 μm. (B) The ratio of actin clouds or comet tails compared to all actin structures formed by the bacteria shows that less comet tails were formed in the SM22-reduced cells. Error bars indicate standard error of mean among quantified host cells. **P<0.003 using Student's *t* test with Welch's correction. (C) In addition to reduced comet tail formation, the comet tails that did form were significantly shorter in SM22-reduced cells. Error bars indicate standard error of mean among quantified host cells. ***P<0.0001 using Student's *t* test with Welch's correction.

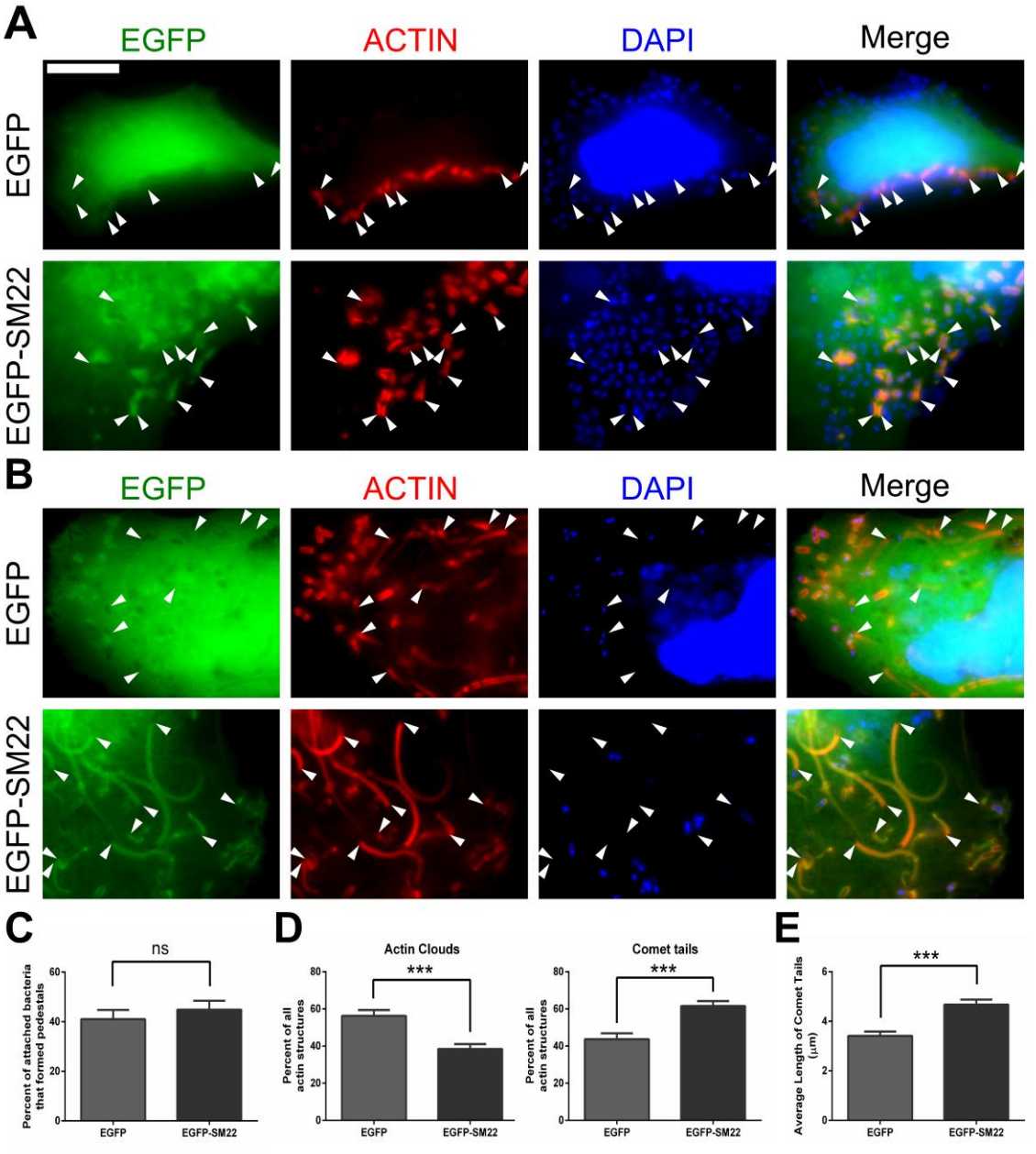

Figure 3.4: Overexpression of SM22 does not increase EPEC pedestal formation, but does increase *L. monocytogenes* comet tail abundance.

All error bars denote standard error of mean amongst the quantified host cells. (A) There was no difference in pedestal formation between EGFP-transfected cells and EGFP-SM22-transfected cells. Arrows indicate bacteria that formed pedestals. Scale bar = 10 μm. (B) Overexpressing SM22 increased the proportion of comet tails observed in transfected cells. Arrows indicate bacteria that formed comet tails. (C) Quantification of EPEC pedestals formed showed no significant difference when SM22 is overexpressed. (D) An increase in the ratio of comet tails compared to all actin structures formed by bacteria was evident in the EGFP-SM22-transfected cells. ***P<0.0001 using Student's *t* test with Welch's correction. (E) Comet tail lengths were also increased when SM22 was overexpressed. ***P<0.0001 using Student's *t* test with Welch's correction.

Figure 3.5: SM22 colocalized with actin through the full length of EPEC pedestals. EPEC-generated pedestals on PtK2 cells were chemically-induced to elongate using 2,3-butanedione monoxime (BDM). XZ cross-section show that SM22 is found throughout the pedestal. Dashed line indicate region of the XZ cross-section. Scale bar = 10 µm.

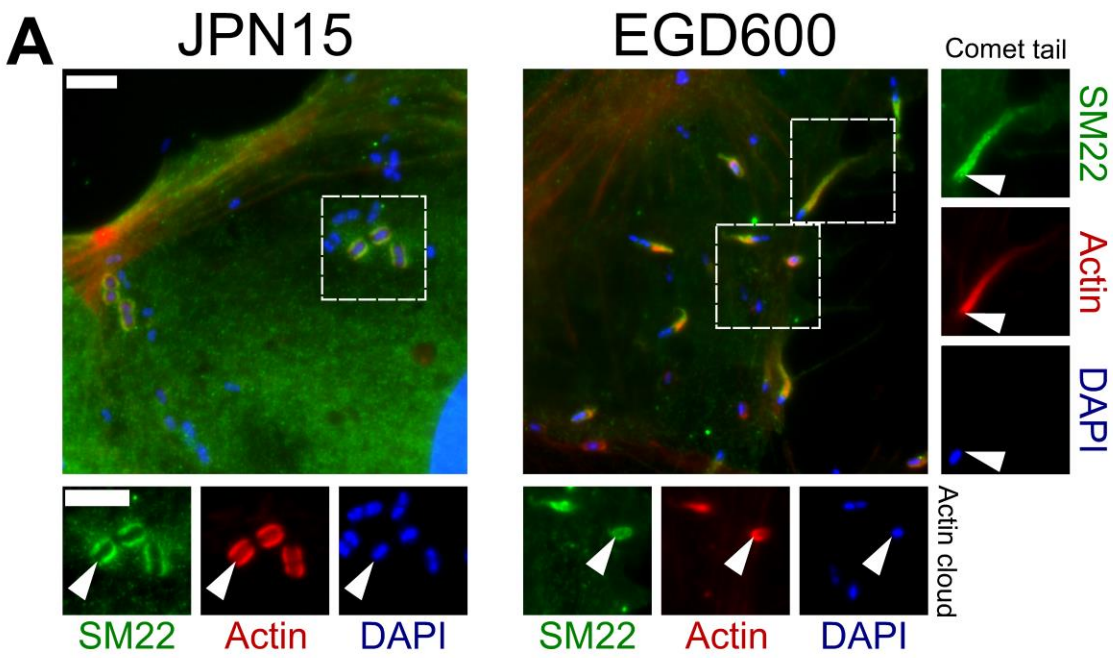
A
JPN15
EGD600
Comet tail
SM22
Actin
DAPI
Actin cloud
SM22
Actin
DAPI
SM22
Actin
DAPI

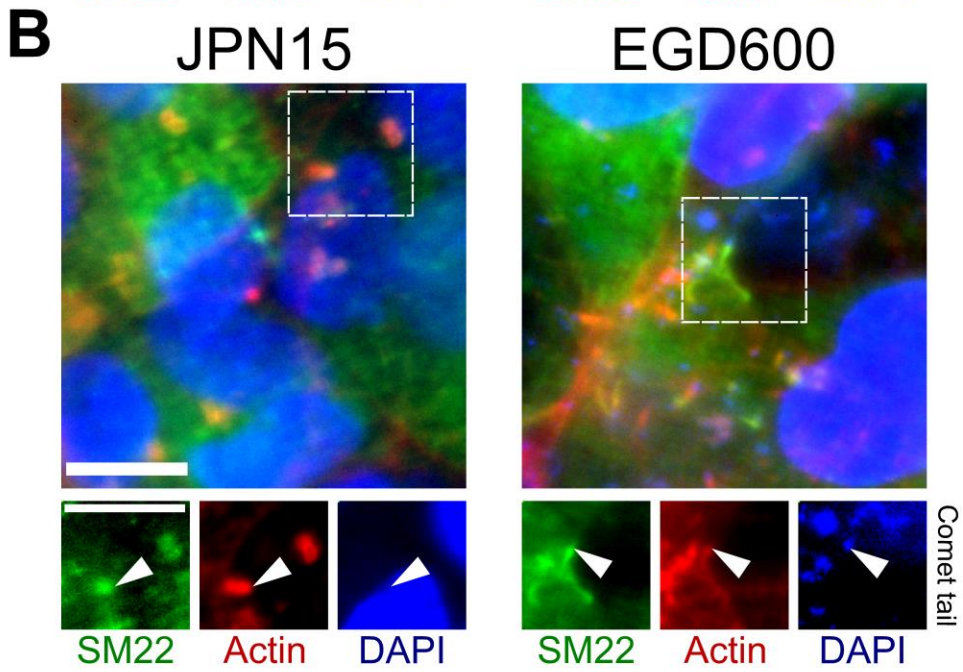
B
JPN15
EGD600
Comet tail
SM22
Actin
DAPI
SM22
Actin
DAPI

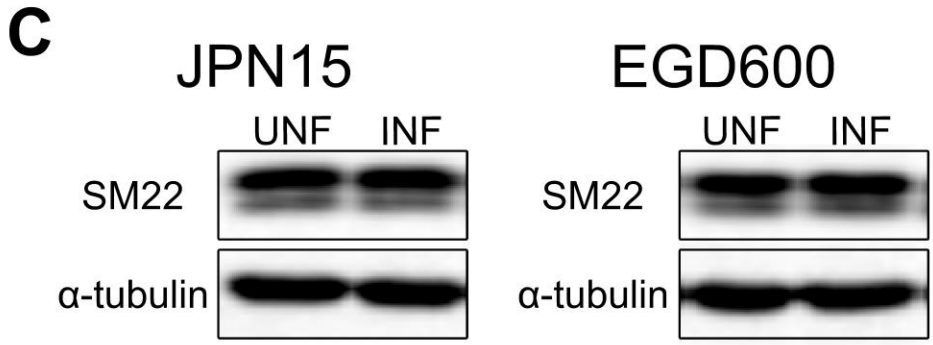
C
JPN15
EGD600
UNF
INF
SM22
α-tubulin
UNF
INF
SM22
α-tubulin

Figure 3.6: SM22 colocalized with actin in EPEC pedestals and *L. monocytogenes* in Caco2 human colorectal cells.

Scale bars = 5 µm. (A) SM22 was enriched in EPEC pedestals as well as in *L. monocytogenes* actin clouds and comet tails in flat Caco2 cells. Arrows indicate the location of some of the bacteria. (B) In polarized Caco2 cells, SM22 was also found in EPEC pedestals and *L. monocytogenes* comet tails. Arrows indicate some of the bacteria. (C) Caco2 cells express endogenous SM22. Neither EPEC nor *L. monocytogenes* infections altered the protein levels of SM22.

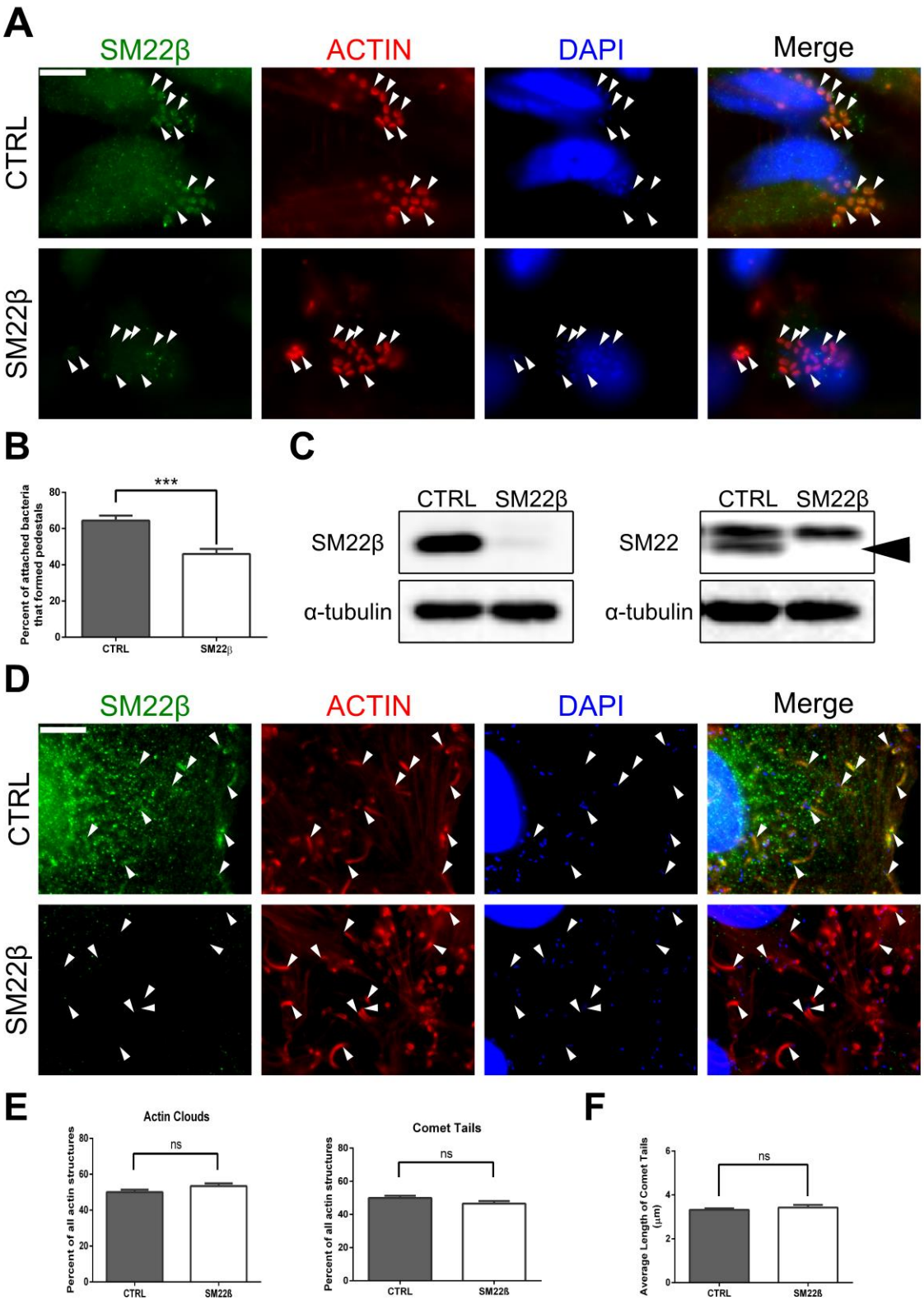
A
SM22β
ACTIN
DAPI
Merge
CTRL
SM22β
B
***
Percent of attached bacteria that formed pedestals
80
60
40
20
0
CTRL
SM22β
C
CTRL
SM22β
SM22β
α-tubulin
CTRL
SM22β
SM22
α-tubulin
D
SM22β
ACTIN
DAPI
Merge
CTRL
SM22β
E
Actin Clouds
ns
Percent of all actin structures
80
60
40
20
0
CTRL
SM22ß
Comet Tails
ns
Percent of all actin structures
80
60
40
20
0
CTRL
SM22ß
F
ns
Average Length of Comet Tails (µm)
6
4
2
0
CTRL
SM22ß

Figure 3.7: Depleting SM22β did not abolish either EPEC pedestal or *L. monocytogenes* comet tail formation.

Scale bars = 10 μm. (A) Pedestals still formed when SM22β was depleted. Arrows indicate pedestal-forming bacteria. (B) Depletion of SM22β slightly reduced pedestal formation. Error bars indicate standard error of mean among quantified host cells. ***P<0.0001 using Student's *t* test with Welch's correction. (C) Transfection of SM22β siRNA reduced SM22β protein levels as well as the lower protein band (black arrow) detected by the SM22 antibody. (D) Comet tail formation was not altered when SM22β was depleted. Arrows indicate comet tail forming bacteria. (E) SM22β depletion did not alter the proportion of actin clouds and comet tails. Significance was determined using Student's *t* test with Welch's correction. (F) Comet tail length was also unaffected by SM22β depletion. Significance was determined using Student's *t* test with Welch's correction.

Chapter 4.

Ube2N is a novel actin-associated protein at *Listeria* actin-rich structures and lamellipodia

The content of this chapter is being prepared for submission to a journal.

Chua MD, Moon KM, Foster LJ, Guttman JA. (2018). Ube2N is a novel actin-associated protein at *Listeria* actin-rich structures and lamellipodia. (*In preparation*).

MDC designed the project with JAG. MDC performed all the experiments, analysed the data and prepared the manuscript. KMM and LJF performed the mass spectrometry identification of actin from the Ube2N immunoprecipitation. JAG supervised the data analysis and wrote the manuscript with MDC. All authors reviewed the manuscript.

4.1. Abstract

The actin cytoskeleton forms much of the structure needed for the intracellular motility of an assortment of microbes as well as entire cells. The co-factor to the ubiquitin conjugating enzyme Ube2N (Ube2V1) has been implicated in both cancer cell metastasis and lysine-63 ubiquitylation of β actin. As this protein complexes with Ube2N, we sought to investigate whether Ube2N itself was involved in actin-based events within the cell. Through examination of *Listeria monocytogenes* actin clouds, comet tails and listeriopods as well as lamellipodia in migrating cells, we show that Ube2N is recruited to actin-rich structures and is crucial for their function when associated with the plasma membrane. This docking occurs directly between Ube2N and actin. The direct association of Ube2N provides the first evidence of an E2 conjugating enzyme at any actin structure and suggests an alternative function of this protein.

4.2. Introduction

Many bacterial pathogens and migrating cells control eukaryotic cell actin filament dynamics for forward motion. The dynamic nature of actin filaments generates the propulsive force necessary for mammalian cell motility[325]. An intricate array of proteins initiates the polymerization of actin filaments through signalling cascades along the leading edge of these cells. As actin accumulates near the plasma membrane, these protein complexes elongate the growing filaments and this provides the power required to extend the lamellipodia of the cell[15]. Thus, characterizing the proteins involved in the dynamics of the actin cytoskeleton and the plasma membrane is crucial for host cell motility. Although the large-scale architecture of the entire actin cytoskeleton has complicated the study of specific signalling cascades that regulate actin dynamics at the leading edge, researchers have utilized bacterial models to identify novel proteins that play key roles in regulating actin filaments[295,326]. These bacterial pathogens recruit actin-polymerizing complexes to generate relatively small actin-rich structures that mimic actin dynamics at the leading edge of mammalian cells.

L. monocytogenes invades its host cell through clathrin-mediated actin-dependent endocytosis[217,218,313]. Once inside the host cell, the bacterium utilizes its bacterial surface protein ActA to mimic the host cell actin polymerizing protein N-WASp and this induces the polymerization of actin filaments around the bacterial surface[91].

Initially, these short filaments appear as an actin-rich ring around the bacterium called an actin cloud. Eventually, ActA polarizes to one end of the microbe and elongation of the filaments from that site commences the formation of an actin network that allow the bacterium to propel itself around the host cell[221,222]. These structures of actin called comet tails enable not only intracellular motility, but also cell-to-cell spreading through protrusions made at the host cell plasma membrane called listeriopods[297]. Using this bacterial model system, researchers can study interactions between the plasma membrane and the actin cytoskeleton when *L. monocytogenes* invades through actin-dependent endocytosis, and when *L. monocytogenes*-induced comet tails form listeriopods at the host cell membrane[218,225].

Many studies have utilized bacterial pathogens to elucidate the protein makeup of the actin cytoskeleton. Previously, a mass-spectrometry analysis of isolated enteropathogenic *Escherichia coli*-induced pedestals identified about 90 novel host cell proteins that do not have known actin associations[299]. From that list of protein candidates, we demonstrated that the Ubiquitin-conjugating Enzyme 2N (Ube2N) is a novel protein found at actin-rich structures. Using *L. monocytogenes* infections as a model to study dynamic actin structures, we show that Ube2N colocalizes at all actin-rich structures formed by the bacteria; invasion sites, actin clouds, comet tails and listeriopods. Functionally-inhibiting Ube2N using the small-molecule NSC697923 diminishes *L. monocytogenes* invasion and cell-to-cell spreading, but does not alter comet tails. Actin co-precipitates with Ube2N in lysates from *L. monocytogenes*-infected cells and we confirm this binding using purified Ube2N together with purified actin. In cultured cells, the docking of Ube2N to actin occurs only at the plasma membrane interface. To further characterize the novel association of Ube2N with the actin cytoskeleton in cells, we show that Ube2N is enriched at lamellipodia and at actin-rich filopodia-like protrusions found at the cell borders. Finally, wound-healing assays to study cell motility demonstrate that functionally-inhibiting Ube2N alters cell movement, thus inhibiting wound closure. Through this work, our data establishes Ube2N as a novel actin regulator at the plasma membrane.

4.3. Materials and Methods

4.3.1. Bacterial growth and Cell culture

Frozen stocks of *Listeria monocytogenes* (strain EGD600 and Δ*actA*)[303,304] were grown on Brain Heart Infusion (BHI) agar (BD Biosciences) at 37˚C for 24 hours and incubated in a BHI broth culture (shaking) at 37˚C for 16 hours. *Potorous tridactylus* kidney PtK2 cells (ATCC CCL-56) were cultured with DMEM/F-12 (1:1 ratio) supplemented with 10% Fetal Bovine Serum (FBS) and were grown at 37˚C and 5% CO2.

4.3.2. *L. monocytogenes* Infections

The overnight cultures of *L. monocytogenes* were diluted 10-fold and were cultured at 37˚C until an optical density (OD600) of approximately 1.00 was obtained. 1 mL of the subculture was centrifuged for 5 minutes at 9600 g, then washed repeatedly with warm PBS. Next, the bacteria were re-suspended in serum-free DMEM/F12, then diluted in serum-free media to obtain a multiplicity of infection (MOI) of 10 bacteria per host cell. The diluted bacteria were added onto the seeded cells and the well plates were spun down at 215 g for 2 minutes. The infections were then incubated at 37˚C. Two hours later, the cells were washed with warm PBS supplemented with magnesium and calcium (PBS +/+) (Corning, Cat. No: MT21030CV) then the media in each well was replaced with fresh DMEM/F12 with 10% FBS containing 50 µg/mL gentamicin to kill extracellular bacteria. The infections were incubated at 37˚C for a total of 1.5-6 hours.

4.3.3. Immunofluorescence Staining and Microscopy

Samples for immunofluorescence staining were washed three times with warm (37ºC) phosphate buffered saline (PBS), fixed with warm 3% paraformaldehyde for 15 minutes, then incubated in -20ºC acetone for 8 minutes then air dried. The coverslips were then blocked with 5% NGS in PBS containing 0.0005% Tween-20 and 0.1% bovine serum albumin (TPBS/BSA). Afterwards, the samples were incubated separately with a mouse anti-Ube2N (Invitrogen Cat. No: 37-1100) diluted at a concentration of 0.01 µg/µL or mouse anti-ezrin (Developmental Studies Hybridoma Bank Cat No: CPTC-Ezrin-1) antibody diluted at a concentration of 0.054 µg/µL in TPBS/BSA at 4˚C overnight.

Following the incubation with the primary antibodies the coverslips were washed three times with TPBS/BSA and then incubated with Alexa-488 conjugated goat anti-mouse antibodies (Invitrogen Cat. No: A11001) diluted at a concentration of 2 µg/µL in TPBS/BSA at room temperature for two hours. The coverslips were then washed another three times with TPBS/BSA and incubated with Alexa-594 conjugated phalloidin (Molecular Probes Cat. No: A12381) diluted at 1:10 in TPBS/BSA at room temperature for 15 minutes. Coverslips were mounted in Prolong Diamond antifade with DAPI (Molecular Probes Cat. No: P36962). Representative images were taken using a Leica DMI4000B inverted microscope fitted with a Hamamatsu Orca R2 CCD camera.

Actin clouds, comet tails, and listeriopods were then enumerated from the resulting images. A bacterium that had an unbroken ring of actin surrounding the bacterium was considered an actin cloud-forming bacterium. Comet tail-forming bacterium were determined as bacterium that had an accumulation of actin on one end of the bacterium. Lastly, listeriopods were identified as comet tails that were immunolabelled with the ezrin antibody.

4.3.4. *L. monocytogenes* Invasion Assay

PtK2 cells were seeded then grown to 100% confluency on 24-well CELLBIND plates (Corning). Dimethyl sulfoxide (DMSO) or 2 µM NSC697923 were added to the media 1 hour before the infections and remained in the media for the duration of the infections. The *L. monocytogenes* infections were conducted using an MOI of 10 bacteria for each host cell. After 1 hour of infection, the media was replaced with fresh culture media also containing 50 µg/mL gentamicin. Two hours post-infection, the cells were washed three times with warm PBS +/+. The host cells were then permeabilized using PBS with 1% Triton-X100 to release the internalized bacteria, then serially diluted using BHI broth. Each dilution was plated on BHI agar and incubated at 37˚C for 24 hours. Bacterial colonies were enumerated from each dilution and the data from triplicate wells were averaged for each trial.

4.3.5. Double Immunofluorescence Staining of internalized *L. monocytogenes* (Inside/Outside Staining)

PtK2 cells were seeded then grown to 100% confluency on 12 mm coverslips in a 24-well plate. The infections were conducted similarly to the *L. monocytogenes* invasion assay, however instead of permeabilizing with 1% Triton-X100, the cells were fixed with warm (37˚C) 3% Paraformaldehyde for 15 minutes. Next, the cells were washed two times with PBS, blocked with 5% NGS in PBS/BSA, and incubated with rabbit anti-*L. monocytogenes* antibodies (BD Difco Cat. No: DF2302500) diluted to 8.2 µg/µL in PBS/BSA at 37˚C for 1 hour. To label extracellular bacteria, the cells were subsequently incubated with Alexa-594 conjugated goat anti-rabbit antibodies (Invitrogen Cat. No: A11012) diluted at 2 µg/µL in PBS/BSA at 37˚C for 1 hour. Then, PBS containing 0.2% Triton-X100 was used to permeabilize the cell membranes and the coverslips were then incubated in 5% NGS in TPBS/BSA. To label the intracellular bacteria, the coverslips were incubated in rabbit anti-*L. monocytogenes* antibodies diluted at 8.2 µg/µL in TPBS/BSA and then with Alexa-488 conjugated goat anti-rabbit antibodies diluted at 2 µg/µL in TPBS/BSA. Alexa-350 conjugated phalloidin (Molecular Probes Cat. No: A-22281) was used to stain for filamentous actin and the coverslips were mounted using Prolong Diamond with DAPI.

4.3.6. *L. monocytogenes* Infection Foci Assay

PtK2 cells were seeded then grown to 100% confluency on 12mm coverslips in 24-well plates. The *L. monocytogenes* infections were conducted using an MOI of 0.01 bacteria for each host cell. Two hours after the infections, spent media was replaced with fresh media with 50 µg/mL gentamicin to kill extracellular bacteria. To study inhibition of Ube2N, 2 µM NSC697923 was also added to the fresh media and compared to DMSO (carrier buffer) controls. Following this media change, the infections were incubated at 37˚C for 4 hours, then fixed for immunofluorescence staining of *L. monocytogenes*. Representative images were taken of infection foci. The area of bacterial spread was determined by taking the images from the immunofluorescence staining of *L. monocytogenes* and creating an area mask using ImageJ[319]. Briefly, fluorescent intensity images thresholds were adjusted to remove background noise and then a binary mask was created. The resulting binary mask was dilated and smoothened

to define the area of bacterial spread and then the area of spread was measured in pixels to get the corresponding area in micrometers.

4.3.7. Immunoprecipitation of Ube2N complexes in *L. monocytogenes*-infected cells

PtK2 cells were seeded to 100% confluency in 6-well plates. The *L. monocytogenes* infections were conducted as mentioned previously using an MOI of 10 bacteria per host cell. Following the infections, the cells in each well were lysed using 80 µL RIPA lysis buffer 150 mM sodium chloride, 50 mM Tris pH 7.5, 5 mM ethylenediaminetetraacetic acid (EDTA), 1% Nonidet P-40, 1% deoxychloic acid, 0.1% sodium dodecyl sulfate) supplemented with cOmplete Mini protease inhibitor cocktail (Roche Cat. No: 11836153001). The lysates from 10 wells were pooled and incubated with 5 µg normalized mouse IgG antibodies and 25 µL Protein G Dynabeads (Novex Cat. No: 10003D) at 4˚C for 1 hour. Afterwards, the IgG and Dynabeads were separated and the pre-cleared lysates were divided into two fresh microfuge tubes. These lysates were then incubated with either 5 µg mouse anti-Ube2N or 5 µg normalized mouse IgG and then incubated at 4˚C overnight. The next day, 25 µL of Protein G Dynabeads were added and incubated at 4˚C overnight. To collect the immunoprecipitated complexes, the incubated lysates were removed and the Dynabeads-bound protein complexes were washed five times with tris-buffered saline (TBS). Protein complexes were then collected by adding 45 µL of sample buffer (0.375M Tris pH 6.8, 12% SDS, 60% glycerol, 0.6M DTT, 0.06% bromophenol blue) and boiling the samples at 100˚C for 10 minutes. The samples were then resolved on 10% sodium dodecyl sulfate polyacrylamide (SDS-PAGE) gels. The gel was either stained using the Pierce Silver Stain kit (Thermo Scientific Cat. No: 24612) or transferred on a nitrocellulose membrane for immunoblotting. The blotted nitrocellulose membrane was then blocked with 4% BSA or 4% BLOTTO (non-fat dry milk) (Santa Cruz Biotechnology, Cat. No: sc-2325) in TBS with 0.1% Tween-20 (TBST). The blots were then incubated in mouse anti-Ube2N (Invitrogen, Cat. No: 37-1100) antibodies diluted at 0.0005 µg/µL in TBST or mouse anti-actin antibodies (Abcam, Cat. No: ab3280) diluted at 0.0002 µg/µL in TBST at 4˚C overnight. The blots were then incubated with horseradish peroxidase-conjugated goat anti-mouse antibodies (Invitrogen Cat. No: G21040) diluted at 0.0002 µg/µL in TBST at room temperature for 2 hours. Successive washes with TBST and TBS were performed to remove unbound antibodies. To develop the immunoblots, the membrane was

incubated in 6 mL of Luminata Crescendo Western HRP substrate (Merck Millipore Cat. No: WBLUR0500) at room temperature for 5 mins, then chemiluminescence was captured using a Fujifilm LAS4000 chemiluminescent scanner.

4.3.8. Mass spectrometry identification of immunoprecipitated proteins

Proteins were excised and digested out of the gel as described (Chan et al., 2006). The resulting peptides were purified by solid phase extraction on C-18 STop And Go Extraction (STAGE) Tips [327] and analyzed by Bruker Impact II QToF[328] using 20 min peptide separation. The data was searched using MaxQuant[329] version 1.5.8.3 with protein databases retrieved from UniProt under *Listeria monocytogenes* and all mammalian species.

4.3.9. Subcellular Fractionation of whole cells

PtK2 cells were seeded on 80 mm culture dishes. Cells were washed twice with ice cold PBS prior to collecting the cells. Total cell lysate was collected by incubating the cells in RIPA lysis buffer. The lysates were centrifuged to remove cellular debris and the supernatant was collected. The Subcellular Protein Fractionation Kit for Cultured Cells (Thermo Scientific Cat. No: 78840) was used to obtain cytosolic, membrane, nuclear and cytoskeletal fractions from PtK2 cells in 10 cm culture dishes. Collected protein fractions were quantified using the Pierce bincinchoninic acid protein quantification kit (Thermo Scientific Cat. No: 23225). Protein samples were then loaded onto a 10% SDS-PAGE gels then blotted onto nitrocellulose membranes. Afterwards, the membranes were blocked with either 4% BSA or 4% BLOTTO for 1 hour prior to incubations with primary antibodies. The following antibodies were diluted in TBST with 1% BSA and were used to probe the membranes at 4°C overnight: mouse anti-Ube2N (0.0005 µg/µL) (Invitrogen Cat. No: 37-1100), mouse anti-actin (0.0002 µg/µL) (Abcam Cat. No: ab3280), mouse anti-GAPDH (0.004 µg/µL) (Developmental Studies Hybridoma Bank Cat. No: DSHB-hGAPDH-4B7), mouse anti-Atp1a1 (0.008 µg/µL) (Developmental Studies Hybridoma Bank Cat. No: a6F), and mouse anti-H2A (0.004 µg/µL) (Proteintech Cat. No: 66095-1-IG). The membranes were washed successively with TBST and then incubated with HRP-conjugated goat anti-mouse antibodies diluted at 2 µg/µL in TBST at room temperature for 2 hours. Then, the membranes were repeatedly washed with TBST and

TBS prior to developing. Developing was conducted by incubating the membranes in Luminata Crescendo Western HRP substrate and then imaging the membranes using a Fujifilm LAS4000 chemiluminescent scanner.

4.3.10. Protein binding assays by Far Western Blotting

Far Western blotting was conducted based on the protocol by Wu and colleagues[330]. Purified actin (Cytoskeleton Cat. No: APHL99-A), Ube2N (Abcam Cat. No: ab95900), and Ube2D1 (Abcam Cat. No: ab90023) were obtained commercially. 2 µg of total cell lysate from PtK2 cells, actin, and BSA were loaded onto 10% SDS-PAGE gels. Consequently, the proteins were transferred onto a nitrocellulose membrane and then the proteins were denatured and renatured using decreasing concentrations of guanidine buffer (0-6 M guanidine-HCl, 100 mM NaCl, 20 mM Tris (pH 7.5), 0.5 mM EDTA, 10% glycerol, 0.1% Tween-20, 2% BLOTTO or BSA and 1 mM DTT19). The membranes were then blocked with 5% BLOTTO or 5% BSA in PBS with 0.05% Tween-20 (PBST) at room temperature for 1 hour, and then incubated with 1 µg/mL of either Ube2N, Ube2D1, or BSA in protein binding buffer (100 mM NaCl, 20 mM Tris (pH 7.5), 0.5 mM EDTA,

10% glycerol, 0.1% Tween-20, 2% BLOTTO or BSA and 1 mM DTT) at 4˚C overnight. The next day, mouse anti-Ube2N (0.0005 µg/µL), rabbit anti-Ube2D1 (0.0005 µg/µL), mouse IgG (0.0005 µg/µL) or rabbit IgG (0.0005 µg/µL) were used to detect binding of Ube2N or Ube2D1 to actin using the procedures outlined previously about western blotting. Similarly, total cell lysate, Ube2N, Ube2D1, and BSA were also loaded on a 10% SDS-PAGE gel, transferred on nitrocellulose membranes and prepared for probing with 1 µg/mL of purified actin. Afterwards, the blots were immunolabelled with mouse anti-actin (0.0002 µg/µL) or mouse IgG (0.004 µg/µL) were used to detect binding of actin to Ube2N or Ube2D1.

4.3.11. Wound Healing Assay

PtK2 cells were seeded and grown to 100% confluency on 18 mm circle coverslips. A wound on the monolayer was created by taking a sterile 20-µL pipet tip and scratching a line in the cell monolayer. The coverslip was then placed in a Chamlide IC Live cell imaging chamber and mounted on the Chamlide IC top-stage incubator system.

The cells were maintained at 37˚C and the chamber was regulated with 5% humidified CO2. Images were taken every 15 minutes and wound areas were traced and measured using ImageJ[319]. Individual cell tracking was done on ImageJ using the MtrackJ plugin[331]. X-Y coordinate plots were created using the Ibidi Chemotaxis and Migration tool.

4.4. Results

4.4.1. Ube2N is enriched at actin-rich structures during *L. monocytogenes* infections

L. monocytogenes generate actin-rich structures that ultimately enable the microbes to gain motility within their host cells and spread from cell-to-cell. To examine the potential for Ube2N to be involved at these structures, we immunolocalized the protein and found that it was concentrated at all actin-rich structures generated by *L. monocytogenes*; invasion sites, actin-clouds, comet tails and listeriopods (Figs. 4.1A, 4.1B). Ube2N recruitment was focused at the zone of actin polymerization and faded throughout the structure, which paralleled the actin concentration at those sites. When bacterial mutants that are unable to recruit actin to the bacteria were used, Ube2N remained cytoplasmic (Fig. 4.1B').

Key to the *L. monocytogenes* infectious process is their ability to invade the cells of their hosts. This process requires clathrin-mediated endocytosis[217]. This event harnesses actin dynamics to bring the bacteria into the eukaryotic cells. Because Ube2N was prominent at invasion sites (Fig. 4.1A), we examined its involvement in *L. monocytogenes* invasion in the presence of the Ube2N-specific inhibitor NSC697923[332,333]. Using gentamicin protection assays coupled with NSC697923, we found that bacterial counts were decreased by ~90% (Fig. 4.1C). To confirm that the calculated decrease was due to a defect in bacterial invasion and not bacterial replication, we performed inside/outside staining to visualize the infections in the presence of NSC697923. Here, we found the similar results (Figs. 4.1D, 4.1E), indicating that bacterial invasion was significantly hampered when Ube2N was inhibited.

Bacterial cell-to-cell spreading is also integral to *L. monocytogenes* infections. To determine the importance of Ube2N in this process, we calculated the distance of bacterial movement from the infection foci when in the presence of NSC697923 or

DMSO (carrier control). We found that in the presence of NSC697923 bacterial spreading was decreased by 40% (Fig. 4.2A, 4.2C, 4.2D). In cells with equivalent levels of bacteria-generated actin-rich structures, the number of listeriopods (determined by counting ezrin-positive comet tails) present during NSC697923 treatments were compared to DMSO controls where we found that their abundance was significantly decreased (Fig. 4.2B). This decrease corresponded to a proportional increase in the numbers of actin clouds present within the cells (Fig. 4.2E, 4.2G). Interestingly, comet tails remained unperturbed by NSC697923 (Fig. 4.2F) suggesting that Ube2N was functionally required only when actin-rich structures had membrane interactions.

4.4.2. Ube2N is a novel actin-binding protein

Because Ube2N seems to play a role in actin dynamics, there is the possibility that Ube2N may interact with components of the actin cytoskeleton. Using *L. monocytogenes* infections as a model, we infected PtK2 cells and immunoprecipitated Ube2N from the lysates. We then immunoblotted these samples and determined that actin co-precipitated with Ube2N (Fig. 4.3A). We confirmed this identification by mass spectrometry. To further confirm this novel interaction, we used purified actin to probe re-natured Ube2N on a nitrocellulose membrane, we did not detect any bound actin to the Ube2N band (Fig. 4.3B). However, Ube2N, and not Ube2D1 (which shares similar domains with Ube2N), was able to bind to re-natured actin on a nitrocellulose membrane (Fig. 4.3C). This suggests that Ube2N can bind directly to actin when in its native conformation. Next, we examined which subcellular fractions of PtK2 epithelial cell lysates contained both Ube2N and actin. Ube2N was concentrated in the cytosolic and cell membrane fractions (Fig. 4.3D). This suggests that the Ube2N we immunoprecipitated (Fig. 4.3A) could be either the cytosolic or membrane-bound species. However, the absence of Ube2N in the cytoskeletal fraction suggests that Ube2N function with the cytoskeleton may be more transient since Ube2N was also inconsistently observed at *L. monocytogenes* comet tails. Taken together, the actin-binding role of Ube2N may be most crucial when actin interacts with structures at the plasma membrane.

4.4.3. Ube2N is a novel protein involved in actin-based motility

To further our study, we examined whether the lamellipodia in migrating cells also contained Ube2N, as those structures are also actin-rich and membrane associated. Immunolocalization of Ube2N in motile cells showed that it was concentrated within those structures at the leading edge of migrating cells (Fig. 4.4A). Furthermore, inhibiting Ube2N using NSC697923 altered the morphology of the leading edge of the cells and Ube2N, which caused a focused band of Ube2N at the lamellipodia periphery (Fig. 4.4B). We also observed this intense accumulation of Ube2N at the edge of the lamellipodia in cells infected with *actA*-deficient *L. monocytogenes* (Fig. 4.5).

Using wound-healing assays to study cell motility, we found Ube2N inhibition (through NSC697923 treatment) blocked the ability of the wound to seal (Fig. 4.4C, 4.4D). Individual tracking of the cells at the wound edge showed that there was barely any displacement in the Ube2N-inhibited cells (Fig. 4.4E) as cells with functional Ube2N (DMSO-treated) moved towards the centre of the wound, but the NSC697923-treated cells showed either little, sideward or reverse movement (Fig. 4.4F).

4.5. Discussion

The canonical role of E2 ubiquitin-conjugating enzyme Ube2N is to position activated ubiquitin monomers onto the growing chain of a Lysine 63-linked polyubiquitin tag on a substrate. This function requires cofactors such as Ube2V1 (or Uev1A) and Ube2V2 (or MMS2), which help align Ube2N with the E3 ligase that covalently joins the ubiquitin molecule from Ube2N with the polyubiquitinated substrate[167]. In NFκB signalling, Ube2N binds with its cofactor Ube2V1 and the E3 ligase TRAF6 and this activates downstream complexes to start gene transcription[166,334]. In DNA damage repair, Ube2N binds with Ube2V2 to ubiquitylate MDC1 to initiate the DNA damage response [335,336]. Notably, Ube2N has been implicated in cancer metastasis. Its binding partner Ube2V1 plays a role in regulating metastasis of breast cancer and Ube2V1 overexpression has been shown to increase movement in wound healing assays[337]. Our study suggests that Ube2N is the key protein linking Ube2V1 to the actin cytoskeleton. Ube2N is localized to actin-rich structures vital to cell motility and loss of Ube2N function impeded cell movement.

The interaction of the actin cytoskeleton and the plasma membrane defines cell motility as protein complexes drive the polymerization of actin and generate the pushing of the plasma membrane forward[19]. Thus, characterizing key components of these protein complexes is crucial for understanding the driving force of cell motility. Interestingly, Ube2N inhibition does not completely obliterate actin dynamics at the plasma membrane since our assays showed that *L. monocytogenes* can still generate actin structures at the membrane and actin-rich lamella and filopodial protrusions were still formed in motile PtK2 cells. Even though Ube2N function may not be required for actin polymerization, it may be involved in the regulation of the actin architecture along the plasma membrane. Aside from this, a previous study has shown that expression of Ube2N is upregulated in metastatic breast cancer and that silencing of Ube2N led to downregulation of adhesion proteins (VCAM1, ICAM1, and CD44) and actin-associated proteins (ACTG2 and CNN2)[338]. Although the co-dependent regulation of cell-motility-related genes provide further evidence that Ube2N plays a pivotal role in actin-based cell motility, it is through our findings that we have solidified the empirical connection of Ube2N with actin and the plasma membrane, both of which are essential in driving cell movement.

More importantly, Ube2N function has always been associated with either a cofactor such as Ube2V1 and UBE2V2 or an E3 ligase such as TRAF6. Those functions focus on ubiquitylation of a substrate[167,333,339–342]. This dependence on other proteins is common with all E2 ubiquitin-conjugating enzymes, and none of these enzymes have been reported to bind directly to a substrate or target protein since substrate binding and specificity is dependent on the corresponding E3 ubiquitin ligase[165,343,344]. Here, we report a novel direct interaction of Ube2N with actin and we have shown *in vitro* that Ube2N is able to bind with actin in the absence of Ube2V1 or an E3 ligase. In previous *in vitro* studies, E2 enzymes were able to dimerize and the E2 conjugating function was conserved and used for autoubiquitination of the E2 enzymes[165]. Quite possibly, the dimerized form of Ube2N could activate a binding interaction with actin at the leading edge of cells to regulate actin dynamics at the plasma membrane. As NSC697923 prevents the formation of a thioester bond between ubiquitin and Ube2N[332,333], it is interesting to speculate that the Ube2N dimerization and actin binding may have been altered and which ultimately could have blocked the regulation of actin at the leading edge of cells.

Through our study, we have shown that Ube2N has a novel role in actin dynamics at the plasma membrane. This also provides the first implication of an E2 ubiquitin conjugating enzyme at actin-plasma membrane interface and this proposes a novel function for Ube2N outside of its role in ubiquitin-based cell signalling.

4.6. Figures

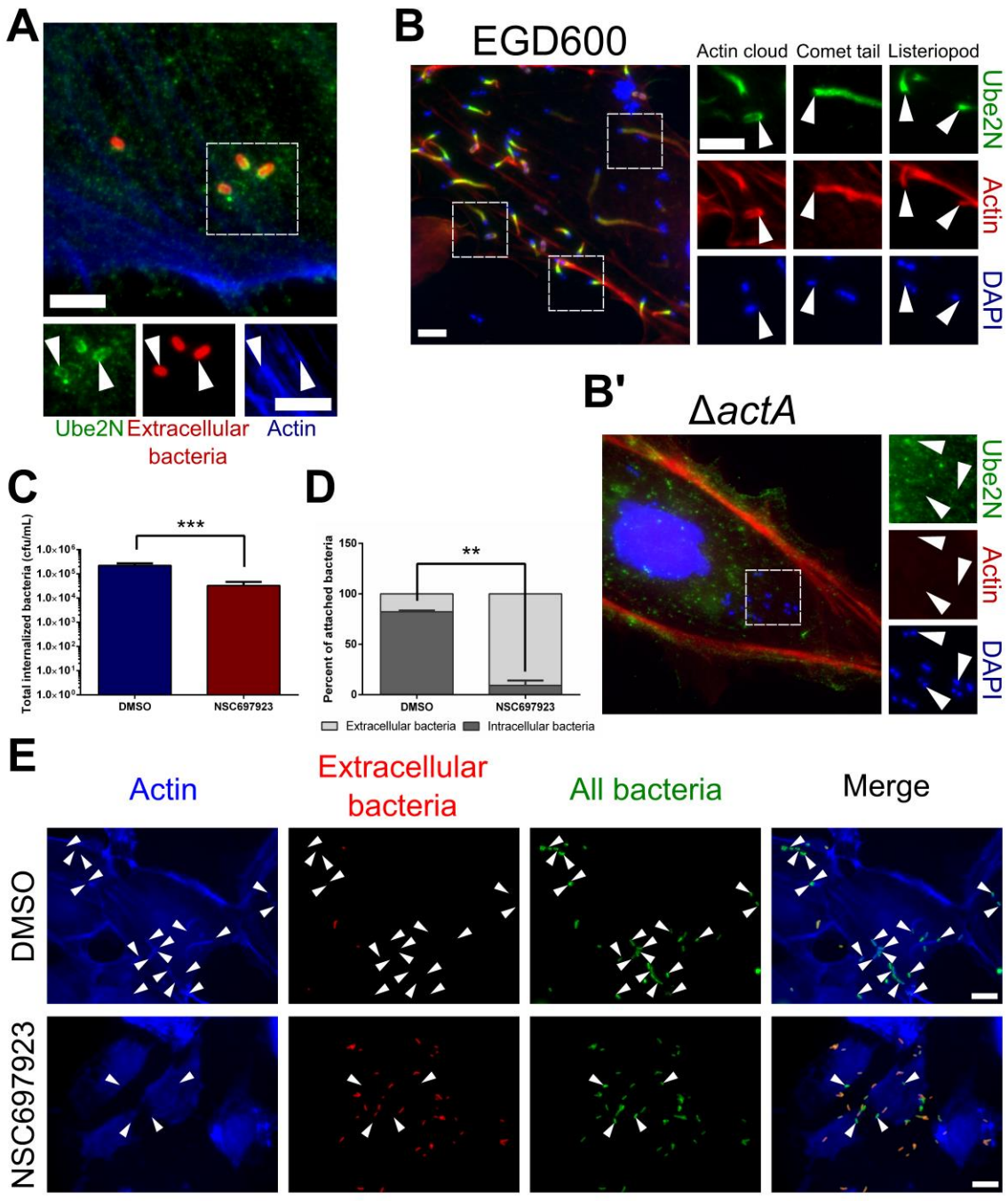

Figure 4.1: Ube2N is involved in bacterial invasion and is present at actin-rich structures generated by *L. monocytogenes*.

(A) Ube2N is recruited during *L. monocytogenes* invasion. Invading bacteria were immunolabelled (red) prior to cell permeabilization. Arrowheads indicate invading bacteria. Scale bars = 5 µm. (B, B') Ube2N colocalizes with actin-rich structures generated by *L. monocytogenes*. Ube2N colocalizes with *L. monocytogenes*-induced actin clouds, comet tails and listeriopods. The internalized *L. monocytogenes* Δ*actA* did not recruit Ube2N. Arrowheads indicate regions of

internalized bacteria. Scale bars = 5 µm. (C) Bacterial enumeration from lysed PtK2 cell monolayers after 2-hour infections with *L. monocytogenes*. Total internalized bacteria in Ube2N-inhibited cells was reduced to 11% of the total internalized bacteria in control cells. Error bars indicate standard error of mean of four trials with triplicate wells for each treatment. *** $P<0.001$ using Student's *t* test with Welch's correction. (D) Quantification of all attached bacteria after the gentamicin protection assay. Ube2N inhibition decreased the proportion of internalized bacteria. Error bars indicate the standard error of mean of three trials. ** $P<0.005$ using Student's *t* test with Welch's correction. (E) Representative images of immunolabelling of *L. monocytogenes* identifies extracellular bacteria in red or yellow while intracellular bacteria are exclusively green. Cell borders were identified by labelling filamentous actin using Alexa-350 conjugated phalloidin. Arrowheads indicate intracellular bacteria. Scale bars = 10 µm.

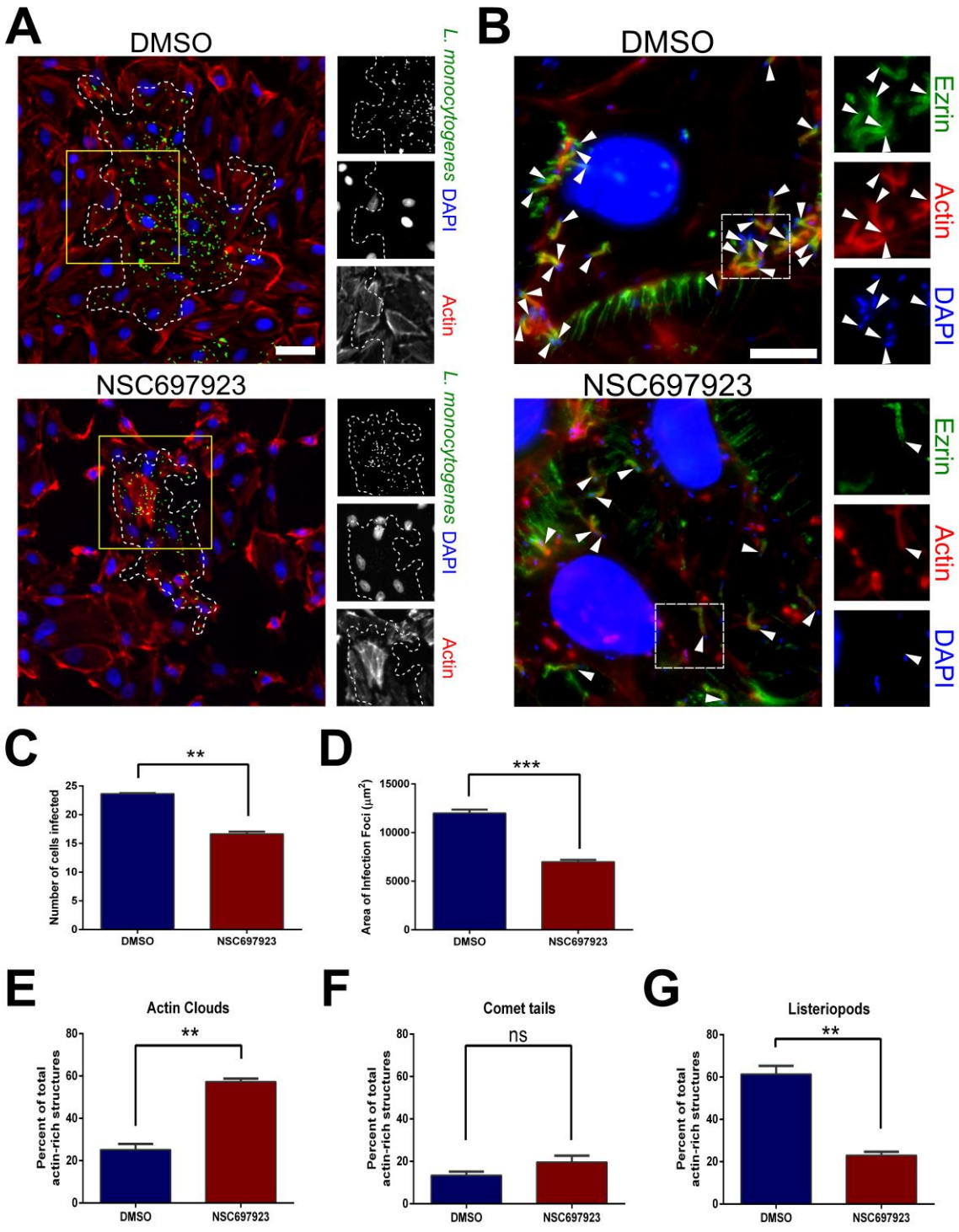

Figure 4.2: Ube2N inhibition reduced the actin-rich membrane protrusions formed by *L. monocytogenes*.

(A) *L. monocytogenes* formed smaller infection foci in Ube2N inhibited cells. Each infection focus was measured by creating a mask on ImageJ based on immunofluorescence labelling of the bacteria. Filamentous actin was labelled using Alexa-594 conjugated phalloidin and was used to

identify the cell borders. Dashed line indicates the border of each infection focus. Scale bar = 10 µm. (B) Immunolabelling of ezrin was used to identify listeriopods in DMSO or NSC697923-treated PtK2 cells. Filamentous actin was labelled using Alexa-594 conjugated phalloidin. Arrowheads indicate ezrin-positive listeriopods. Scale bar = 10 µm. (C, D) Quantification of the number of cells and area of each infection focus, respectively. Error bars indicate the standard error of mean from three trials. **P<0.005 using Student's *t* test with Welch's correction. ***P<0.001 using Student's t test with Welch's correction. (E- G) Proportion of actin-rich structures in *L. monocytogenes*-infected PtK2 cells. The proportion of listeriopods out of all the *L. monocytogenes*-generated actin-rich structures in Ube2N-inhibited cells is decreased compared to infected DMSO-treated cells. Error bars indicate standard error of mean for three trials. **P<0.005 using Student's *t* test with Welch's correction.

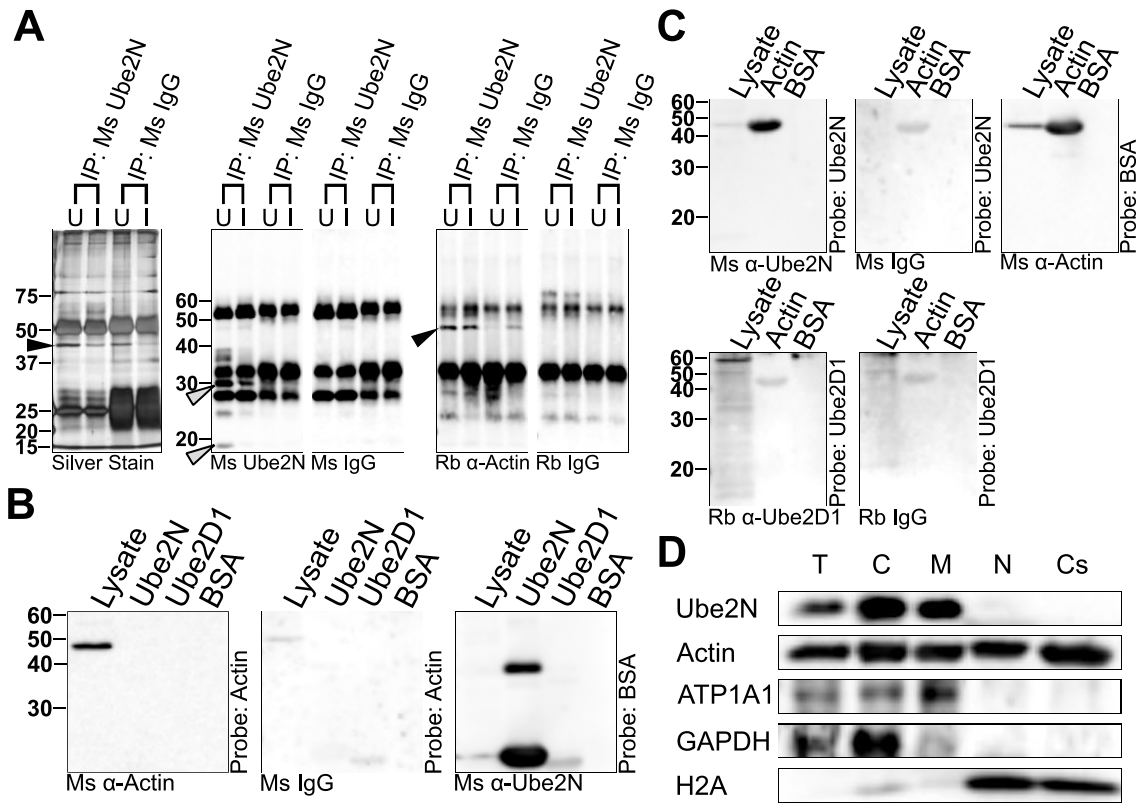

Figure 4.3: Ube2N binds directly to actin.
(A) Immunoprecipitation of Ube2N from *L. monocytogenes* infected PtK2 cells reveal a 42 kDa band of interest (black arrowhead in the silver stain gel). Western blot analysis shows Ube2N (gray arrowheads) was immunoprecipitated and actin (black arrowhead in the actin western blot) was co-immunoprecipitated with Ube2N. (U = uninfected lysates, I = *L. monocytogenes*-infected lysates) (B) Far Western Blotting of Ube2N and Ube2D1 shows that purified actin cannot bind to either Ube2N or Ube2D1. (C) Purified Ube2N binds to actin, but Ube2D1 cannot. (D) Subcellular fractionation of Ube2N from PtK2 cells shows that the interaction with actin is concentrated at the cytosol and the membrane fractions. (T = total cell lysate, C = cytosolic fraction, M = membrane fraction, N = nuclear fraction, Cs = cytoskeletal fraction)

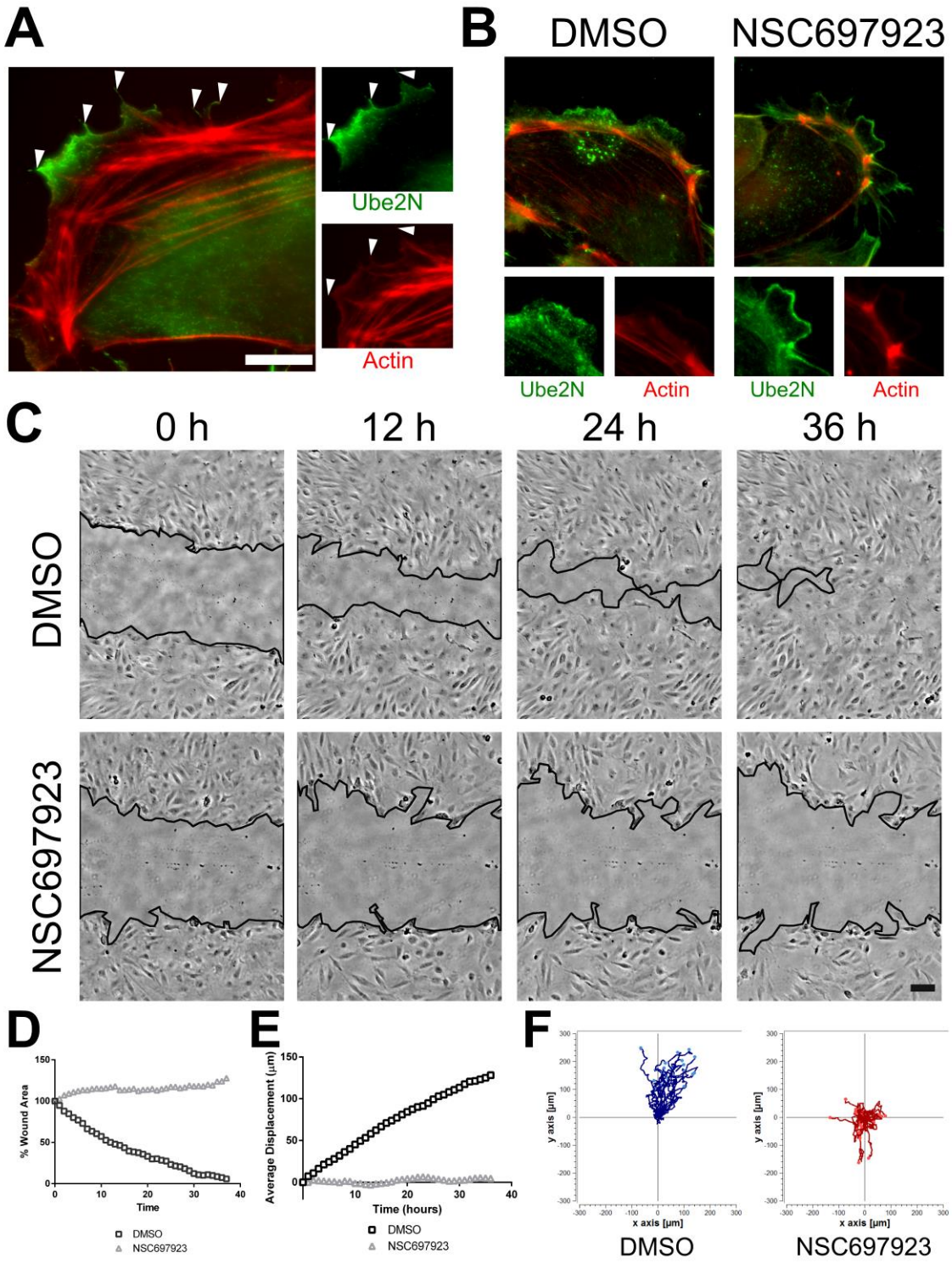

Figure 4.4: Ube2N is a novel actin-associated membrane-bound protein that is crucial for cell motility.

(A) Immunofluorescence labelling of Ube2N shows an enrichment at the protruding edge of a PtK2 cell. Filamentous actin is labelled using Alexa-594 conjugated phalloidin. Arrowheads indicate cell protrusions where Ube2N is enriched. Scale bar = 10 µm. (B) Ube2N is enriched at

the edge of a lamellipodium in NSC697923-inhibited cells. (C) Wound healing assay of DMSO or NSC697923-treated cells shows that Ube2N is involved in cell motility. Wound closure is achieved in DMSO-treated cells after 36 hours, while wound area is increased in NSC697923-treated cells. Black solid lines indicate the area of the wound. Scale bar = 40 μm. (D) The wound area was measured using ImageJ and percent of wound healing was determined by the proportion of the wound area at the time measured and the wound area at the start of the assay. (E) Individual cells at the edge of the wound were tracked using the MtrackJ plugin for ImageJ. The average displacement of DMSO-treated cells increased over time while the cells tracked in the NSC697923-treated monolayer had a significantly decreased average displacement over time. (F) The tracks for each cell analysed were plotted on an X-Y coordinate plane. DMSO-treated cells migrated tangentially from the wound line while most NSC697923-treated cells moved sideward or in a reverse direction from the wound area.

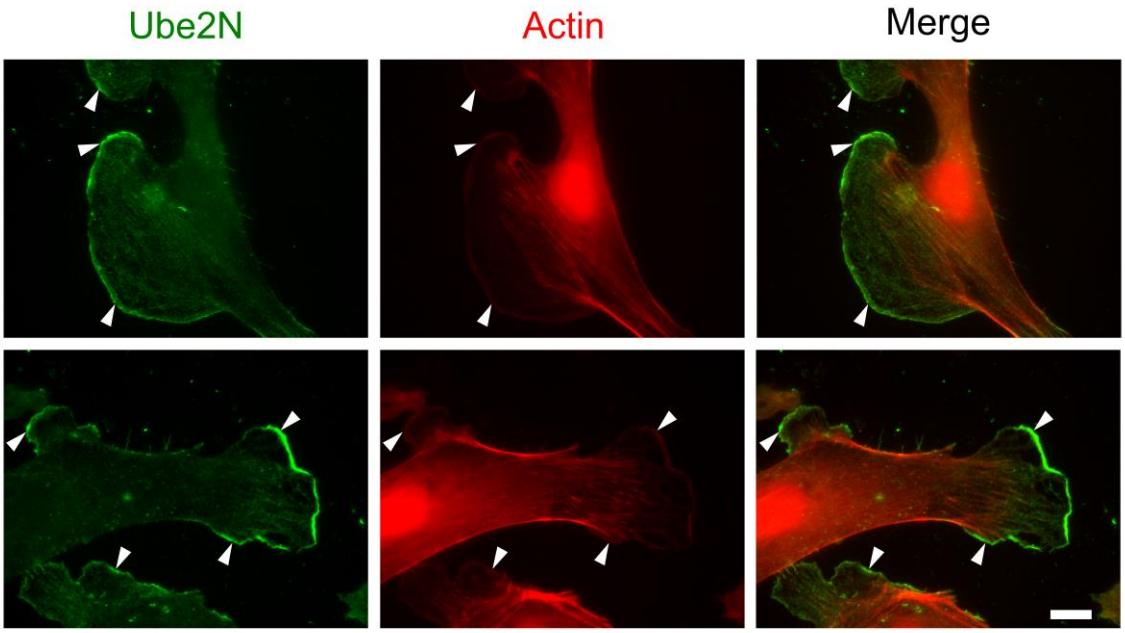

Figure 4.5: Ube2N is enriched at the lamellipodia.
PtK2 cells infected with the *L. monocytogenes actA* mutant showed increased formation of lamellipodia. Ube2N is concentrated at the edge of the lamellipodia. Arrowheads indicate sites of Ube2N enrichment at the lamellipodia. Scale bar = 10 µm.

Chapter 5.

Klebsiella pneumoniae disassembles host microtubules in lung epithelial cells

The content of this chapter is in revision for publication.

Chua MD, Liou CH, Bogdan AC, Law HT, Yeh KM, Lin JC, Siu LK, Guttman JA. (2018). *Klebsiella pneumoniae* disassembles host microtubules in lung epithelial cells. *Cell Microbiol*. (*In revision*).

MDC and JAG designed the project. MDC conducted all the bacterial infections and analysed the data. CHL, JCL, and LKS generated all the bacterial stocks and the *K. pneumoniae* genomic library. ACB identified KATNB1 as one of the microtubule severing proteins. KMY conducted the experiments for the preliminary identification of the microtubule disassembly phenotype and the identification of KATNAL1. KMY and HTL generated the live cell imaging of the microtubule severing. JAG supervised the data analysis and wrote the manuscript with MDC. All authors reviewed the manuscript.

5.1. Abstract

Klebsiella pneumoniae raises significant concern to the health care industry as these microbes are the source of widespread contamination of medical equipment, cause pneumonia as well as other multi-organ metastatic infections and have gained multi-drug resistance. Despite soaring mortality rates, the host cell alterations occurring during these infections remain poorly understood. Here, we show that during *in vitro* and *in vivo K. pneumoniae* infections of lung epithelia, microtubules are severed and then eliminated. This destruction does not require direct association of *K. pneumoniae* with the host cells, as microtubules are disassembled in cells that are distant from the infecting bacteria. This microtubule dismantling is dependent on the *K. pneumoniae* (Kp) gene *ytfL* as non-pathogenic *E. coli* expressing Kp *ytfL* disassemble microtubules in the absence of *K. pneumoniae* itself. Our data points to the host katanin catalytic subunit A like 1 protein (KATNAL1) and the katanin regulatory subunit B1 protein (KATNB1) as the gatekeepers to the microtubule-severing event as both proteins localize specifically to microtubule cut sites. Infected cells that had either of these proteins knocked-out maintained intact microtubules. Taken together, we have identified a novel mechanism in which a bacterial pathogen can cause microtubule destruction within the host epithelia.

5.2. Introduction

Klebsiella pneumoniae are pathogenic Gram-negative bacteria capable of causing a spectrum of illnesses ranging from pneumonia to meningitis [258,262,283,345]. *K. pneumoniae*-induced pneumonia has led to alarmingly worse survival rates than the pneumonia typically generated by *Streptococcus pneumoniae*, with *K. pneumoniae* mortality rates as high as 44% in highly infected individuals [262]. Unfortunately, only a few virulence factors have been characterized from these microbes. These include the capsular polysaccharide, outer membrane porins, and the type VI secretion system (T6SS), which show decreased virulence in bacteria mutated in their components[257,273,346–349]. The spread of *K. pneumoniae* is significant in hospital settings as these bacteria can form biofilms on contaminated hospital equipment[256,261]. Moreover, the misuse of antibiotics has led to many multi-drug resistant strains making treatment increasingly difficult[276–278,350,351]. As a result, hypervirulent strains have arisen and *K.*

pneumoniae has become one of the most common causes of multi-drug resistant bacterial infections[258]. Although their virulence is of concern, the sub-cellular mechanisms involved during their infectious process have remained largely elusive.

The microtubule-based cytoskeleton is an essential network for the trafficking of material throughout the cell, maintaining cellular structure and the regulation of an assortment of other cellular processes[1,2,97]. Microtubules are comprised of α- and β-tubulin dimers that arrange into protofilaments forming a hollow tube[97,352]. Due to their ubiquity in cells, bacterial pathogens have devised strategies to control microtubules for their benefits[353,354] (Radhakrishnan and Splitter, 2012; Mostowy, 2014).

To examine the sub-cellular alterations caused during *K. pneumoniae* infections, we examined the cytoskeleton of both infected A549 lung epithelial cells and lung epithelia from C57Bl/6J mice and found that the microtubule network was destroyed during the infections. This disassembly occurred through the release of a factor from *K. pneumoniae* into the supernatant as the spent supernatants of the infections caused the dismantling of microtubules in naïve cells. To identify the bacterial component responsible for the phenotype, we generated and screened a *K. pneumoniae* genome fosmid vector library containing 1000 random gene fragments of *K. pneumoniae* DNA that spanned the full genome. We identified *ytfL* as a crucial gene responsible for inducing microtubule disassembly. Through immunolocalization of microtubule severing enzymes and CRISPR-based knock-outs we found the katanin catalytic subunit A like 1 protein (KATNAL1) and the katanin regulatory subunit B1 protein (KATNB1) were the crucial proteins needed for the microtubule severing and ultimate network destruction caused by *Klebsiella pneumoniae*.

5.3. Materials and Methods

5.3.1. Cell Culture and Bacterial growth

A549 human lung epithelial cells (ATCC CCL-185) were grown in F12 media (Kaighn's modification) with 10% fetal bovine serum (FBS) or Roswell Park Memorial institute (RPMI) 1640 with 10% FBS. NCI-H23 human lung epithelial cells (ATCC CRL-5800), NCI-H358 human lung epithelial cells (ATCC CRL-5807), and NCI-460 human lung epithelial cells (ATCC HTB-177) were grown in RPMI 1640 media with 10% FBS.

All cultured cells were maintained at 37˚C with 5% CO2. *K. pneumoniae* K1-serotype (NVT1001) were obtained from a patient with liver abscesses in Taiwan (Table 1). The deletion mutants of *K. pneumoniae* were generated using in-frame deletion mutagenesis as mentioned previously (Table 1). To culture *K. pneumoniae*, frozen stocks were streaked on tryptic soy agar (TSA) plates and grown at 37˚C. Single colonies were inoculated into 7 mL tryptic soy broth (TSB) and grown as a shaking culture at 37˚C for 16 hours.

5.3.2. *K. pneumoniae* infections of cultured lung cells

A549 cells were seeded on glass coverslips in 24-well plates. Once confluent, the cell culture media was replaced with 300 µL of F12K containing 10% FBS. Bacteria were grown and 2 µL of the inoculum was added onto each well resulting in an MOI of ~10 cfu/host cell. Infected cells were then incubated at 37˚C for 4-8 hours. The cells were then fixed for immunofluorescent staining. To compare the different cultured lung cell lines, A549, NCI-H23, NCI-H358, and NCI-H460 were grown similarly on 24-well plates and 300 µL of RPMI with 10% FBS was used instead of F12K with 10% FBS. The same volume of bacteria was added, but the infection was incubated at 37˚C for 8 hours. For the spent supernatant experiments, ciprofloxacin was added to the infection supernatant at the 6-hour time point, and the infection was run for 1 additional hour. For denaturing studies, the spent supernatant was boiled at 100˚C for 10 minutes. Then, the spent supernatant was removed, and centrifuged at 13,000 rpm to pellet the bacteria. The spent supernatant was then added to naïve A549 cells and incubated for 4 hours, while the initial infection was fixed for immunofluorescent staining.

5.3.3. Immunofluorescence staining and microscopy

After the bacterial infections, the cells were fixed using -20˚C methanol for 10 minutes, permeabilized using PBS with 0.2% Triton-X100 for 5 minutes, then blocked with 5% normal goat serum in PBS with 0.05% Tween-20 and 0.1% bovine serum albumin (TPBS/BSA) for 20 minutes. The coverslips were then incubated in mouse anti-α-tubulin antibodies (Developmental Studies Hybridoma Bank, 12G10) diluted to 0.18 µg/µL in TPBS/BSA and either rabbit anti-KATNAL1 antibodies (Atlas Antibodies, HPA046205) diluted to 0.001 µg/µL or rabbit anti-KATNB1 antibodies (ProteinTech, 14969-1-AP) diluted to 0.004 µg/µL and incubated overnight at 4˚C. To immunolabel *K.*

pneumoniae, the coverslips were incubated in rabbit anti-*K. pneumoniae* antibodies (Invitrogen, PA1-7226) diluted to 0.1 µg/µL in TPBS/BSA. Afterwards, the cells were incubated with Alexa-488 conjugated goat anti-mouse antibodies (Invitrogen, A-11001) and Alexa-594 conjugated goat anti-rabbit antibodies (Invitrogen, A-11008) used at 2 µg/µL in TPBS/BSA for 2 hours at room temperature. Finally, the coverslips were washed with TPBS/BSA before mounting on glass slides using Prolong Diamond with DAPI. Fluorescence microscopy was conducted using a Leica DMI4000B inverted microscope fitted with a 100x oil immersion objective and imaged with a Hamamatsu Orca R2 CCD camera.

5.3.4. *K. pneumoniae* infections of C57BL/6J mice

Six to eight week old female C57BL/6J mice (Jackson Labs) were obtained then housed and maintained at the SFU animal care facility in accordance with the regulations of the Canadian Council of Animal Care. On the day of infection, the mice were anesthetized using 5% vaporized isoflurane. Overnight bacterial cultures were diluted in phosphate buffered saline (PBS), and the mice were intranasally inoculated with either 2.0 x 105 CFU of bacteria in two 10 µL aliquots (one aliquot per nostril) or two 10 µL aliquots of PBS. The mice were infected for 3 days, then euthanized by 5% carbon dioxide inhalation and cervical dislocation, and then the lungs were removed and immersion fixed in warm 3% paraformaldehyde for 3 hours, washed extensively in PBS then mounted onto cryostat stubs. 5 µm sections were taken from each lung and collected on poly-L-lysine coated slides. The sections on the slides were then permeabilized using PBS with 0.2% Triton-X100 for 5 minutes and subsequently treated for immunofluorescence staining of α-tubulin.

5.3.5. Western Blotting

Following the infections, A549 cells were washed with warm PBS, then lysed using RIPA lysis buffer. Equal amounts of protein were loaded for each lane on 10% sodium dodecyl sulfate polyacrylamide gels. Following the transfer to nitrocellulose, the membranes were blocked with 4% BLOTTO (Santa Cruz Biotechnology, sc-2325) in tris-buffered saline with 0.1% tween-20 (TBST) and then incubated with mouse anti-α-tubulin antibodies (Developmental Studies Hybridoma Bank, 12G10) diluted to 0.01 µg/µL in TBST with 1% BSA (TBST/BSA) overnight at 4˚C. The next day the membranes were

washed with TBST before incubating with horseradish peroxidase (HRP)-conjugated goat anti-mouse antibodies (Invitrogen, G21040) diluted to 0.0002 µg/µL in TBST/BSA. After successive washes, the membranes were analysed using the Millipore Luminata Crescendo HRP substrate and imaged on a Fujifilm LAS4000 chemiluminescent scanner. As a loading control, the membrane blot was stripped using stripping buffer, washed extensively, blocked then re-probed with mouse anti-calnexin antibodies (BD Biosciences, 610523) diluted to 0.25 µg/µL and HRP-conjugated goat anti-mouse antibodies (Invitrogen, G21040) diluted to 0.0002 µg/µL in TBST/BSA.

5.3.6. Creating the *K. pneumoniae* genome library and screening for the microtubule disassembly phenotype

K. pneumoniae genomic DNA from the NVT2001 strain was sheared and inserted into fosmid vectors using the Copycontrol Fosmid Library Production Kit (Epibio). Genomic DNA was sheared into approximately 25-40 kb fragments then inserted into the pCC2FOS vector (Epibio). The packaged vectors were transduced into Escherichia coli (EPI 300 strain) using the MaxPlax Lambda phage. The transduced bacteria were grown on Luria-Bertani (LB) media with 12.5 µg/mL chloramphenicol and single clones were isolated. One thousand bacterial clones (FL clone) were generated such that each FL clone contains a single random fragment of *K. pneumoniae* DNA. Then, the inoculum from each of 50 bacterial clones was combined to make pools of clones (FLP pool). The resulting genome library contained 20 pools of 50 FL clones with random *K. pneumoniae* DNA fragments (FLP pool) and 1000 bacterial clones with a single *K. pneumoniae* DNA fragment (FL clones) such that each FL clone belonged to a specific FLP pool.

To screen the library, A549 cells were seeded on 96-well glass-bottom plates and bacterial clones or pools of clones were grown in 500 µL brain heart infusion broth (BHIB) with 12.5 µg/mL chloramphenicol for 16 hrs as shaking cultures at 37˚C. The bacterial inocula were used either undiluted or diluted in BHIB with 12.5 µg/mL chloramphenicol up to 1:4 dilution. Once the A549 cells grew to confluency, fresh F12K with 10% FBS was added to the cells and 1 µL of each bacterial culture was used to infect each well of the glass-bottom well plate. The bacterial infections were incubated at 37˚C for up to 6 hrs. Afterwards, the cells were fixed using 37˚C 3% paraformaldehyde then stained for α-tubulin as mentioned above. The degree of microtubule disassembly

was then assessed and the clones that consistently showed high microtubule disassembly across trials were further examined. We screened the FLP pools to identify a subset of FL clones candidates. The FL clone that consistently showed microtubule disassembly was then used for bacterial infections as described above.

5.3.7. Insertion of clusters of *K. pneumoniae* genes into *E. coli*

The selected FL clone from the library contained several genes from *K. pneumoniae*. Gene clusters were PCR amplified from the fosmid vector and re-inserted as either clusters of adjacent genes or singular genes into the empty fosmid vector. The newly transduced *E. coli* clones were then selected and a similar phenotype screening as mentioned above was used to identify the precise gene that caused the microtubule disassembly.

5.3.8. Live cell imaging

A549 cells were grown on 18mm circle coverglass in 12-well plates. After 24hours, mKate2-EB3 (Evrogen, FP316) was transfected into the cells using jetPEI (Polyplus Transfections) according to the manufacturer's procedures to visualize the cellular microtubules without altering the amount of tubulin in the cells. The next day, the transfected cells were transferred into a Chamlide live cell imaging chamber and infected with 2 µL of wildtype *K. pneumoniae* inoculum. After 4 hours of infection, the imaging chamber was transferred to a Chamlide IC top stage incubator and then imaged using the Leica DMI4000B microscope and Hamamatsu Orca R2 CCD camera. The Chamlide incubator was maintained under identical infection parameters at 37˚C and supplemented with 5% humidified CO2.

5.3.9. Creating and infecting Katanin-deficient A549 cells

A549 cells were transfected with constructs containing scrambled guide RNA (gRNA) (Genecopoeia, pCRISPR-SG01), 3 KATNAL1-targeting gRNAs (Genecopoeia, HCP263473-SG01-3-B), or 3 KATNB1-targeting gRNAs (Genecopoeia, HCP200373-SG01-3-B). Single clones stably-expressing the gRNAs were selected, then seeded at 5000 cells per well and incubated with 2 µL of Cas9 nuclease lentivirus (Applied Biological Materials, K003) for 24 hrs. Then, the cells were selected for Cas9 expression

and protein levels of KATNAL1 and KATNB1 determined using immunofluorescence localization at the microtubule organizing centres of mitotic cells as well as immunoblotting for KATNAL1 or KATNB1. The generated stable cells were seeded on glass coverslips in 24 well plates and infected as mentioned previously. *K. pneumoniae* infections were carried out for 6 hrs at 37˚C and prepared for fluorescence microscopy of α-tubulin.

5.4. Results

5.4.1. Host cell microtubules are disassembled during *K. pneumoniae* infections

To examine the effects *K. pneumoniae* has on the host cytoskeleton, we studied the microtubule network of A549 lung epithelial cells at various *K. pneumoniae* infection time-points by localizing α-tubulin. In uninfected cells, microtubules appeared in radiating filamentous strands towards the edges of the cells (Fig. 5.1A). After 6-hour infections, the cells showed varying degree of microtubule network disassembly. Some cells had fully intact microtubule networks, others had no microtubules present, while many cells contained microtubules with random breaks along their lengths (Fig. 5.1A, 5.5B). Although *K. pneumoniae* has been found reduce actin filament levels[268], we found that microtubule disassembly precedes the alterations of the actin cytoskeleton (Fig. 5A). After 8-hour infections, none of the host cells had intact microtubules (Fig. 5.5B, 5.5C). This occurred without the host cell nuclei displaying any evident DNA condensation, which would have been indicative of the initiation of mitosis. The microtubule alterations did not require bacterial attachment or internalization into the host cell at the time of microtubule disassembly as cells far from the bacteria (at the end of the frame or not even in the same frame) had altered microtubules (Fig. 5.5B). Moreover, even though the proportion of host cells with attached bacteria did not increase over time, less intact cells were observed through the various infection timepoints (Fig. 5.5D). In addition, there was no noticeable affect on overall α-tubulin levels in the cells (Fig. 5.1B). The ability of microtubules to disassemble far from the location of the *K. pneumoniae* bacteria suggested that the bacteria may be releasing a factor to cause the microtubule disassembly to distant cells. To test this, following our standard 6-hour infections, ciprofloxacin was added to kill the bacteria. Following removal of the bacteria, we transferred the ciprofloxacin-treated spent supernatant to fresh A549 cells and saw the

same microtubule disassembly. (Fig. 5.1C). When we boiled the spent supernatant (instead of treating with ciprofloxacin), microtubules remained intact. This indicates that the secreted factor is most likely a released protein effector.

Expanding on our findings, we also examined other human lung epithelial cells. We recorded microtubule disassembly in all cell lines tested [NCI-23, NCI-358, and NCI-H460 lung cells] (Fig. 5.6A, 5.6B). To determine whether the observed collapse of the microtubule network was evident during *in vivo* infections, we infected C57/Bl6 mice intranasally with *K. pneumoniae* and examined the microtubules in the lung epithelium. Immunostaining of α-tubulin showed filamentous strands within and at the apical periphery of the epithelial cells in sham infected mice (Fig. 5.1D). In contrast, dramatic morphological changes were observed in *K. pneumoniae* infected epithelia (Fig. 5.1D) as the cells were shorter, had less staining in the area of the cilia and the microtubule network within the cells was dismantled.

5.4.2. Known virulence factors of *K. pneumoniae* are not responsible for microtubule severing

K. pneumoniae expresses virulence factors such as the capsular polysaccharide, outer membrane porins, and those secreted through a T6SS. Because all of these have been correlated to disease progression [257,273,346–348,355], we examined if any of those factors induced microtubule severing. Using mutated bacteria, we infected A549 cells for 6 hours and saw that all still caused microtubule disassembly indicating that none of those components were responsible for the microtubule severing phenotype. (Fig. 5.7)

5.4.3. *K. pneumoniae ytfL* is required for microtubule severing

To identify the *Klebsiella pneumoniae* gene(s) responsible for the observed microtubule disassembly phenotype, we screened a genomic library of *Escherichia coli* clones containing random ~40 kb segments of the *K. pneumoniae* genome (Fig. 5.2A). Initially, we infected A549 cells with the FLP pools to determine which pool of bacterial clones caused microtubule severing as those would be further pursued (Fig. 5.2B). We identified the “FLP 601-650 pool” of bacterial clones that reproducibly caused microtubule disassembly in A549 cells (Fig. 5.2C, 5.3A). We then screened the 50 clones in the FLP 601-650 pool and identified FL 647 as the clone containing genes that

cause the microtubule disassembly (Fig. 5.2D, 5.3A). Further examination of segments of genes in FL 647 was conducted by expressing each gene or small gene clusters into *E. coli* EPI 300 strain (Fig. 5.2E). Ultimately, we inserted only the *K. pneumoniae* gene *ytfL* (Kp *ytfL*) into *E. coli* EPI 300 and observed microtubule severing (Fig. 5.3B). *E. coli* also expresses the gene *ytfL* (Ec *ytfL*) but does not disassemble microtubules without the transduced Kp *ytfL* vectors (Fig. 5.3B).

The crystal structure of Kp ytfL has not been solved. However, to get an idea of the organization of the protein, we conducted bioinformatics analysis on the known amino acid structure of Kp ytfL. Using Phyre2 (www.sbg.bio.ic.ac.uk/phyre2/) [356], we identified 2 main domains of Kp ytfL – a putative N-terminal transmembrane domain consisting of 4 α-helices and a C-terminal domain that contains 6 α-helices and 11 β-sheets (Fig. 5.8A). Phyre2 predicted that the N-terminal domain contains four transmembrane domains but with low confidence, and thus, we used TMHMM (www.cbs.dtu.dk/services/TMHMM/)[357] to predict the location of the transmembrane helices. Phyre2 predicted with 100% confidence that the C-terminal domain of Kp ytfL shares a 24% amino acid identity with the *E. coli* magnesium efflux protein *corC* (Ec *corC*). Ec *corC* and the C-terminal domain of Kp ytfL have multiple binding domains that include an adenosine monophosphate (AMP) binding domain in the central pocket and two cystathionine β-synthase domains (Fig. 5.8B). Interestingly, Kp ytfL and Ec ytfL have additional amino acids on its C-terminal tail, which are absent in Ec *corC*. Strikingly, the C-terminal tail of Kp ytfL is predicted to be stabilized within its catalytic domain whereas the C-terminal tail of Ec ytfL dangles outside its catalytic domain (Fig. 5.8C). Several amino acids (N427, V431, E441, S442, and N445) that are present on Kp ytfL but absent on Ec ytfL could be responsible for the different orientation of this portion of Kp ytfL (Fig. 5.8D).

5.4.4. *K. pneumoniae*-induced microtubule severing is mediated by KATNAL1 and KATNB1.

Our observation of microtubule breaks and then the complete dissolution of the microtubule cytoskeleton as the infections progressed suggested that the *K. pneumoniae* infections caused microtubule severing, which led to the complete breakdown of microtubules in host cells. To confirm this, we conducted time-lapse imaging of *K. pneumoniae*-infected A549 cells expressing fluorescently-tagged EB3

protein (mKate2-EB3). mKate2-EB3 initially localized along the full length of microtubules, then showed microtubule severing and complete dissolution of the microtubule array (Fig. 5.9).

Microtubule severing in epithelial cells is caused by microtubule severing proteins, which include katanins, spastin, and fidgetins. We attempted to immunolocalize all three of the severing enzymes and found that the katanin catalytic subunit A1 like 1 protein (KATNAL1) and the katanin regulatory subunit B1 (KATNB1) localized precisely at the break in the microtubules suggesting a role in the cutting events (Fig. 5.4A). We then hypothesized that if these proteins are involved, then microtubule severing will not occur when we knock out KATNAL1 or KATNB1. To do this, we expressed scrambled or KATNAL1 specific guide RNA (gRNA) as well as the nickase Cas9. From this, we generated populations of scrambled gRNA-transfected cells (control) (Fig. 5.10A) and KATNAL1-deficient cells which had no KATNAL1 staining at the microtubule organizing center (Fig. 5.10A'). Even though we depleted this katanin protein, the microtubules were not altered in these cells (Fig. 5.10C). Western blotting of KATNAL1 showed that the protein levels of this protein was also reduced (Fig. 5.10D). After 6 hours of infection with *K. pneumoniae*, only 21% of host cells had intact microtubules, whereas 41% of KATNAL1-deficient cells had intact microtubules (Fig. 5.4B). Similarly, we knocked out KATNB1 (Fig. 5.10B') and intact microtubule networks were observed in 63% of *K. pneumoniae*-infected cells that were deficient of KATNB1 (Fig. 5.4B).

5.5. Discussion

Microtubule disassembly is common amongst bacterial pathogens. *Shigella flexneri* secretes the bacterial protein effector VirA, which cleaves α/β tubulin dimers, causing localized destabilization of microtubules around the bacteria[353,358]. *Pseudomonas aeruginosa*, secretes ExoY, which induces a signalling cascade in the host cell and causes instability of the microtubules[359,360] resulting in shorter and fewer host cell microtubules [156]. Our study is unique as the microtubule array is attacked in cells that are not in direct contact with the microbes. Our evidence that *K. pneumoniae* releases a protein and that Kp *ytfL* expression in laboratory strain *E. coli* causes the disassembly of microtubules together suggests several possible mechanisms. One possibility is that a portion of Kp ytfL, whether it is the entire periplasmic domain or just the short fragment at its C-terminal tail, could be the released factor responsible for

triggering the microtubule breakdown event. Whether this protein or protein fragment is endocytosed or binds to a receptor on the host cell surface to ultimately activate KATNAL1 requires further study. Alternatively, the periplasmic domain of Kp ytfL could potentially be the initiator of a signalling cascade either on the bacterial surface or the host cell surface and this leads to either the secretion of a bacterial protein effector or the activation of host cell secretory mechanism. In both instances, the mere addition of the Kp *ytfL* gene into non-pathogenic *E. coli* suggests that we found the activator of this novel mechanism.

Although bioinformatic predictions suggest that Kp ytfL and Ec ytfL have similar secondary structures, the fact that laboratory strain *E. coli* cannot cause microtubule disassembly in the absence of Kp ytfL suggests that differences between the two proteins are at the crux of the microtubule disassembly triggering event. We found that several residues present only on Kp ytfL allows for the hydrogen-bonding of its C-terminal tail within its catalytic domain. Based on the two possible mechanisms we have mentioned, this unique orientation of the Kp ytfL C-terminal tail could possibly allow for the cleavage of the C-terminal tail into a short peptide effector. Alternatively, it could stabilize the catalytic domain of Kp ytfL and enhance the activity of this protein to effectively initiate a signalling mechanism.

Within the cytosol, microtubules can only be cut by microtubule severing proteins such as katanins, spastins, and fidgetins [361–363]. Katanins form a complex containing a regulatory subunit and a catalytic subunit [131,133,139]. To sever microtubules, a regulatory subunit binds to the microtubule to recruit a katanin catalytic subunit that initiates microtubule severing[132–134]. We have shown that the regulatory subunit KATNB1 and one of the catalytic subunits KATNAL1 are involved in *K. pneumoniae*-triggered microtubule severing and that depletion of these proteins increased the number of host cells with intact microtubules. Interestingly, depleting KATNB1 yielded more intact cells than depleting KATNAL1. Perhaps the katanin catalytic subunit A 1 protein (KATNA1) that also has microtubule severing activity compensates for the loss of KATNAL1 and only the depletion of KATNB1, which is the regulatory subunit for both catalytic enzymes, resulted in more cells with intact microtubules.

Our findings indicate that *K. pneumoniae* utilizes a novel mechanism to alter the host lung epithelia. Kp ytfL is at the core of this event that ultimately activates the

microtubule severing proteins KATNAL1 and KATNB1 to completely eliminate the host microtubule network.

5.6. Figures

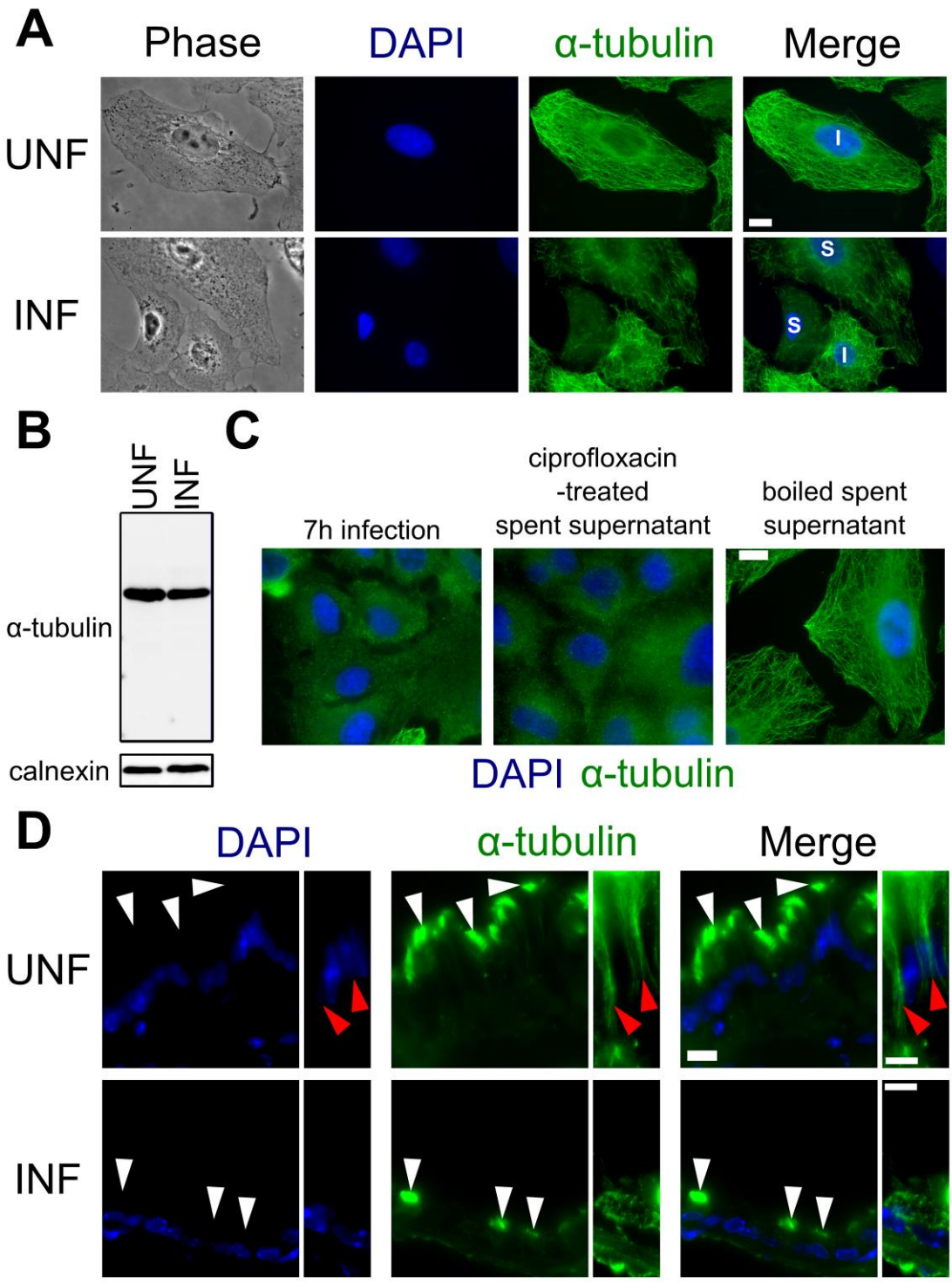

Figure 5.1: Disassembly of microtubules occurs in *K. pneumoniae*-infected A549 lung epithelial cells and lung epithelia from infected C57Bl/6J mice.

(A) Microtubules are severed in A549 cells during *Klebsiella pneumoniae* infections. The nuclei of each cell are labelled to indicate the state of the cytoplasmic microtubule network as I (intact microtubules) and S (severing microtubules). (B) Immunoblot of cell lysates collected after infection. Infected and uninfected samples show equivalent levels of α-tubulin. Anti-calnexin antibodies were used to determine lane loading levels. (C) Microtubules are disassembled in infected cells and cells treated with ciprofloxacin-treated spent supernatant. All microtubules remain intact when the spent supernatant is boiled. (D) Microtubules are absent in infected mouse lung epithelial cells. Rectangle panels show a region of the epithelia where brightness was enhanced to highlight cytosolic microtubules. Cilia are labelled with white arrowheads and red arrowheads point to cytosolic microtubules. DAPI (blue) shows DNA to identify individual cells. Scale bar =10 µm. In the rectangle panels, scale bar = 5 µm.

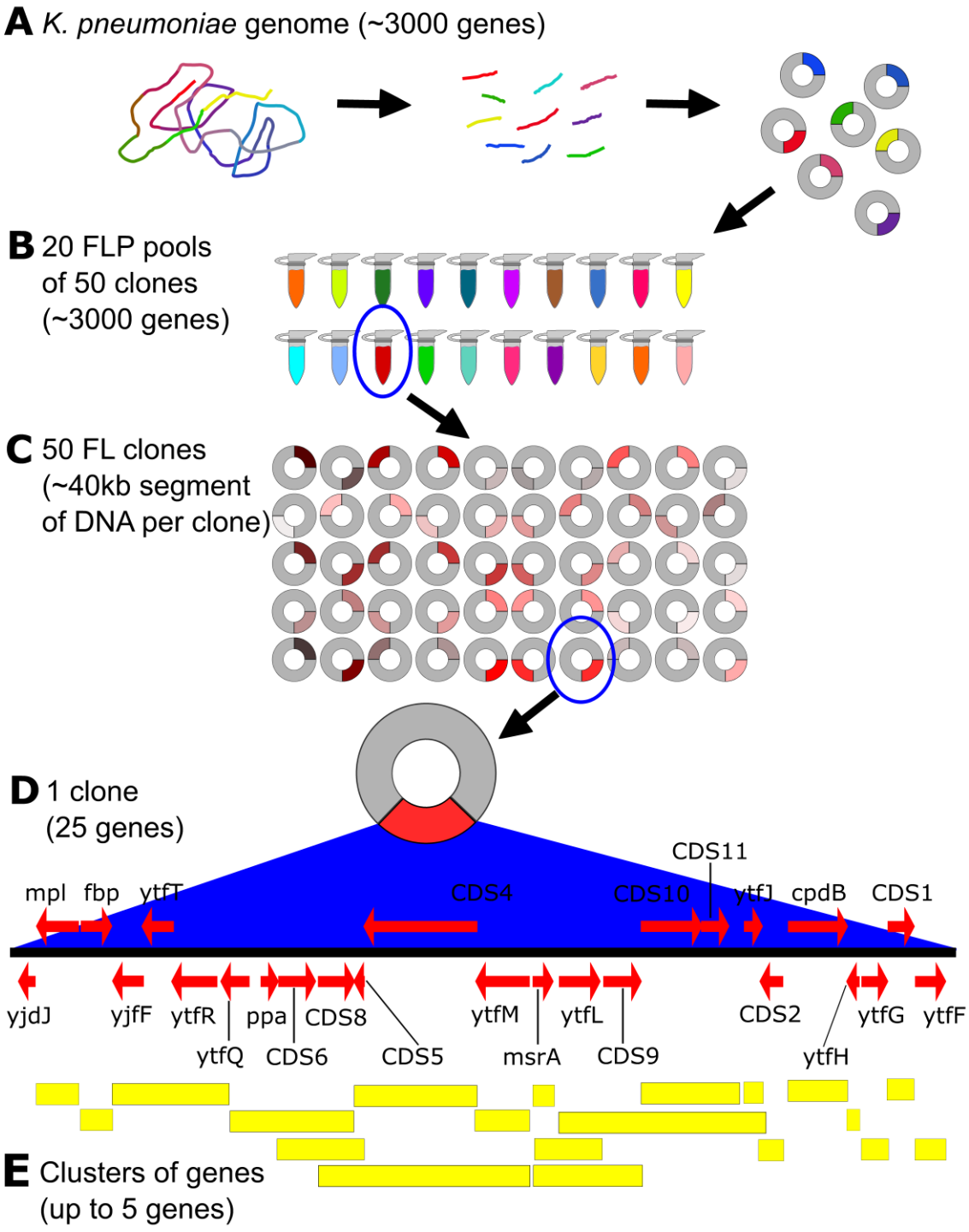

Figure 5.2: Schematic diagram of the screening strategy to uncover the *Klebsiella pneumoniae* gene responsible for host cell microtubule disassembly.

(A) Genomic DNA from *K. pneumoniae* (NVT-2001 strain) was sheared and packaged into vectors. (B) FLP pools were created by combining cultures from 50 E. coli clones. (C) Screening

of the 20 FLP pools identified a pool of 50 clones such that each clone contained a random ~40 kb segment of the *K. pneumoniae* genome. (D) A single clone containing 23 genes was able to consistently cause microtubule disassembly. (E) Single genes or clusters of genes from the identified clone were assessed for microtubule disassembly.

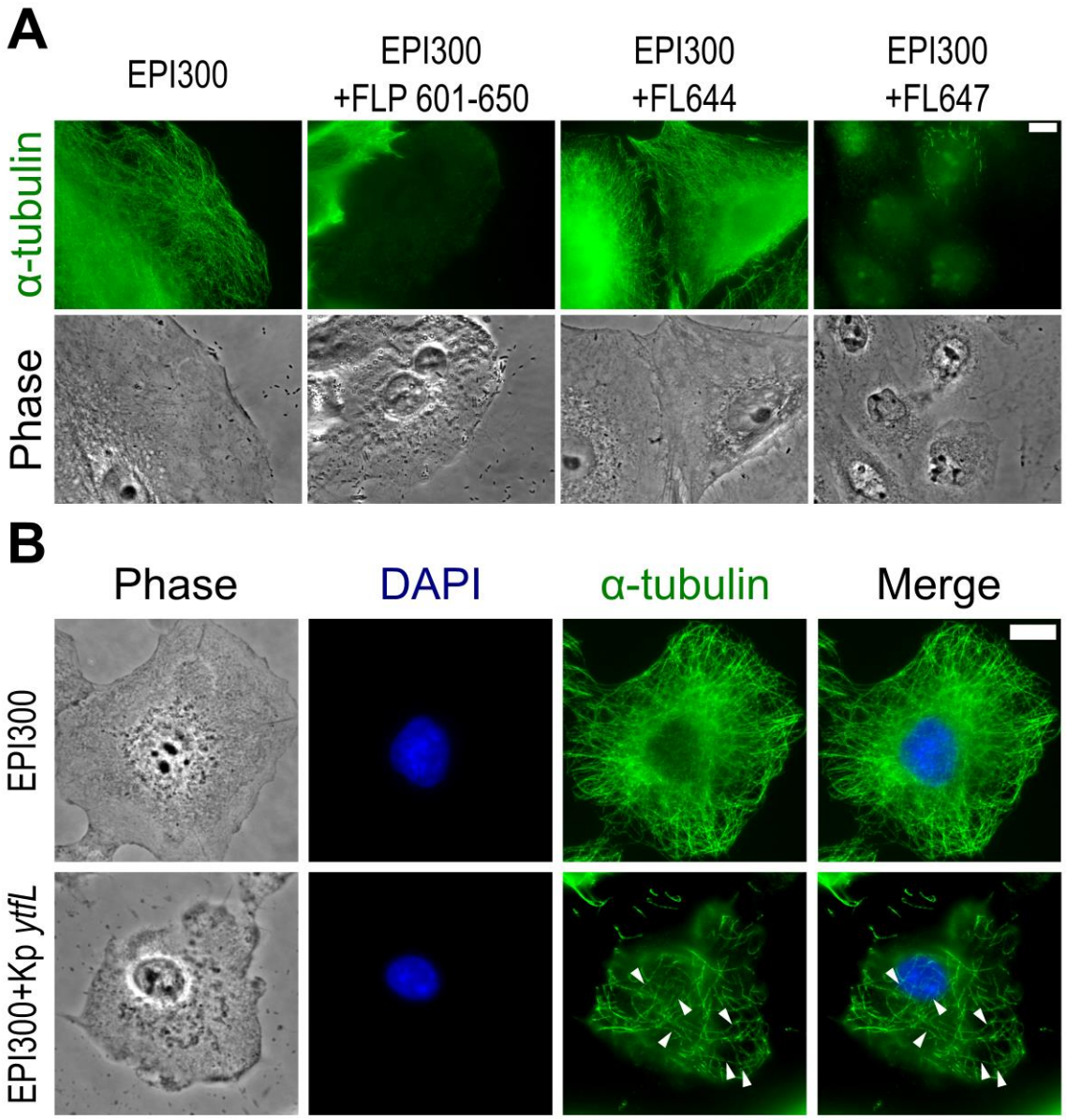

Figure 5.3: Kp *ytfL* causes microtubule severing.
(A) FLP601-650 and FL647 caused disassembly of microtubules in A549 lung cells. Cells were infected and fixed for staining with anti-α-tubulin antibodies. EPI300 alone does not cause microtubule disassembly. FLP601-650 contains a mix population of clones from FL601 to FL650. FL644 is an example of a clone that does not cause microtubule disassembly. FL647 consistently causes microtubule disassembly among the FLP601-650 bacterial clones and contains the gene Kp *ytfL*. Scale bar = 10 µm. (B) Infection with *E. coli* (EPI300 strain) does not cause microtubule severing. Infection with *E. coli* (EPI300 strain) expressing Kp *ytfL* causes microtubule severing (arrowheads) Scale bar = 10 µm.

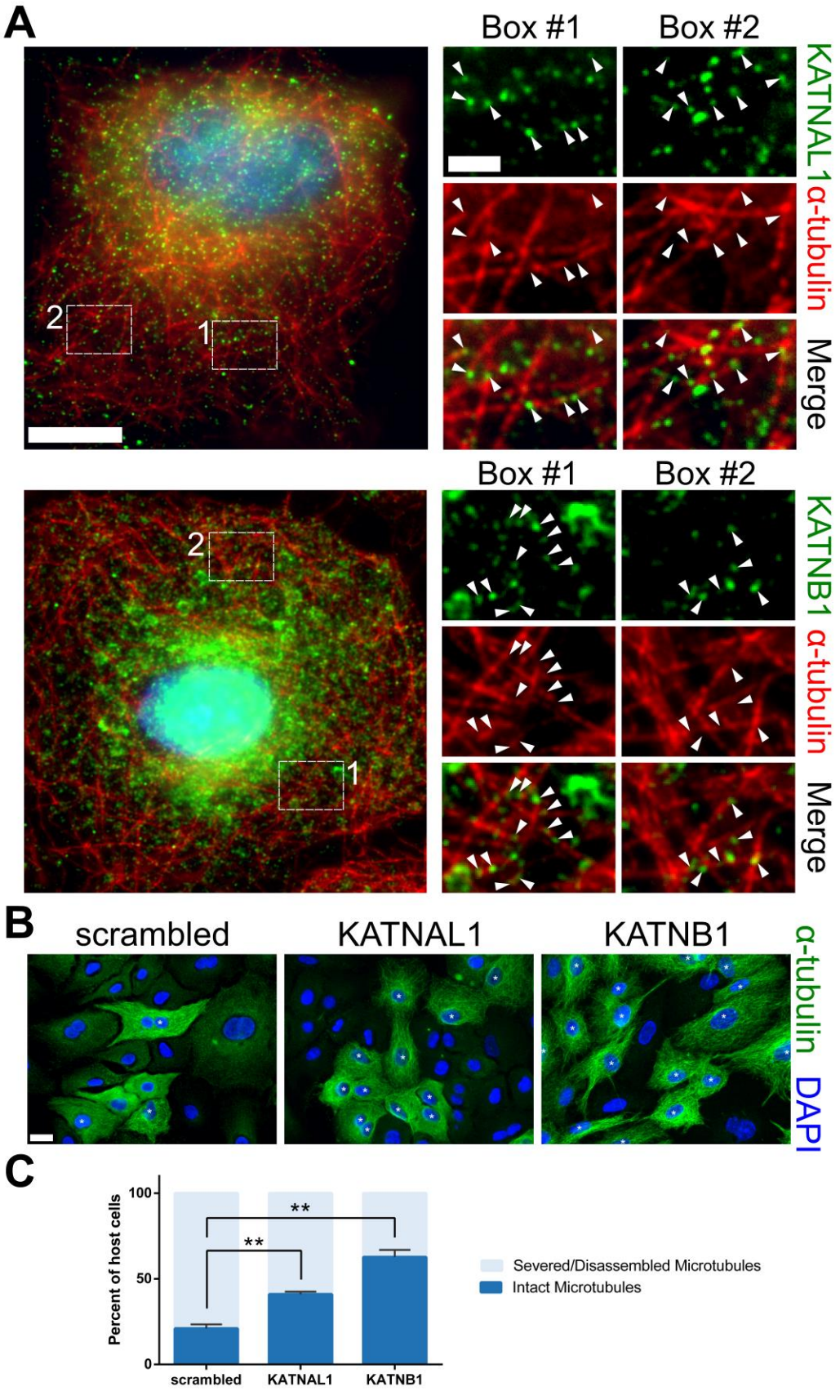
A
Box #1
Box #2
KATNAL1
α-tubulin
Merge
2
1
Box #1
Box #2
KATNB1
α-tubulin
Merge
2
1
B
scrambled
KATNAL1
KATNB1
α-tubulin
DAPI
C
Percent of host cells
100
50
0
**
**
scrambled
KATNAL1
KATNB1
Severed/Disassembled Microtubules
Intact Microtubules

Figure 5.4: KATNAL1 and KATNB1 are involved in microtubule severing during *Klebsiella pneumoniae* infections of A549 cells.

(A) KATNAL1 and KATNB1 (green and arrowheads) were immunolocalized to the cut sites on microtubules (red) during *K. pneumoniae* infections. DAPI (blue) was used to stain DNA. Scale bar = 10 µm. For Box #1 and Box #2 of each image, scale bar = 2 µm. (B) More host cells that are either KATNAL1 or KATNB1 deficient had intact microtubules compared to scrambled gRNA-treated cells. (*) indicate cells with intact microtubules. Scale bar = 20 µm (C) Quantification showed a significant increase in the number of host cells with intact microtubules in KATNAL1- or KATNB1-deficient cells. ** $P<0.005$ using Student's *t* test with Welch's correction.

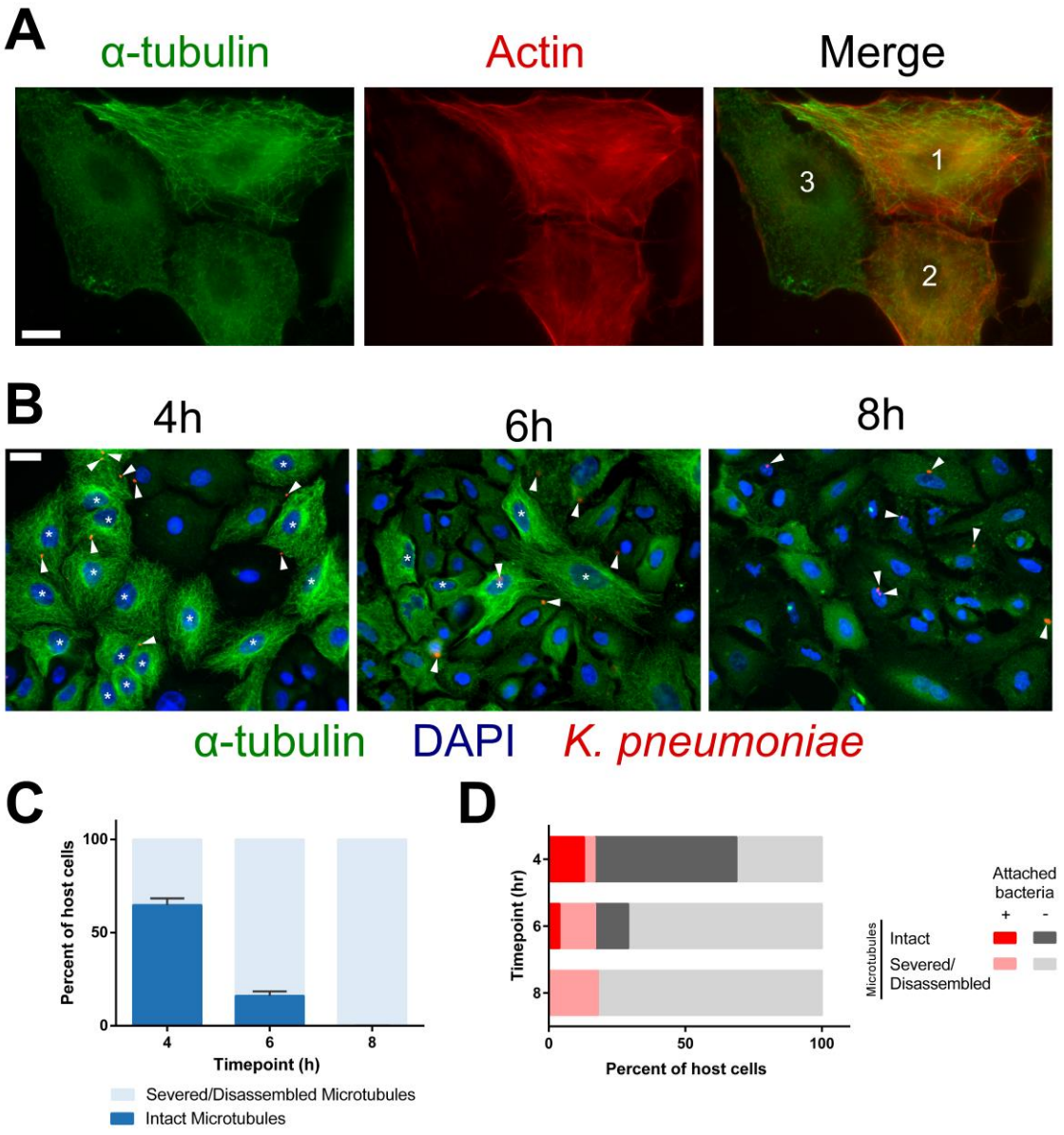

Figure 5.5: Microtubules are severed over time.
(A) Microtubule disassembly preceded the known reduction of actin filaments during *K. pneumoniae* infections. 1) Actin filaments were present when microtubules begin to sever. 2) When only microtubule fragments were in the cytosol, actin filaments were still present. 3) In cells with disassembled microtubules, traces of cortical actin remained within the host cell. Scale bar - = 20 µm (B) At later time-points of the infection, less cells had intact microtubules. At 8 hours, all cells had disassembled microtubules. Arrowheads indicate attached bacteria. (*) indicate host cells with intact microtubules. Scale bar = 20 µm (C) The percent of host cells with intact microtubules reduced over time. (D) While the proportion of host cells with attached bacteria did was consistently under 20% of host cells, more cells had severed or disassembled microtubules over time.

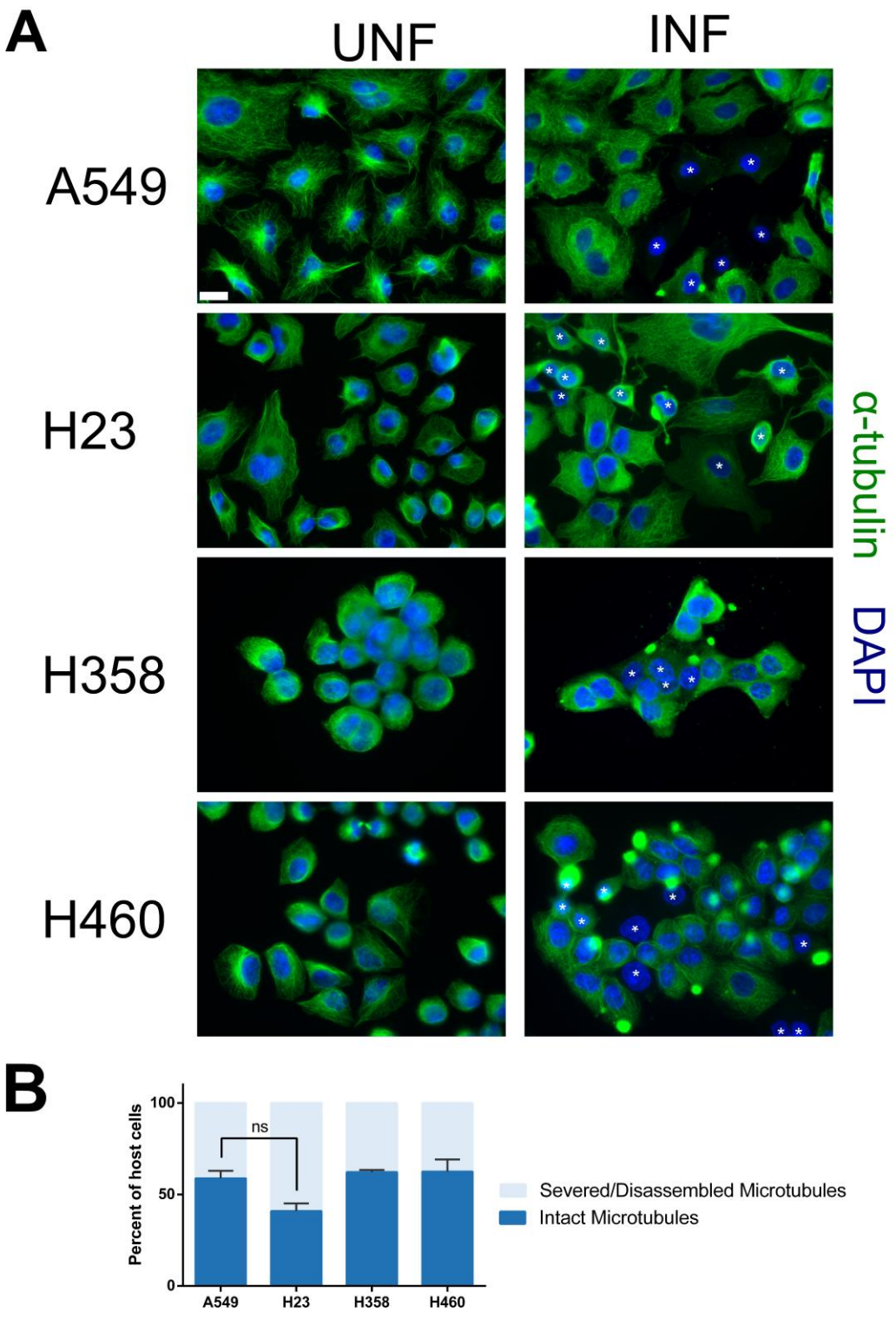
A
UNF
INF
A549
H23
H358
H460
α-tubulin
DAPI
B
Percent of host cells
100
50
0
ns
A549
H23
H358
H460
Severed/Disassembled Microtubules
Intact Microtubules

Figure 5.6: *K. Pneumoniae* induces microtubule disassembly in various lung epithelial cells.

(A) A549, H23, H358, and H460 lung cells had disassembled microtubules during *K. pneumoniae* infections. (*) indicates cells with disassembled microtubules. Scale bar = 20 µm (B) All lung cells had similar proportions of host cells with intact microtubules. Significance was determined using Student's *t* test with Welch's correction.

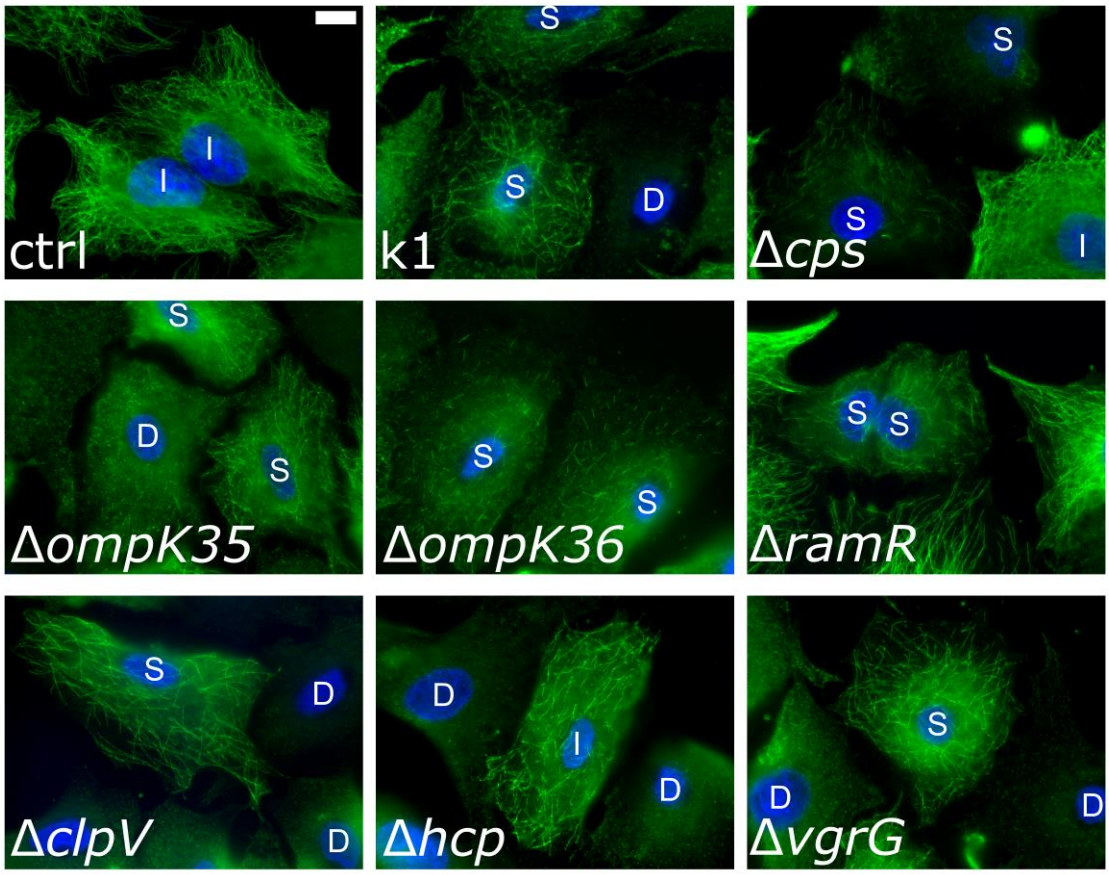

Figure 5.7: Mutants of known *K. pneumoniae* effectors do not inhibit microtubule disassembly.

A549 cells were infected with single gene mutants of *K. pneumoniae* and stained with anti-α-tubulin antibodies (Green) and DAPI (Blue). The control (ctrl) was incubated in culture broth only, k1 was infected with the wild-type *K. pneumoniae* (K1 strain), and the Δ*cps* mutant does not express capsular polysaccharide. The outer membrane porin mutants consist of Δ*ompK35*, Δ*ompK36*, and Δ*ramR*. The Δ*clpV*, Δ*hcp*, and Δ*vgrG* mutants are lacking components of the T6SS. The nuclei of each cell are labelled with I to indicate “intact microtubules” in the cytosol, S (severing microtubules), D (disassembled microtubules). Scale bar =10 μm.

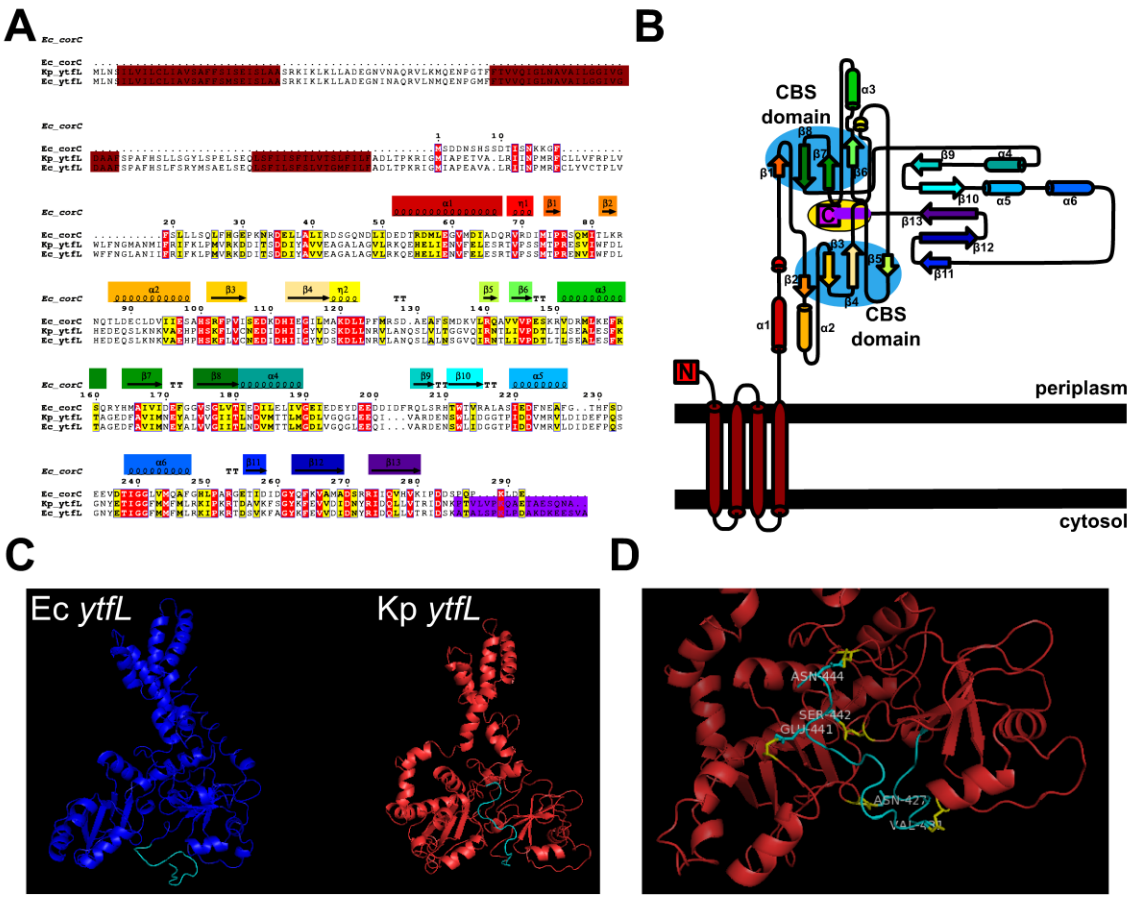

Figure 5.8: Kp *ytfL* and Ec *ytfL* sequence alignment and predicted structure.
The α-helices and β-strands are colour-coordinated between panel (A) and (B). (A) Phyre2 predicts with 100% confidence that Kp ytfL and Ec ytfL have a 24% identity with Ec corC. The sequences were then aligned and illustrated using Clustal Omega and ESPript 3 to depict the segments of α-helices (coils) and β-strands (arrows). The amino acid sequence of the first 3 transmembrane helices were predicted by TMHMM (pale red). The fourth transmembrane helix is not shown due to the gap in the alignment denoted in position 134. The sequence alignments of the three proteins show strictly conserved amino acids (bright red boxes) and differences in the sequence of the C-terminal tail (purple). (B) The suggested topology of Kp ytfL were generated based on the predicted transmembrane domain and the known crystal structure of Ec corC. The N-terminal transmembrane domain anchors the protein on the inner membrane, while the C-terminal tail is in the core of the periplasmic domain of Kp ytfL. Putative binding sites are the central pocket where the C-terminal tail is located (light yellow oval) and the two cystathionine β-synthase (CBS) domains (highlighted by light blue ovals) show additional possible binding sites. The difference between Kp ytfL and Ec ytfL lies in the short amino acid sequence at the C-terminal tail (highlighted by the light yellow oval). (C) The C-terminal tail of Kp ytfL (cyan) is predicted to loop into the catalytic domain whereas the Ec ytfL C-terminal tail (cyan) remains outside the catalytic domain. (D) The C-terminal tail of Kp ytfL interacts through hydrogen bonds with other residues (yellow) from the catalytic domain.

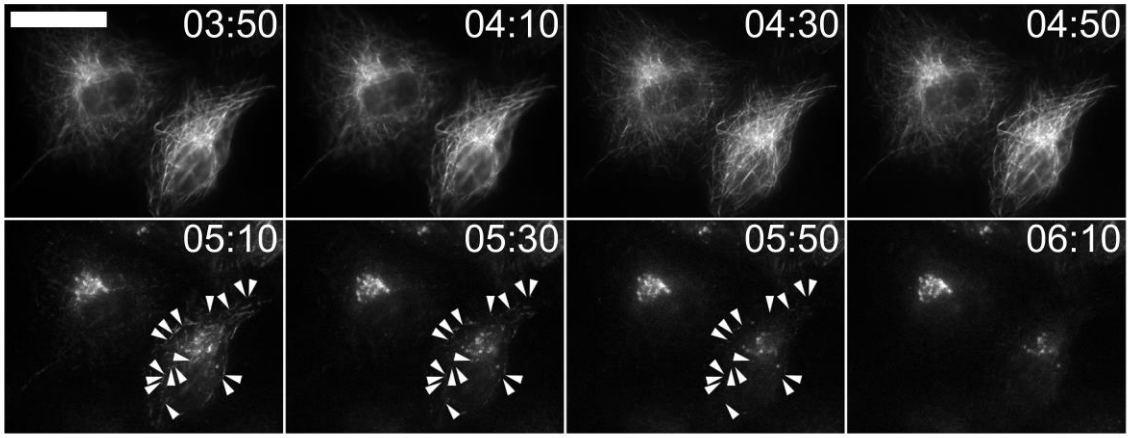

Figure 5.9: Microtubule severing occurs during K. pneumoniae infections.
Distinct cuts on microtubules (arrowheads) precede the destruction of the microtubule network. Time-lapse images were taken at 10-minute intervals. Scale bar = 10 µm.

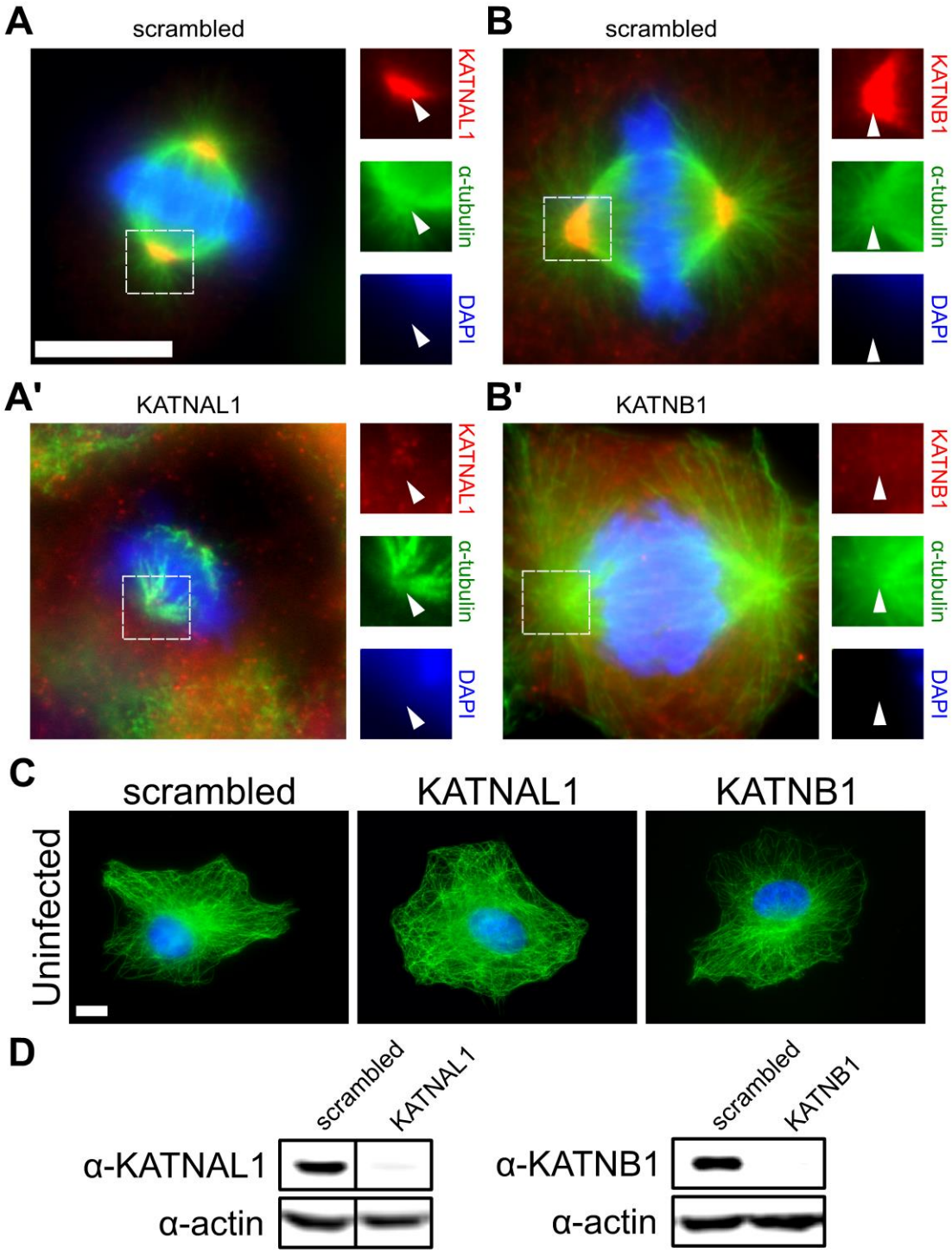

Figure 5.10: KATNAL1 and KATNB1 were depleted using CRISPR-Cas9 gene-editing techniques.

Arrowheads indicate the region of the MTOC. Scale bar = 10 μm (A, A') KATNAL1-deficient cells had no KATNAL1 immunolocalization at the MTOC. Cells were selected for stable expression of scrambled guide RNA or KATNAL1 guide RNA as well as Cas9. (B, B') No KATNB1 immunolocalization was observed at the MTOC of KATNB1-deficient cells. Cells were selected

for stable expression of scrambled guide RNA or KATNB1 guide RNA as well as Cas9. (C) Microtubules appear normal in all the transfected cells. (D) Western blot of the generated stable cell lines showed depletion of KATNAL1 in KATNAL1 gRNA transfected cells and depletion of KATNB1 in KATNB1 gRNA transfected cells.

5.7. Tables

Table 1: List of bacterial strains used for this study

Strain	Characteristics	Source
K1 (NVT1001)	Serotype wildtype K1 strain	[273]
NVT1001-Δ*wzy*	Capsule deficient K1 strain	[355]
NVT1001-Δ*ompK35*	*ompK35*-deficient K1 strain	[273]
NVT1001-Δ*ompK36*	*ompK36*-deficient K1 strain	[273]
NVT1001-Δ*ramR*	*ramR*-deficient K1 strain	This study
NVT1001-Δ*clpV*	*clpV*-deficient K1 strain (non-functional T6SS)	This study
NVT1001-Δ*hcp*	*hcp*-deficient K1 strain (non-functional T6SS)	This study
NVT1001-Δ*vgrG*	*vgrG*-deficient K1 strain (non-functional T6SS)	This study
EPI300	Laboratory strain *E. coli* used for the *K. pneumoniae* genomic library	EpicentreBio

Chapter 6.

General Discussion

6.1. Bacterially-generated actin-rich structures

Previous mass spectrometry analysis conducted by Dr. HT Law in our laboratory provided a list of proteins enriched at EPEC pedestals[299]. This screen identified proteins that have not been associated with any bacterially-generated actin-rich structures as well as some proteins that are not yet known to be associated with actin. Using a variety of bacterial infection models, I selected an assortment of proteins from the proteomics screen and divided my research program into three stages: (1) I immunolocalized each protein during EPEC, *L. monocytogenes*, and *S.* Typhimurium infections, (2) I characterized the functional role of each protein during the generation of actin-rich structures by these bacteria, and (3) if these protein(s) had novel functional roles, I examined their involvement in general mammalian cell actin dynamics.

Extensive work has been done to determine the importance of actin-stabilizing proteins in EPEC pedestal formation and many of these proteins such as α-actinin, spectrin and plastin have been localized to the stalk of pedestals[364,365]. All of these have calponin homology domains, but surprisingly the major of calponin homology-containing proteins (calponin 1, calponin 2, and SM22) have not been studied during any of those infections. Thus, since these calponins were enriched in EPEC pedestals, I investigated the role of calponin 1, calponin 2, and SM22 during the three aforementioned bacterial infections. Most work on calponin 1 and calponin 2 demonstrated that these proteins play differential roles in stabilizing cytosolic stress fibres and actin filaments at the cell periphery in smooth muscle cells and keratinocytes[308]. Calponin 1 had an affinity for cytosolic stress fibres whereas calponin 2 was recruited to cortical actin filaments[62]. Calponin 2 only localized to cytosolic stress fibres upon deletion of its inhibitory C-terminal tail[68]. My immunolocalization of calponin 1 and calponin 2 provided similar results such that calponin 1 was found throughout EPEC pedestals, *L. monocytogenes* comet tails and *S.* Typhimurium membrane ruffles whereas calponin 2 was enriched towards the membrane-associated regions of these actin-rich structures. Unfortunately, studying these calponins was difficult as simply reseeding cells from a stock flask to a

well plate affected the expression levels of calponins[308]. Compounding the studies were that calponin-specific antibodies were inefficient in immunofluorescence labelling in human intestinal epithelial cells. Nonetheless, I have shown that calponins were recruited to actin in EPEC pedestals, *L. monocytogenes* actin clouds and comet tails, and *S.* Typhimurium membrane ruffles. My investigation of SM22 provided more insight into the role of calponins in bacterially-generated actin structures. First, I validated the mass spectrometry analysis by immunolocalizing one of the most abundant novel proteins from the proteomics screen, SM22, at EPEC pedestals[299]. Next, I showed that similar to its known colocalization with actin in the host cell, SM22 immunolocalized to the full length of EPEC pedestals and *L. monocytogenes* comet tails. Lastly, consistent with known effects of SM22 depletion on cell motility, I found similar detrimental effects for EPEC pedestal formation and *L. monocytogenes* infections. As such, even though other actin-stabilizing proteins like α-actinin, spectrin and plastin were not experimentally altered in those studies and were likely unaltered, compensation for the loss of SM22 function was not evident. As a result, my work reveals that the stability of EPEC pedestals and *L. monocytogenes* comet tails relies on the function of SM22.

My research also analysed another protein enriched in the EPEC pedestal protein screen, Ube2N, an E2 ubiquitin-conjugating enzyme. Interestingly, several studies have indirectly associated Ube2N with actin dynamics. In breast cancer cells, overexpressing Ube2V1, one of the binding partners of Ube2N, was essential for inducing metastatic cell movement, which is an actin-based process[337]. Another study showed that the Ube2N-Ube2V1 complex is involved in ubiquitylating actin in hyperglycemic conditions in kidney cells[366]. This association seems to occur in a highly specific context, and in the context of EPEC infections, previous studies in our laboratory have already shown that overall ubiquitylation levels were depleted[367]. At first glance, it seems quite contrary to have a ubiquitin-conjugating enzyme to be enriched in pedestals when overall, ubiquitylation is downregulated. To further confound this, E1 ubiquitin-activating enzymes and E3 ubiquitin-ligating enzymes were not enriched in the mass spectrometry screen[299]. However, my initial immunolocalization of Ube2N showed that this protein was indeed enriched at the tips of EPEC pedestals (Appendix Figure A1). This suggested that Ube2N may have a novel function separate from its traditional ubiquitylation functions. Possibly, as a consequence of shutting down the ubiquitylation system, a ubiquitylation enzyme such as Ube2N can function in other cellular processes.

Admittedly, it was difficult to discern the role of Ube2N in EPEC pedestals as my preliminary inhibition of the Ube2N ubiquitylation function during EPEC infections did not show any discernible effects on the ability of EPEC to form pedestals or on the morphology of these pedestals at the end of a 6-hour infection (data not shown). I ceded to focus my Ube2N research on the other actin-polymerizing bacteria *L. monocytogenes*. Although Ube2N immunolocalized to all of the induced actin-rich structures during these infections including invasion sites, only the membrane-associated invasion events and listeriopods were diminished following Ube2N inhibition. Because both invasion and cell-to-cell spreading are important for bacterial colonization of epithelia, my research discovered that Ube2N plays a critical role for the plasma membrane-based events during *L. monocytogenes* infections.

Further exploration of this involvement of Ube2N in listeriopods revealed that Ube2N directly interacts with actin and my results suggest that this interaction occurs at the plasma membrane. Protein function at the interface of the actin cytoskeleton and the plasma membrane is reminiscent of the regulation of actin-based mammalian cell motility, and so, I studied the role of Ube2N in mammalian cell motility using a wound-healing assay. Ube2N inhibition halted cells in my wound healing assay and when taken together with the study which showed that Ube2V1 overexpression increased cell motility [337], Ube2N activities play a pivotal role in regulating mammalian cell movement. Another breast cancer study suggested that along with proteins involved in regulating cell adhesion, Ube2N is upregulated during cancer metastasis[338]. These lines of evidence support the notion that Ube2N is part of the protein repertoire that orchestrates cell motility and my research is the first to show empirical proof of the direct binding between Ube2N and actin and that this novel function of Ube2N drives cell motility.

Although I was unable to determine the exact molecular mechanism of the interaction between Ube2N and actin, previous work on E2 ubiquitin-conjugating enzymes and several pieces of evidence that I have gathered could begin to shed some light on this. E2 enzymes have been shown to dimerize when they are inhibited[165] and I speculate that this could generate a dimer with a novel binding site. Although I could not determine if the Ube2N species that bound to actin suspended in my far western membrane dimerized, the negative result in the converse experiment where purified actin did not bind to Ube2N could suggest that a specific polymerized orientation of Ube2N may be required. Although this speculation is based on correlative evidence and

needs more empirical experiments, my studies have shown that the functional inhibition of Ube2N caused an enrichment of Ube2N at the tip lamellipodia. The role of inhibited Ube2N may be important for binding to branched actin structures at the plasma membrane as *L. monocytogenes* cell-to-cell spreading and mammalian cell motility were reduced when Ube2N was inhibited. In the instance of EPEC pedestals where ubiquitylation is diminished and consequently, Ube2N is quite possibly functionally inhibited already, further chemical inhibition would yield, as I have tested, no discernible effects. Through these, my research points to a novel function of Ube2N outside of its known ubiquitylation function and this novel function is important for regulating actin at the plasma membrane of mammalian cells.

Therefore, my research claims to include calponin 1, calponin 2, SM22, and Ube2N in the proteome of bacterially-generated actin-rich structures. My findings suggest that calponin 1 and SM22 may both be involved in providing structural support for actin filaments whereas the plasma membrane associations of calponin 2 and Ube2N point to a unique functional role near the plasma membrane. This coincidental parallelism between the immunolocalizations of calponin 2 and Ube2N is quite intriguing as several studies implies some degree of association between the two proteins. Both proteins have been shown to be upregulated in metastatic cancer cells[338] and several studies suggest that both of these proteins are markers for these highly motile cells [61,337]. Knockdown of Ube2N has also been shown to down-regulate calponin 2 expression[338] and this adds to the correlative data of these proteins having a shared function. With this, we can begin to identify novel protein-protein interactions that are vital for actin dynamics.

6.2. Novel *Klebsiella pneumoniae*-induced microtubule disassembly

The microtubule disassembly of an entire population of cells has not been previously discovered during any bacterial infection. To date, bacteria-induced destruction of microtubules is either localized around the bacterium or occurs in the host cell where the bacterium attaches[156,353,368]. We found that unique to *K. pneumoniae* is its ability to cause microtubule disassembly in cells distant from its host cell and this suggests that a released factor may be involved. Despite being unable to determine if the Kp ytfL protein was secreted, or a cleaved portion was released to the host cells, I

did find that this protein activates the signalling cascade that eventually leads to the activation of the katanin proteins KATNAL1 and KATNB1. As such, I have discovered the activating signal from the bacteria and the resulting host cell effector proteins that are triggered in this novel *K. pneumoniae*-induced phenotype.

Elucidating the entire mechanism requires laborious scrutiny as there are many possible permutations. For instance, analysing Kp ytfL and its putative domains suggest multiple modes of action. Through my Phyre modelling, the C-terminal tail of Kp ytfL, unlike its *E. coli* (Ec) ytfL counterpart, presumably binds to the central pocket of the protein. This conformation of the Kp ytfL C-terminal tail could align this peptide for cleavage, releasing the peptide effector to the environment. If the C-terminal tail is not cleaved, this conformation could potentially amplify the ability of Kp ytfL to bind either adenosine monophosphate (AMP) or ATP. Altering the concentration of either AMP or ATP could then activate signalling cascades such as two-component regulatory mechanisms within the bacteria[369] or alternatively, Kp ytfL could alter AMP or ATP levels in the infection media leading to an activation of host cell processes. In any of these possible scenarios, Kp ytfL shows unique structural properties that could instigate the microtubule disassembly phenotype.

If AMP or ATP levels are altered in the infection media and consequently within the host cell, many cellular signalling processes could lead to microtubule severing. Increasing cytosolic ATP levels can directly enhance the ATPase activity of KATNAL1 leading to more severing events[370]. Alternatively, increased ATP can provide the phosphate analogs required for kinase activity and, of note, tau phosphorylation leads to increased katanin-mediated microtubule severing[371]. Increased ATP could also potentially generate purine-based compounds and previous work has shown that incubation with specific purine-based compounds leads to katanin-induced severing in lung cells[372]. With all of these, there are various ways of inducing katanin-based severing within the host cell. Nonetheless, regarding the katanins, I have shown that the KATNAL1 and KATNB1 subunits are involved in *K. pneumoniae*-induced microtubule severing.

Although it is tempting to surmise that Kp ytfL causes AMP or ATP alterations that lead to katanin activation, it is still possible that other proteins from the bacteria or the host are involved in the series of events in between bacterial Kp ytfL and the host

cell katanins. Yet, my work highlights potential mechanisms for this novel bacterially-induced disassembly of entire microtubule networks in host lung cells.

Chapter 7.

Future Directions

7.1. Further characterization of the actin-associated proteins

Additional studies for calponin 1 and calponin 2 would increase our overall understanding of the role of calponins in bacterially-generated actin-rich structures. Interestingly, a previous study examined EGFP-tagged constructs of calponin 2, which lacks the inhibitory C-terminal tail and binds to stress fibres similar to calponin 1[305]. It would be interesting to determine if this construct could alter the formation of EPEC pedestals, *L. monocytogenes* listeriopods, and *S.* Typhimurium membrane ruffles. Furthermore, deletion mutants for the calponin homology domain would also provide insight to the potential role of calponin 1 and calponin 2 as scaffolding proteins that could allow the binding of signalling proteins such as extracellular regulated kinase 1 (ERK1) and extracellular regulated kinase 2 (ERK2)[59]. As such, manipulation of the calponin structures would improve our understanding of their role during bacterial infections.

The stabilizing role of SM22 suggests that the actin filaments are protected from actin severing enzymes[62]. Overexpressing or constitutively activating actin severing enzymes (such as gelsolin or cofilin) would provide data on the extent of protection that SM22 provides actin filaments. With this, we can extract the mechanism of how SM22 stabilizes actin-rich structures.

Examining the exact mechanism of Ube2N binding to actin would direct further studies with this novel actin-associated protein. Because inhibited Ube2N can dimerize, incubating crosslinked Ube2N dimers with single actin filaments will determine if inhibited Ube2N binds in a particular fashion to actin filaments. Furthermore, examining the localization of the calponins in Ube2N inhibited cells would provide additional correlative evidence to which proteins interact with Ube2N during actin dynamics.

7.2. Expanding our understanding of *K. pneumoniae*-induced microtubule severing

As mentioned in the previous chapter, AMP and ATP levels could be altered during *K. pneumoniae* infections. Using a fluorescent biosensor for ATP levels such as Perceval HR[373], it would be interesting to determine if ATP levels are altered. Then, tracking phosphorylation using radiolabelled phosphates would identify which kinases are involved in this mechanism. Still, many possible proteins could be involved between Kp ytfL and the activated host katanins. Inhibiting known kinases such as Aurora kinase A and Protein kinase C could also identify key pathways that could be activated during *K. pneumoniae* infections. By doing these, the complete mechanism from Kp ytfL to KATNAL1 and KATNB1 could be elucidated. From there, we could determine novel therapeutics that could prevent exacerbation of *K. pneumoniae* infections in humans.

Furthermore, because *K. pneumoniae* presents a novel pathway to induce microtubule disassembly, its potential for anticancer therapeutics can be examined. Currently, paclitaxel, vinca alkaloids, and colchicine-based chemicals serve as microtubule-targeting agents for cancer cells[374,375]. *K. pneumoniae* could provide novel strategy to inhibit the proliferation of lung cancer cells.

Chapter 8.

Conclusion

In summary, both the actin cytoskeleton and the microtubule network can be altered during bacterial infections. Calponin 1, calponin 2, SM22, and Ube2N are novel proteins implicated in the formation of bacterially-generated actin-rich structures. Further analysis of the interactions of these proteins as well as other novel proteins at these structures will increase our understanding of general actin dynamics. *K. pneumoniae*-induced microtubule severing occurs through the bacterial protein Kp ytfL which leads to the activation of the host cell katanins KATNAL1 and KATNB1. This contributes to our understanding of novel mechanisms for eliciting microtubule disassembly not only at localized areas within a single cell, but also throughout an entire cell monolayer *in situ* or epithelial tissue *in vivo*.

References

1. Kast, D. J. & Dominguez, R. The Cytoskeleton–Autophagy Connection. *Curr Biol* **27,** R318–R326 (2017).

2. Gurel, P. S., Hatch, A. L. & Higgs, H. N. Connecting the Cytoskeleton to the Endoplasmic Reticulum and Golgi. *Curr Biol* **24,** R660–R672 (2014).

3. Ciobanasu, C., Faivre, B. & Clainche, C. Integrating actin dynamics, mechanotransduction and integrin activation: The multiple functions of actin binding proteins in focal adhesions. *Eur J Cell Biol* **92,** 339–348 (2013).

4. Diz-Muñoz, A., Fletcher, D. A. & Weiner, O. D. Use the force: membrane tension as an organizer of cell shape and motility. *Trends Cell Biol* **23,** 47–53 (2013).

5. Vignjevic, D. & Montagnac, G. Reorganisation of the dendritic actin network during cancer cell migration and invasion. *Semin Cancer Biol* **18,** 12–22 (2008).

6. Lee, S. & Dominguez, R. Regulation of actin cytoskeleton dynamics in cells. *Mol Cells* **29,** 311–325 (2010).

7. Holmes, K. C., Popp, D., Gebhard, W. & Kabsch, W. Atomic model of the actin filament. *Nature* **347,** 44–49 (1990).

8. Skruber, K., Read, T.-A. & Vitriol, E. A. Reconsidering an active role for G-actin in cytoskeletal regulation. *J Cell Sci* **131,** jcs203760 (2018).

9. Pennanen, P. *et al.* Diversity of actin architecture in human osteoclasts: network of curved and branched actin supporting cell shape and intercellular micrometer-level tubes. *Mol Cell Biochem* **432,** 131–139 (2017).

10. Janmey, P. A., Hvidt, S., Lamb, J. & Stossel, T. P. Resemblance of actin-binding protein/actin gels to covalently crosslinked networks. *Nature* **345,** 345089a0 (1990).

11. Bray, D. & White, J. G. Cortical flow in animal cells. *Science (80-.).* **239,** 883–888 (1988).

12. NAUMANEN, P., LAPPALAINEN, P. & HOTULAINEN, P. Mechanisms of actin stress fibre assembly. *J Microsc* **231,** 446–454 (2008).

13. Niessen, C. M. & Gottardi, C. J. Molecular components of the adherens junction. *Biochim. Biophys. Acta Bba - Biomembr* **1778,** 562–571 (2008).

14. Hartsock, A. & Nelson, J. W. Adherens and tight junctions: Structure, function and connections to the actin cytoskeleton. *Biochim. Biophys. Acta Bba - Biomembr* **1778,** 660–669 (2008).

15. Le Clainche, C. & Carlier, M.-F. F. Regulation of actin assembly associated with protrusion and adhesion in cell migration. *Physiol. Rev.* **88,** 489–513 (2008).

16. Svitkina, T. *Electron Microscopic Analysis of the Leading Edge in Migrating Cells*. **79,** (2007).

17. Wang, Y. L. Exchange of actin subunits at the leading edge of living fibroblasts: possible role of treadmilling. *J Cell Biol.* **101,** 597–602 (1985).

18. Theriot, J. A. & Mitchison, T. J. Actin microfilament dynamics in locomoting cells. *Nature* **352,** 352126a0 (1991).

19. Pontes, B. *et al.* Membrane tension controls adhesion positioning at the leading edge of cells. *J. Cell Biol.* **216,** 2959–2977 (2017).

20. Small, J. V., Stradal, T., Vignal, E. & Rottner, K. The lamellipodium: where motility begins. *Trends Cell Biol* **12,** 112–120 (2002).

21. Bugyi, B. & Carlier, M.-F. Control of Actin Filament Treadmilling in Cell Motility. *Annu Rev Biophys* **39,** 449–470 (2010).

22. Koestler, S. A. *et al.* F- and G-Actin Concentrations in Lamellipodia of Moving Cells. *PLoS One* **4,** e4810 (2009).

23. Khurana, S. & George, S. P. The role of actin bundling proteins in the assembly of filopodia in epithelial cells. *Cell Adhes. Migr* **5,** 409–420 (2014).

24. Mattila, P. K. & Lappalainen, P. Filopodia: molecular architecture and cellular functions. *Nat Rev Mol Cell Bio* **9,** 446–454 (2008).

25. Dominguez, R. & Holmes, K. C. Actin Structure and Function. *Annu Rev Biophys* **40,** 169–186 (2011).

26. Cooper, J. A., Buhle, E. L., Walker, S. B., Tsong, T. Y. & Pollard, T. D. Kinetic evidence for a monomer activation step in actin polymerization. *Biochemistry-us* **22,** 2193–2202 (1983).

27. Frieden, C. Polymerization of actin: mechanism of the Mg2+-induced process at pH 8 and 20 degrees C. *Proc Natl. Acad Sci* **80,** 6513–6517 (1983).

28. group, C. *et al.* Control of polarized assembly of actin filaments in cell motility. *Cell Mol Life Sci* **72,** 3051–3067 (2015).

29. Graceffa, P. & Dominguez, R. Crystal Structure of Monomeric Actin in the ATP State STRUCTURAL BASIS OF NUCLEOTIDE-DEPENDENT ACTIN DYNAMICS. *J Biol Chem* **278,** 34172–34180 (2003).

30. McCullagh, M., Saunders, M. G. & Voth, G. A. Unraveling the Mystery of ATP

Hydrolysis in Actin Filaments. *J Am Chem Soc* **136,** 13053–13058 (2014).

31. Pollard, T. D. Rate constants for the reactions of ATP- and ADP-actin with the ends of actin filaments. *J Cell Biol.* **103,** 2747–2754 (1986).

32. Shekhar, S., Pernier, J. & Carlier, M.-F. Regulators of actin filament barbed ends at a glance. *J Cell Sci* **129,** 1085–1091 (2016).

33. Machesky, L. M., Atkinson, S. J., Ampe, C., Vandekerckhove, J. & Pollard, T. D. Purification of a cortical complex containing two unconventional actins from Acanthamoeba by affinity chromatography on profilin-agarose. *J Cell Biol.* **127,** 107–115 (1994).

34. Higgs, H. N. Formin proteins: a domain-based approach. *Trends Biochem Sci* **30,** 342–353 (2005).

35. Baum, B. & Kunda, P. Actin Nucleation: Spire — Actin Nucleator in a Class of Its Own. *Curr Biol* **15,** R305–R308 (2005).

36. Mullins, D. R., Heuser, J. A. & Pollard, T. D. The interaction of Arp2/3 complex with actin: Nucleation, high affinity pointed end capping, and formation of branching networks of filaments. *Proc Natl. Acad Sci* **95,** 6181–6186 (1998).

37. Marchand, J.-B., Kaiser, D. A., Pollard, T. D. & Higgs, H. N. Interaction of WASP/Scar proteins with actin and vertebrate Arp2/3 complex. *Nat Cell Biol* **3,** 76–82 (2000).

38. Ti, S.-C., Jurgenson, C. T., Nolen, B. J. & Pollard, T. D. Structural and biochemical characterization of two binding sites for nucleation-promoting factor WASp-VCA on Arp2/3 complex. *Proc Natl. Acad Sci* **108,** E463–E471 (2011).

39. Yamaguchi, H. *et al.* Two tandem verprolin homology domains are necessary for a strong activation of Arp2/3 complex-induced actin polymerization and induction of microspike formation by N-WASP. *Proc Natl. Acad Sci* **97,** 12631–12636 (2000).

40. Rohatgi, R. *et al.* The Interaction between N-WASP and the Arp2/3 Complex Links Cdc42-Dependent Signals to Actin Assembly. *Cell* **97,** 221–231 (1999).

41. Beltzner, C. C. & Pollard, T. D. Pathway of Actin Filament Branch Formation by Arp2/3 Complex. *J Biol Chem* **283,** 7135–7144 (2008).

42. Amann, K. J. & Pollard, T. D. The Arp2/3 complex nucleates actin filament branches from the sides of pre-existing filaments. *Nat Cell Biol* **3,** ncb0301_306 (2001).

43. Svitkina, T. M. & Borisy, G. G. Arp2/3 Complex and Actin Depolymerizing Factor/Cofilin in Dendritic Organization and Treadmilling of Actin Filament Array in

Lamellipodia. *J Cell Biol.* **145,** 1009–1026 (1999).

44. Shekhar, S. *et al.* Formin and capping protein together embrace the actin filament in a menage a trois. *Nat Commun* **6,** 8730 (2015).

45. Kovar, D. R., Harris, E. S., Mahaffy, R., Higgs, H. N. & Pollard, T. D. Control of the Assembly of ATP- and ADP-Actin by Formins and Profilin. *Cell* **124,** 423–435 (2006).

46. Paul, A. S., Paul, A., Pollard, T. D. & Pollard, T. The Role of the FH1 Domain and Profilin in Formin-Mediated Actin-Filament Elongation and Nucleation. *Curr Biol* **18,** 9–19 (2008).

47. Paul, A. S. & Pollard, T. D. Energetic Requirements for Processive Elongation of Actin Filaments by FH1FH2-formins. *J Biol Chem* **284,** 12533–12540 (2009).

48. Vavylonis, D., Kovar, D. R., O'Shaughnessy, B. & Pollard, T. D. Model of Formin-Associated Actin Filament Elongation. *Mol Cell* **21,** 455–466 (2006).

49. Quinlan, M. E., Heuser, J. E., Kerkhoff, E. & Mullins, D. R. Drosophila Spire is an actin nucleation factor. *Nature* **433,** 382–388 (2005).

50. Sitar, T. *et al.* Molecular architecture of the Spire-actin nucleus and its implication for actin filament assembly. *Proc. Natl. Acad. Sci. U. S. A.* **108,** 19575–80 (2011).

51. Stevenson, R. P., Veltman, D. & Machesky, L. M. Actin-bundling proteins in cancer progression at a glance. *J Cell Sci* **125,** 1073–1079 (2012).

52. Winder, S. J. & Ayscough, K. R. Actin-binding proteins. *J Cell Sci* **118,** 651–654 (2005).

53. Vignjevic, D. *et al.* Role of fascin in filopodial protrusion. *J Cell Biol.* **174,** 863–875 (2006).

54. Gimona, M. & Mital, R. The single CH domain of calponin is neither sufficient nor necessary for F-actin binding. *J Cell Sci* **111 (Pt 13),** 1813–1821 (1998).

55. Gimona, M., Djinovic-Carugo, K., Kranewitter, W. J. & Winder, S. J. Functional plasticity of CH domains. *Febs Lett* **513,** 98–106 (2002).

56. Galkin, V. E., Orlova, A., Fattoum, A., Walsh, M. P. & Egelman, E. H. The CH-domain of Calponin does not Determine the Modes of Calponin Binding to F-actin. *J Mol Biol* **359,** 478–485 (2006).

57. Fu, Y. *et al.* Mutagenesis analysis of human SM22: characterization of actin binding. *J Appl Physiol* **89,** 1985–1990 (2000).

58. Mino, T., Yuasa, U., Nakamura, F., Naka, M. & Tanaka, T. Two distinct actin-

binding sites of smooth muscle calponin. *Eur. J. Biochem.* **251,** 262–268 (1998).

59. LEINWEBER, B. D., LEAVIS, P. C., GRAREK, Z., WANG, C.-L. & MORGAN, K. G. Extracellular regulated kinase (ERK) interaction with actin and the calponin homology (CH) domain of actin-binding proteins. *Biochem J* **344,** 117–123 (1999).

60. Kaneko, T. *et al.* Identification of Calponin as a Novel Substrate of Rho-Kinase. *Biochem Bioph Res Co* **273,** 110–116 (2000).

61. Ulmer, B. *et al.* Calponin 2 Acts As an Effector of Noncanonical Wnt-Mediated Cell Polarization during Neural Crest Cell Migration. *Cell Rep.* **3,** 615–621 (2013).

62. Gimona, M., Kaverina, I., Resch, G. P., Vignal, E. & Burgstaller, G. Calponin repeats regulate actin filament stability and formation of podosomes in smooth muscle cells. *Mol. Biol. Cell* **14,** 2482–2491 (2003).

63. Rozenblum, G. T. & Gimona, M. Calponins: Adaptable modular regulators of the actin cytoskeleton. *Int. J. Biochem. Cell Biol.* **40,** 1990–1995 (2008).

64. Liu, R. & Jin, J.-P. Calponin isoforms CNN1, CNN2 and CNN3: Regulators for actin cytoskeleton functions in smooth muscle and non-muscle cells. *Gene* **585,** 143–153 (2016).

65. Jensen, M. *et al.* Mechanism of Calponin Stabilization of Cross-Linked Actin Networks. *Biophys J* **106,** 793–800 (2014).

66. Jensen, M. *et al.* Effects of basic calponin on the flexural mechanics and stability of F-actin. *Cytoskeleton* **69,** 49–58 (2012).

67. Zhang, J. *et al.* SM22β encodes a lineage-restricted cytoskeletal protein with a unique developmentally regulated pattern of expression. *Mech Dev.* **115,** 161–166 (2002).

68. Burgstaller, G., Kranewitter, W. J. & Gimona, M. The molecular basis for the autoregulation of calponin by isoform-specific C-terminal tail sequences. *J. Cell. Sci.* **115,** 2021–2029 (2002).

69. Lawson, D., Harrison, M. & Shapland, C. Fibroblast transgelin and smooth muscle SM22α are the same protein, the expression of which is down-regulated in many cell lines. *Cell Motil Cytoskel* **38,** 250–257 (1997).

70. Thompson, O., Moghraby, J. S., Ayscough, K. R. & Winder, S. J. Depletion of the actin bundling protein SM22/transgelin increases actin dynamics and enhances the tumourigenic phenotypes of cells. *BMC Cell Biol.* **13,** 1 (2012).

71. Sjöblom, B., Salmazo, A. & Djinović-Carugo, K. α-Actinin structure and regulation. *Cell Mol Life Sci* **65,** 2688–2701 (2008).

72. McGough, A., Way, M. & DeRosier, D. Determination of the alpha-actinin-binding site on actin filaments by cryoelectron microscopy and image analysis. *J Cell Biol.* **126,** 433–443 (1994).

73. Schultheiss, T. *et al.* A sarcomeric alpha-actinin truncated at the carboxyl end induces the breakdown of stress fibers in PtK2 cells and the formation of nemaline-like bodies and breakdown of myofibrils in myotubes. *Proc Natl. Acad Sci* **89,** 9282–9286 (1992).

74. Pavalko, F. M. & Burridge, K. Disruption of the actin cytoskeleton after microinjection of proteolytic fragments of alpha-actinin. *J Cell Biol.* **114,** 481–491 (1991).

75. Galkin, V. E., Orlova, A., Cherepanova, O., Lebart, M.-C. & Egelman, E. H. High-resolution cryo-EM structure of the F-actin–fimbrin/plastin ABD2 complex. *Proc Natl. Acad Sci* **105,** 1494–1498 (2008).

76. Delanote, V., Vandekerckhove, J. & Gettemans, J. Plastins: versatile modulators of actin organization in (patho)physiological cellular processes. *Acta Pharm Sin.* **26,** aps2005114 (2005).

77. Nag, S. *et al.* Ca2+ binding by domain 2 plays a critical role in the activation and stabilization of gelsolin. *Proc Natl. Acad Sci* **106,** 13713–13718 (2009).

78. Allen, P. G. Functional consequences of disulfide bond formation in gelsolin. *Febs Lett* **401,** 89–94 (1997).

79. McLaughlin, P. J., Gooch, J. T., Mannherz, H.-G. & Weeds, A. G. Structure of gelsolin segment 1-actin complex and the mechanism of filament severing. *Nature* **364,** 685–692 (1993).

80. Cruz, E. M. Cofilin Binding to Muscle and Non-muscle Actin Filaments: Isoform-dependent Cooperative Interactions. *J Mol Biol* **346,** 557–564 (2005).

81. Cruz, E. M. & Sept, D. The Kinetics of Cooperative Cofilin Binding Reveals Two States of the Cofilin-Actin Filament. *Biophys J* **98,** 1893–1901 (2010).

82. Suarez, C. *et al.* Cofilin Tunes the Nucleotide State of Actin Filaments and Severs at Bare and Decorated Segment Boundaries. *Curr Biol* **21,** 862–868 (2011).

83. Breitsprecher, D. *et al.* Cofilin cooperates with fascin to disassemble filopodial actin filaments. *J Cell Sci* **124,** 3305–3318 (2011).

84. Colonne, P. M., Winchell, C. G. & Voth, D. E. Hijacking Host Cell Highways: Manipulation of the Host Actin Cytoskeleton by Obligate Intracellular Bacterial Pathogens. *Front. Cell Infect Microbiol* **6,** 107 (2016).

85. Bhavsar, A. P., Guttman, J. a & Finlay, B. B. Manipulation of host-cell pathways

by bacterial pathogens. *Nature* **449,** 827–834 (2007).

86. Lai, Y., Rosenshine, I., Leong, J. M. & Frankel, G. Intimate host attachment: Enteropathogenic and enterohaemorrhagic Escherichia coli. *Cell. Microbiol.* **15,** 1796–1808 (2013).

87. Hume, P. J., Singh, V., Davidson, A. C. & Koronakis, V. Swiss Army Pathogen: The Salmonella Entry Toolkit. *Front. Cell Infect Microbiol* **7,** 348 (2017).

88. Lee, J., Park, H. & Park, Y. Molecular Mechanisms of Host Cytoskeletal Rearrangements by Shigella Invasins. *Int J Mol Sci* **15,** 18253–18266 (2014).

89. Veiga, E. & Cossart, P. Listeria hijacks the clathrin-dependent endocytic machinery to invade mammalian cells. *Nat Cell Biol* **7,** 894–900 (2005).

90. Egile, C. *et al.* Activation of the Cdc42 Effector N-Wasp by the Shigella flexneri Icsa Protein Promotes Actin Nucleation by Arp2/3 Complex and Bacterial Actin-Based Motility. *J Cell Biol.* **146,** 1319–1332 (1999).

91. Boujemaa-Paterski, R. *et al.* Listeria protein ActA mimics WASp family proteins: it activates filament barbed end branching by Arp2/3 complex. *Biochemistry* **40,** 11390–11404 (2001).

92. Robbins, J. R. *et al.* Listeria monocytogenes exploits normal host cell processes to spread from cell to cell. *J. Cell Biol.* **146,** 1333–1349 (1999).

93. Bernardini, M. L., Mounier, J., d'Hauteville, H., Coquis-Rondon, M. & Sansonetti, P. J. Identification of icsA, a plasmid locus of Shigella flexneri that governs bacterial intra- and intercellular spread through interaction with F-actin. *Proc Natl. Acad Sci* **86,** 3867–3871 (1989).

94. Farache, D., Emorine, L., Haren, L. & Merdes, A. Assembly and regulation of γ-tubulin complexes. *Open Biol.* **8,** 170266 (2018).

95. Meng, W., Mushika, Y., Ichii, T. & Takeichi, M. Anchorage of Microtubule Minus Ends to Adherens Junctions Regulates Epithelial Cell-Cell Contacts. *Cell* **135,** 948–959 (2008).

96. Goodson, H. V & Jonasson, E. M. Microtubules and Microtubule-Associated Proteins. *Csh Perspect Biol* **10,** a022608 (2018).

97. Barisic, M. & Maiato, H. The Tubulin Code: A Navigation System for Chromosomes during Mitosis. *Trends Cell Biol.* **26,** 766–775 (2016).

98. Shen, F. *et al.* Vinblastine differs from Taxol as it inhibits the malignant phenotypes of NSCLC cells by increasing the phosphorylation of Op18/stathmin. *Oncol Rep* **37,** 2481–2489 (2017).

99. Miceli, C., Tejada, A., Castaneda, A. & Mistry, S. J. Cell cycle inhibition therapy that targets stathmin in in vitro and in vivo models of breast cancer. *Adv Exp Med Biol* **20,** 298 (2013).

100. Parker, A. L., Kavallaris, M. & McCarroll, J. A. Microtubules and Their Role in Cellular Stress in Cancer. *Front. Oncol* **4,** 153 (2014).

101. Khan, S. & Scholey, J. M. Assembly, Functions and Evolution of Archaella, Flagella and Cilia. *Curr Biol. Cb* **28,** R278–R292 (2018).

102. Hu, Z., Liang, Y., Meng, D., Wang, L. & Pan, J. *Microtubule-depolymerizing kinesins in the regulation of assembly, disassembly, and length of cilia and flagella*. **317,** (2015).

103. Sanchez, A. D. & Feldman, J. L. Microtubule-organizing centers: from the centrosome to non-centrosomal sites. *Curr Opin Cell Biol* **44,** 93–101 (2017).

104. Lin, T. C., Neuner, A. & Schiebel, E. Targeting of γ-tubulin complexes to microtubule organizing centers: conservation and divergence. *Trends Cell Biol.* **25,** 296–307 (2015).

105. Wieczorek, M., Bechstedt, S., Chaaban, S. & Brouhard, G. J. Microtubule-associated proteins control the kinetics of microtubule nucleation. *Nat Cell Biol* **17,** 907 (2015).

106. Roostalu, J. & Surrey, T. Microtubule nucleation: beyond the template. *Nat Rev Mol Cell Bio* **18,** nrm.2017.75 (2017).

107. Voter, W. A. & Erickson, H. P. The kinetics of microtubule assembly. Evidence for a two-stage nucleation mechanism. *J Biol. Chem* **259,** 10430–10438 (1984).

108. Gardel, M. L. *et al.* Elastic Behavior of Cross-Linked and Bundled Actin Networks. *Science (80-.).* **304,** 1301–1305 (2004).

109. Stearns, T. & Kirschner, M. In vitro reconstitution of centrosome assembly and function: The central role of γ-tubulin. *Cell* **76,** 623–637 (1994).

110. Bowne-Anderson, H., Hibbel, A. & Howard, J. Regulation of Microtubule Growth and Catastrophe: Unifying Theory and Experiment. *Trends Cell Biol* **25,** 769–779 (2015).

111. Toya, M. & Takeichi, M. Organization of non-centrosomal microtubules in epithelial cells. *Cell Struct Funct* **41,** 127–135 (2016).

112. Pedersen, L. B., Schrøder, J. M., Satir, P. & Christensen, S. T. *The ciliary cytoskeleton*. **2,** (2012).

113. Piedra, F.-A. A. *et al.* GDP-to-GTP exchange on the microtubule end can

contribute to the frequency of catastrophe. *Mol. Biol. Cell* **27,** 3515–3525 (2016).

114. Mitchison, T. & Kirschner, M. Dynamic instability of microtubule growth. *Nature* **312,** 312237a0 (1984).

115. Dehmelt, L. & Halpain, S. The MAP2/Tau family of microtubule-associated proteins. *Genome Biol* **6,** 204 (2004).

116. Lewis, S. A., Wang, D. H. & Cowan, N. J. Microtubule-associated protein MAP2 shares a microtubule binding motif with tau protein. *Science (80-.).* **242,** 936–939 (1988).

117. Garner, C. C., Brugg, B. & Matus, A. A 70-Kilodalton Microtubule-Associated Protein (MAP2c), Related to MAP2. *J Neurochem* **50,** 609–615 (1988).

118. Kosik, K. S., Orecchio, L. D., Bakalis, S. & Neve, R. L. Developmentally regulated expression of specific tau sequences. *Neuron* **2,** 1389–1397 (1989).

119. Kotani, S., Murofushi, H., Maekawa, S., Aizawa, H. & Sakai, H. Isolation of rat liver microtubule-associated proteins. Evidence for a family of microtubule-associated proteins with molecular mass of around 200,000 which distribute widely among mammalian cells. *J Biol. Chem* **263,** 5385–5389 (1988).

120. Al-Bassam, J., Ozer, R. S., Safer, D., Halpain, S. & Milligan, R. A. MAP2 and tau bind longitudinally along the outer ridges of microtubule protofilaments. *J Cell Biol.* **157,** 1187–1196 (2002).

121. Lewis, S. A., Ivanov, I. E., Lee, G.-H. & Cowan, N. J. Organization of microtubules in dendrites and axons is determined by a short hydrophobic zipper in microtubule-associated proteins MAP2 and tau. *Nature* **342,** 342498a0 (1989).

122. Kaech, S., Ludin, B. & Matus, A. Cytoskeletal Plasticity in Cells Expressing Neuronal Microtubule-Associated Proteins. *Neuron* **17,** 1189–1199 (1996).

123. Ramkumar, A., Jong, B. Y. & Ori-McKenney, K. M. ReMAPping the microtubule landscape: How phosphorylation dictates the activities of microtubule-associated proteins. *Dev Dynam* **247,** 138–155 (2017).

124. Moores, C. A. *et al.* Mechanism of Microtubule Stabilization by Doublecortin. *Mol Cell* **14,** 833–839 (2004).

125. Brouhard, G. J. *et al.* XMAP215 Is a Processive Microtubule Polymerase. *Cell* **132,** 79–88 (2008).

126. Fox, J. C., Howard, A. E., Currie, J. D., Rogers, S. L. & Slep, K. C. The XMAP215 family drives microtubule polymerization using a structurally diverse TOG array. *Mol Biol Cell* **25,** mbc.E13-08-0501 (2014).

127. Morrison, E. E., Wardleworth, B. N., Askham, J. M., Markham, A. F. & Meredith, D. M. EB1, a protein which interacts with the APC tumour suppressor, is associated with the microtubule cytoskeleton throughout the cell cycle. *Oncogene* **17,** 1202247 (1998).

128. Zanic, M., Stear, J. H., Hyman, A. A. & Howard, J. EB1 Recognizes the Nucleotide State of Tubulin in the Microtubule Lattice. *PLoS One* **4,** e7585 (2009).

129. Zanic, M., Widlund, P. O., Hyman, A. A. & Howard, J. Synergy between XMAP215 and EB1 increases microtubule growth rates to physiological levels. *Nat Cell Biol* **15,** 688–693 (2013).

130. Lopus, M. *et al.* Cooperative Stabilization of Microtubule Dynamics by EB1 and CLIP-170 Involves Displacement of Stably Bound Piat Microtubule Ends. *Biochemistry-us* **51,** 3021–3030 (2012).

131. Quarmby, L. M. & Lohret, T. A. Microtubule severing. *Cell Motil. Cytoskeleton* **43,** 1–9 (1999).

132. Hartman, J. J. *et al.* Katanin, a Microtubule-Severing Protein, Is a Novel AAA ATPase that Targets to the Centrosome Using a WD40-Containing Subunit. *Cell* **93,** 277–287 (1998).

133. Cheung, K. *et al.* Proteomic Analysis of the Mammalian Katanin Family of Microtubule-severing Enzymes Defines Katanin p80 subunit B-like 1 (KATNBL1) as a Regulator of Mammalian Katanin Microtubule-severing. *Mol Cell Proteom* **15,** 1658–1669 (2016).

134. McNally, K. P., Bazirgan, O. A. & McNally, F. J. Two domains of p80 katanin regulate microtubule severing and spindle pole targeting by p60 katanin. *J Cell Sci* **113 (Pt 9),** 1623–1633 (2000).

135. Ververis, A. *et al.* A novel family of katanin-like 2 protein isoforms (KATNAL2), interacting with nucleotide-binding proteins Nubp1 and Nubp2, are key regulators of different MT-based processes in mammalian cells. *Cell Mol Life Sci* **73,** 163–184 (2016).

136. Godek, K. M., Kabeche, L. & Compton, D. A. Regulation of kinetochore-microtubule attachments through homeostatic control during mitosis. *Nat. Rev. Mol. Cell Biol.* **16,** 57–64 (2015).

137. Hochegger, H., Hégarat, N. & Pereira-Leal, J. B. Aurora at the pole and equator: overlapping functions of Aurora kinases in the mitotic spindle. *Open Biol* **3,** 120185 (2013).

138. Quarmby, L. Cellular Samurai: katanin and the severing of microtubules. *J. Cell Sci.* **113 (Pt 1,** 2821–2827 (2000).

139. Ghosh, D., Dasgupta, D. & Guha, A. Models, Regulations, and Functions of Microtubule Severing by Katanin. **2012,** 1–14 (2012).

140. Johjima, A. *et al.* Microtubule Severing by Katanin p60 AAA+ ATPase Requires the C-terminal Acidic Tails of Both α- and β-Tubulins and Basic Amino Acid Residues in the AAA+ Ring Pore. *J Biol Chem* **290,** 11762–11770 (2015).

141. Iwaya, N. *et al.* Effect of Ca2+ on the microtubule-severing enzyme p60-katanin. Insight into the substrate-dependent activation mechanism. *Febs J* **279,** 1339–1352 (2012).

142. Taylor, J. L., White, S., Lauring, B. & Kull, F. J. Crystal structure of the human spastin AAA domain. *J Struct Biol* **179,** 133–137 (2012).

143. Eckert, T., Le, D., Link, S., Friedmann, L. & Woehlke, G. Spastin's Microtubule-Binding Properties and Comparison to Katanin. *PLoS One* **7,** e50161 (2012).

144. Yu, W. *et al.* The Microtubule-severing Proteins Spastin and Katanin Participate Differently in the Formation of Axonal Branches. *Mol Biol Cell* **19,** 1485–1498 (2008).

145. Park, S. *et al.* Fidgetin-Like 1 Gene Inhibited by Basic Fibroblast Growth Factor Regulates the Proliferation and Differentiation of Osteoblasts. *J Bone Min. Res* **22,** 889–896 (2007).

146. Mukherjee, S. *et al.* Human Fidgetin is a microtubule severing the enzyme and minus-end depolymerase that regulates mitosis. *Cell Cycle* **11,** 2359–2366 (2012).

147. Diaz-Valencia, J. D., Bailey, M. & Ross, J. L. *Purification and biophysical analysis of microtubule-severing enzymes in vitro*. **115,** (2013).

148. Zhao, X. *et al.* Fidgetin-like 1 is a ciliogenesis-inhibitory centrosome protein. *Cell Cycle* **15,** 0 (2016).

149. Elliott, S. *et al.* EspG, a Novel Type III System-Secreted Protein from Enteropathogenic Escherichia coli with Similarities to VirA of Shigella flexneri. *Infect Immun* **69,** 4027–4033 (2001).

150. Yoshida, S. *et al.* Shigella deliver an effector protein to trigger host microtubule destabilization, which promotes Rac1 activity and efficient bacterial internalization. *EMBO J.* **21,** 2923–2935 (2002).

151. Xie, H. *et al.* EseG, an Effector of the Type III Secretion System of Edwardsiella tarda, Triggers Microtubule Destabilization. *Infect Immun* **78,** 5011–5021 (2010).

152. Pfeuffer, T., Goebel, W., Laubinger, J., Bachmann, M. & Kuhn, M. LaXp180, a mammalian ActA-binding protein, identified with the yeast two-hybrid system, co-

localizes with intracellular Listeria monocytogenes. *Cell Microbiol* **2,** 101–114 (2000).

153. Maucuer, A., Camonis, J. H. & Sobel, A. Stathmin interaction with a putative kinase and coiled-coil-forming protein domains. *Proc Natl. Acad Sci* **92,** 3100–3104 (1995).

154. Zalevsky, J., Grigorova, I. & Mullins, D. R. Activation of the Arp2/3 Complex by the Listeria ActA Protein ActA BINDS TWO ACTIN MONOMERS AND THREE SUBUNITS OF THE Arp2/3 COMPLEX. *J Biol Chem* **276,** 3468–3475 (2001).

155. Belmont, L. D. & Mitchison, T. J. Identification of a Protein That Interacts with Tubulin Dimers and Increases the Catastrophe Rate of Microtubules. *Cell* **84,** 623–631 (1996).

156. Balczon, R. *et al.* Pseudomonas aeruginosa Exotoxin Y-Mediated Tau Hyperphosphorylation Impairs Microtubule Assembly in Pulmonary Microvascular Endothelial Cells. *PLoS One* **8,** (2013).

157. Prasain, N., Alexeyev, M., Balczon, R. & Stevens, T. Soluble adenylyl cyclase-dependent microtubule disassembly reveals a novel mechanism of endothelial cell retraction. *Am. J. Physiol. Lung Cell. Mol. Physiol.* **297,** L73–L83 (2009).

158. Hochstrasser, M. Origin and function of ubiquitin-like proteins. *Nature* **458,** 422–429 (2009).

159. Erpapazoglou, Z., Walker, O. & Haguenauer-Tsapis, R. Versatile Roles of K63-Linked Ubiquitin Chains in Trafficking. *Cells* **3,** 1027–1088 (2014).

160. Ye, Y. & Rape, M. Building ubiquitin chains: E2 enzymes at work. *Nat Rev Mol Cell Bio* **10,** nrm2780 (2009).

161. Jin, J., Li, X., Gygi, S. P. & Harper, W. J. Dual E1 activation systems for ubiquitin differentially regulate E2 enzyme charging. *Nature* **447,** 1135 (2007).

162. Burroughs, M. A., Jaffee, M., Iyer, L. M. & Aravind, L. Anatomy of the E2 ligase fold: Implications for enzymology and evolution of ubiquitin/Ub-like protein conjugation. *J Struct Biol* **162,** 205–218 (2008).

163. Zheng, N. & Shabek, N. Ubiquitin Ligases: Structure, Function, and Regulation. *Annu Rev Biochem* **86,** 1–29 (2015).

164. Komander, D. & Rape, M. The Ubiquitin Code. *Annu Rev Biochem* **81,** 203–229 (2012).

165. David, Y., Ziv, T., Admon, A. & Navon, A. The E2 ubiquitin-conjugating enzymes direct polyubiquitination to preferred lysines. *J. Biol. Chem.* **285,** 8595–8604 (2010).

166. Petroski, M. D. *et al.* Substrate modification with lysine 63-linked ubiquitin chains through the UBC13-UEV1A ubiquitin-conjugating enzyme. *J. Biol. Chem.* **282,** 29936–29945 (2007).

167. Andersen, P. L. *et al.* Distinct regulation of Ubc13 functions by the two ubiquitin-conjugating enzyme variants Mms2 and Uev1A. *J. Cell Biol.* **170,** 745–755 (2005).

168. Lin, A. E. & Guttman, J. A. The Escherichia coli adherence factor plasmid of enteropathogenic Escherichia coli causes a global decrease in ubiquitylated host cell proteins by decreasing ubiquitin E1 enzyme expression through host aspartyl proteases. *Int. J. Biochem. Cell Biol.* **44,** 2223–2232 (2012).

169. Tobe, T. *et al.* An extensive repertoire of type III secretion effectors in Escherichia coli O157 and the role of lambdoid phages in their dissemination. *Proc Natl. Acad Sci* **103,** 14941–14946 (2006).

170. Piscatelli, H. *et al.* The EHEC Type III Effector NleL Is an E3 Ubiquitin Ligase That Modulates Pedestal Formation. *PLoS One* **6,** e19331 (2011).

171. Kim, D. *et al.* The Shigella flexneri effector OspG interferes with innate immune responses by targeting ubiquitin-conjugating enzymes. *P Natl Acad Sci Usa* **102,** 14046–14051 (2005).

172. Rohde, J. R., Breitkreutz, A., Chenal, A., Sansonetti, P. J. & Parsot, C. Type III Secretion Effectors of the IpaH Family Are E3 Ubiquitin Ligases. *Cell Host Microbe* **1,** 77–83 (2007).

173. Nishide, A. *et al.* Structural basis for the recognition of Ubc13 by the Shigella flexneri effector ospi. *J. Mol. Biol.* **425,** 2623–2631 (2013).

174. Fu, P. *et al.* Complex Structure of OspI and Ubc13: The Molecular Basis of Ubc13 Deamidation and Convergence of Bacterial and Host E2 Recognition. *PLoS Pathog.* **9,** (2013).

175. Zhou, Y. & Zhu, Y. Diversity of bacterial manipulation of the host ubiquitin pathways. *Cell. Microbiol.* **17,** 26–34 (2015).

176. Nataro, J. P. & Kaper, J. B. Diarrheagenic Escherichia coli. *Clin. Microbiol. Rev.* **11,** 142–201 (1998).

177. Secher, T., Brehin, C. & Oswald, E. Early settlers: which E. coli strains do you not want at birth? *Am J Physiol-gastr L* **311,** G123–G129 (2016).

178. Canizalez-Roman, A. *et al.* Surveillance of Diarrheagenic Escherichia coli Strains Isolated from Diarrhea Cases from Children, Adults and Elderly at Northwest of Mexico. *Front. Microbiol* **7,** 1924 (2016).

179. Yang, S.-C., Lin, C.-H., Aljuffali, I. A. & Fang, J.-Y. Current pathogenic

Escherichia coli foodborne outbreak cases and therapy development. *Arch Microbiol* **199,** 811–825 (2017).

180. Furniss, C. R. D., Clements, A. & Margolin, W. Regulation of the Locus of Enterocyte Effacement in Attaching and Effacing Pathogens. *J Bacteriol* **200,** e00336-17 (2017).

181. Levine, J. A. *et al.* H-NST induces LEE expression and the formation of attaching and effacing lesions in enterohemorrhagic Escherichia coli. *PLoS One* **9,** 1–14 (2014).

182. Donnenberg, M. S. & Finlay, B. B. Combating enteropathogenic Escherichia coli (EPEC) infections: The way forward. *Trends Microbiol.* **21,** 317–319 (2013).

183. Batabyal, P., Mookerjee, S., Sur, D. & Palit, A. Diarrheogenic Escherechia coli in potable water sources of West Bengal, India. *Acta Trop.* **127,** 153–157 (2013).

184. Chellapandi, K. *et al.* Prevalence of multi drug resistant enteropathogenic and enteroinvasive Escherichia coli isolated from children with and without diarrhea in Northeast Indian population. *Ann Clin Microbiol Antimicrob* **16,** 49 (2017).

185. Paulozzi, L. J. *et al.* Diarrhea associated with adherent enteropathogenic Escherichia coli in an infant and toddler center, Seattle, Washington. *Pediatrics* **77,** 296–300 (1986).

186. Shifrin, D. A., Crawley, S. W., Grega-Larson, N. E. & Tyska, M. J. Dynamics of brush border remodeling induced by enteropathogenic E. coli. *Gut Microbes* **5,** 504–516 (2014).

187. Hicks, S., Frankel, G., Kaper, J. B., Dougan, G. & Phillips, A. D. Role of intimin and bundle-forming pili in enteropathogenic Escherichia coli adhesion to pediatric intestinal tissue in vitro. *Infect Immun* **66,** 1570–1578 (1998).

188. Girón, J. A., Torres, A. G., Freer, E. & Kaper, J. B. The flagella of enteropathogenic Escherichia coli mediate adherence to epithelial cells. *Mol Microbiol* **44,** 361–379 (2002).

189. Deng, W. *et al.* Dissecting virulence: Systematic and functional analyses of a pathogenicity island. *P Natl Acad Sci Usa* **101,** 3597–3602 (2004).

190. Gauthier, A., Puente, J. & Finlay, B. B. Secretin of the Enteropathogenic Escherichia coli Type III Secretion System Requires Components of the Type III Apparatus for Assembly and Localization. *Infect Immun* **71,** 3310–3319 (2003).

191. Neves, B. C. *et al.* CesD2 of Enteropathogenic Escherichia coli Is a Second Chaperone for the Type III Secretion Translocator Protein EspD CesD2 of Enteropathogenic Escherichia coli Is a Second Chaperone for the Type III Secretion Translocator Protein EspD. *Infect. Immun.* **71,** 2130–2141 (2003).

192. DeVinney, R., Puente, J., Gauthier, A., Goosney, D. & Finlay, B. B. Enterohaemorrhagic and enteropathogenic Escherichia coli use a different Tir-based mechanism for pedestal formation. *Mol Microbiol* **41,** 1445–1458 (2001).

193. Campellone, K. G. *et al.* Clustering of Nck by a 12-residue Tir phosphopeptide is sufficient to trigger localized actin assembly. *J. Cell Biol.* **164,** 407–416 (2004).

194. Gruenheid, S. *et al.* Enteropathogenic E. coli Tir binds Nck to initiate actin pedestal formation in host cells. *Nat Cell Biol* **3,** ncb0901-856 (2001).

195. Campellone, K. G. Cytoskeleton-modulating effectors of enteropathogenic and enterohaemorrhagic Escherichia coli: Tir, EspFU and actin pedestal assembly. *FEBS J.* **277,** 2390–2402 (2010).

196. Sanger, J. M., Chang, R., Ashton, F., Kaper, J. B. & Sanger, J. W. Novel form of actin-based motility transports bacteria on the surfaces of infected cells. *Cell Motil Cytoskel* **34,** 279–287 (1996).

197. Guttman, J. A., Lin, A. E., Veiga, E., Cossart, P. & Finlay, B. B. Role for CD2AP and other endocytosis-associated proteins in enteropathogenic Escherichia coli pedestal formation. *Infect. Immun.* **78,** 3316–3322 (2010).

198. Lin, A. E., Benmerah, A. & Guttman, J. A. Eps15 and Epsin1 are crucial for enteropathogenic Escherichia coli pedestal formation despite the absence of adaptor protein 2. *J. Infect. Dis.* **204,** 695–703 (2011).

199. Cantarelli, V. V. *et al.* Cortactin is essential for F-actin assembly in enteropathogenic Escherichia coli (EPEC)- and enterohaemorrhagic E. coli (EHEC)-induced pedestals and the ??-helical region is involved in the localization of cortactin to bacterial attachment sites. *Cell. Microbiol.* **8,** 769–780 (2006).

200. Ruetz, T. J., Vogl, A. W. & Guttman, J. A. Detailed Examination of Cytoskeletal Networks Within Enteropathogenic Escherichia coli Pedestals. *Anat. Rec.* **295,** 201–207 (2012).

201. Ruetz, T., Cornick, S. & Guttman, J. A. The spectrin cytoskeleton is crucial for adherent and invasive bacterial pathogenesis. *PLoS One* **6,** (2011).

202. Viswanathan, V. K. *et al.* Cytokeratin 18 interacts with the enteropathogenic Escherichia coli secreted protein F (EspF) and is redistributed after infection. *Cell Microbiol* **6,** 987–997 (2004).

203. Batchelor, M. *et al.* Involvement of the intermediate filament protein cytokeratin-18 in actin pedestal formation during EPEC infection. *Embo Rep* **5,** 104–110 (2004).

204. Nieto-Pelegrin, E., Kenny, B. & Martinez-Quiles, N. Nck adaptors, besides promoting N-WASP mediated actin-nucleation activity at pedestals, influence the cellular levels of enteropathogenic Escherichia coli Tir effector. *Cell Adh Migr* **8,**

404–417 (2014).

205. Wong, A. R. *et al.* Enteropathogenic and enterohaemorrhagic Escherichia coli: even more subversive elements. *Mol. Microbiol.* **80,** 1420–1438 (2011).

206. Martinez-Argudo, I., Sands, C. & Jepson, M. A. Translocation of enteropathogenic Escherichia coli across an in vitro M cell model is regulated by its type III secretion system. *Cell Microbiol* **9,** 1538–1546 (2007).

207. Guttman, J. A. *et al.* Aquaporins contribute to diarrhoea caused by attaching and effacing bacterial pathogens. *Cell Microbiol* **9,** 131–141 (2007).

208. Guttman, J. *et al.* Gap junction hemichannels contribute to the generation of diarrhoea during infectious enteric disease. *Gut* **59,** 218–226 (2010).

209. Cole, M. B., Jones, M. V & Holyoak, C. The effect of pH, salt concentration and temperature on the survival and growth of Listeria monocytogenes. *J Appl Bacteriol* **69,** 63–72 (1990).

210. Glaser, P. *et al.* Comparative Genomics of {}i{}Listeria{}/i{} Species. *Science (80-.).* **294,** 849–852 (2001).

211. Desai, R. & Smith, M. Pregnancy-related listeriosis. *Birth Defects Res* **109,** 324–335 (2017).

212. Madjunkov, M., Chaudhry, S. & Ito, S. Listeriosis during pregnancy. *Arch Gynecol Obs.* **296,** 143–152 (2017).

213. Radoshevich, L. & Cossart, P. Listeria monocytogenes: towards a complete picture of its physiology and pathogenesis. *Nat Rev Microbiol* **16,** 32 (2017).

214. Stavru, F., Archambaud, C. & Cossart, P. Cell biology and immunology of Listeria monocytogenes infections: Novel insights. *Immunol. Rev.* **240,** 160–184 (2011).

215. Lecuit, M. *et al.* Targeting and crossing of the human maternofetal barrier by Listeria monocytogenes: Role of internalin interaction with trophoblast E-cadherin. *P Natl Acad Sci Usa* **101,** 6152–6157 (2004).

216. Shen, Y., Naujokas, M., Park, M. & Ireton, K. InlB-Dependent Internalization of Listeria Is Mediated by the Met Receptor Tyrosine Kinase. *Cell* **103,** 501–510 (2000).

217. Mostowy, S. & Cossart, P. Cytoskeleton rearrangements during Listeria infection: clathrin and septins as new players in the game. *Cell Motil. Cytoskelet.* **66,** 816–823 (2009).

218. Veiga, E. & Cossart, P. The role of clathrin-dependent endocytosis in bacterial internalization. *Trends Cell Biol.* **16,** 499–504 (2006).

219. Hamon, M. A., Ribet, D., Stavru, F. & Cossart, P. Listeriolysin O: the Swiss army knife of Listeria. *Trends Microbiol.* **20,** 360–368 (2012).

220. Kocks, C. *et al.* L. monocytogenes-induced actin assembly requires the actA gene product, a surface protein. *Cell* **68,** 521–531 (1992).

221. Rafelski, S. M. & Theriot, J. A. Bacterial shape and ActA distribution affect initiation of Listeria monocytogenes actin-based motility. *Biophys. J.* **89,** 2146–2158 (2005).

222. Rafelski, S. M. & Theriot, J. A. Mechanism of polarization of Listeria monocytogenes surface protein ActA. *Mol. Microbiol.* **59,** 1262–1279 (2006).

223. Giganti, A. *et al.* Actin-filament cross-linking protein T-plastin increases Arp2/3-mediated actin-based movement. *J Cell Sci* **118,** 1255–1265 (2005).

224. Jasnin, M. *et al.* Three-dimensional architecture of actin filaments in Listeria monocytogenes comet tails. *Proc Natl. Acad Sci* **110,** 20521–20526 (2013).

225. Czuczman, M. A. *et al.* Listeria monocytogenes exploits efferocytosis to promote cell-to-cell spread. *Nature* **509,** 230–234 (2014).

226. Fattouh, R. *et al.* The Diaphanous-Related Formins Promote Protrusion Formation and Cell-to-Cell Spread of Listeria monocytogenes. *J Infect Dis* **211,** 1185–1195 (2015).

227. Tilney, L. G. & Portnoy, D. A. Actin filaments and the growth, movement, and spread of the intracellular bacterial parasite, Listeria monocytogenes. *J. Cell Biol.* **109,** 1597–1608 (1989).

228. Stavru, F., Bouillaud, F., Sartori, A., Ricquier, D. & Cossart, P. Listeria monocytogenes transiently alters mitochondrial dynamics during infection. *Proc. Natl. Acad. Sci.* **108,** 3612–3617 (2011).

229. Pillich, H., Loose, M., Zimmer, K.-P. & Chakraborty, T. Activation of the unfolded protein response by Listeria monocytogenes. *Cell. Microbiol.* **14,** 949–964 (2012).

230. Samba-Louaka, A., Stavru, F. & Cossart, P. Role for Telomerase in Listeria monocytogenes Infection. *Infect. Immun.* **80,** 4257–4263 (2012).

231. Citro, S. & Chiocca, S. Listeria monocytogenes: a bacterial pathogen to hit on the SUMO pathway. *Cell Res.* **20,** 738–740 (2010).

232. Valdez, Y., Ferreira, R. B. R. & Finlay, B. B. Molecular Mechanisms of Salmonella Virulence and Host Resistance. in *Current topics in microbiology and immunology* **337,** 93–127 (2009).

233. Fàbrega, A. & Vila, J. Salmonella enterica Serovar Typhimurium Skills To

Succeed in the Host: Virulence and Regulation. *Clin Microbiol Rev* **26,** 308–341 (2013).

234. Parry, C. M., Hien, T. T., Dougan, G., White, N. J. & Farrar, J. J. Typhoid fever. *N. Engl. J. Med.* **347,** 1770–82 (2002).

235. Ohl, M. E. & Miller, S. I. Salmonella: A Model for Bacterial Pathogenesis. *Annu. Rev. Med.* **52,** 259–274 (2001).

236. Gordon, M. A. Salmonella infections in immunocompromised adults. *J. Infect.* **56,** 413–22 (2008).

237. Liss, V. *et al.* Salmonella enterica Remodels the Host Cell Endosomal System for Efficient Intravacuolar Nutrition. *Cell Host Microbe* **21,** 390–402 (2017).

238. Figueira, R., Watson, K. G., Holden, D. W. & Helaine, S. Identification of salmonella pathogenicity island-2 type III secretion system effectors involved in intramacrophage replication of S. enterica serovar typhimurium: implications for rational vaccine design. *MBio* **4,** e00065 (2013).

239. Misselwitz, B. *et al.* Salmonella enterica serovar Typhimurium binds to HeLa cells via Fim-mediated reversible adhesion and irreversible type three secretion system 1-mediated docking. *Infect. Immun.* **79,** 330–41 (2011).

240. Kubori, T. *et al.* Supramolecular structure of the Salmonella typhimurium type III protein secretion system. *Science* **280,** 602–5 (1998).

241. Stender, S. *et al.* Identification of SopE2 from Salmonella typhimurium, a conserved guanine nucleotide exchange factor for Cdc42 of the host cell. *Mol Microbiol* **36,** 1206–1221 (2000).

242. Piscatelli, H. L., Li, M. & Zhou, D. Dual 4- and 5-phosphatase activities regulate SopB-dependent phosphoinositide dynamics to promote bacterial entry. *Cell Microbiol* **18,** 705–719 (2016).

243. Galán, J. E. & Zhou, D. Striking a balance: Modulation of the actin cytoskeleton by Salmonella. *Proc Natl. Acad Sci* **97,** 8754–8761 (2000).

244. Ehrbar, K., Mirold, S., Friebel, A., Stender, S. & Hardt, W.-D. Characterization of effector proteins translocated via the SPI1 type III secretion system of Salmonella typhimurium. *Int J Med Microbiol* **291,** 479–485 (2001).

245. Zhou, D., Mooseker, M. S. & Galán, J. E. Role of the S. typhimurium Actin-Binding Protein SipA in Bacterial Internalization. *Science (80-.).* **283,** 2092–2095 (1999).

246. Zhou, D., Mooseker, M. S. & Galán, J. E. An invasion-associated Salmonella protein modulates the actin-bundling activity of plastin. *Proc Natl. Acad Sci* **96,** 10176–10181 (1999).

247. Perrett, C. A. & Jepson, M. A. Regulation of Salmonella-induced membrane ruffling by SipA differs in strains lacking other effectors. *Cell Microbiol* **11,** 475–487 (2009).

248. Miao, E. A. *et al.* Salmonella effectors translocated across the vacuolar membrane interact with the actin cytoskeleton. *Mol. Microbiol.* **48,** 401–15 (2003).

249. Brumell, J. H., Tang, P., Mills, S. D. & Finlay, B. B. Characterization of Salmonella-Induced Filaments (Sifs) Reveals a Delayed Interaction Between Salmonella-Containing Vacuoles and Late Endocytic Compartments. *Traffic* **2,** 643–653 (2001).

250. Knodler, L. A. & Steele-Mortimer, O. The Salmonella effector PipB2 affects late endosome/lysosome distribution to mediate Sif extension. *Mol. Biol. Cell* **16,** 4108–23 (2005).

251. Chu, Y. *et al.* A novel contribution of spvB to pathogenesis of Salmonella Typhimurium by inhibiting autophagy in host cells. *Oncotarget* **7,** 8295–8309 (2016).

252. Bernal-Bayard, J., Cardenal-Muñoz, E. & Ramos-Morales, F. The Salmonella type III secretion effector, salmonella leucine-rich repeat protein (SlrP), targets the human chaperone ERdj3. *J. Biol. Chem.* **285,** 16360–8 (2010).

253. Boyle, E. C., Brown, N. F. & Finlay, B. B. Salmonella enterica serovar Typhimurium effectors SopB, SopE, SopE2 and SipA disrupt tight junction structure and function. *Cell Microbiol* **8,** 1946–1957 (2006).

254. McCormick, B. A., Colgan, S. P., Delp-Archer, C., Miller, S. I. & Madara, J. L. Salmonella typhimurium attachment to human intestinal epithelial monolayers: transcellular signalling to subepithelial neutrophils. *J. Cell Biol.* **123,** 895–907 (1993).

255. Ullmann, U. Klebsiella spp . as Nosocomial Pathogens : Epidemiology , Taxonomy , Typing Methods , and Pathogenicity Factors. **11,** 589–603 (1998).

256. Yinnon, A. M., Butnaru, A., Raveh, D., Jerassy, Z. & Rudensky, B. Klebsiella bacteraemia: community versus nosocomial infection. *Qjm Int J Med.* **89,** 933–942 (1996).

257. Siu, L. K., Yeh, K. M., Lin, J. C., Fung, C. P. & Chang, F. Y. Klebsiella pneumoniae liver abscess: A new invasive syndrome. *Lancet Infect. Dis.* **12,** 881–885 (2012).

258. Shon, A. S., Bajwa, R. P. S. & Russo, T. A. Hypervirulent (hypermucoviscous) Klebsiella pneumoniae: a new and dangerous breed. *Virulence* **4,** 107–118 (2013).

259. Russo, T. A. *et al.* Hypervirulent K. pneumoniae secretes more and more active iron-acquisition molecules than 'classical' k. pneumoniae thereby enhancing its virulence. *PLoS One* **6,** (2011).

260. Shon, A. S. & Russo, T. A. Hypervirulent Klebsiella pneumoniae: the next superbug? *Future Microbiol.* **7,** 669–671 (2012).

261. Schroll, C., Barken, K. B., Krogfelt, K. A. & Struve, C. Role of type 1 and type 3 fimbriae in Klebsiella pneumoniae biofilm formation. **10,** 179 (2010).

262. Jung, J. *et al.* Comparison of the clinical characteristics and outcomes of Klebsiella pneumoniae and Streptococcus pneumoniae meningitis. (2015). doi:10.1016/j.diagmicrobio.2015.02.006

263. Lawlor, M. S., Hsu, J., Rick, P. D. & Miller, V. L. Identification of Klebsiella pneumoniae virulence determinants using an intranasal infection model. *Mol. Microbiol.* **58,** 1054–1073 (2005).

264. Lawlor, M., O'Connor, C. & Miller, V. Yersiniabactin Is a Virulence Factor for Klebsiella pneumoniae during Pulmonary Infection. *Infect Immun* **75,** 1463–1472 (2007).

265. Ye, P. *et al.* Interleukin-17 and lung host defense againstKlebsiella pneumoniae infection. *Am J Respir Cell Mol Biol* **25,** 335–340 (2001).

266. Oelschlaeger, T. a & Tall, B. D. Invasion of cultured human epithelial cells by Klebsiella pneumoniae isolated from the urinary tract. *Infect. Immun.* **65,** 2950–2958 (1997).

267. Hsu, C. R. *et al.* Klebsiella pneumoniae translocates across the intestinal epithelium via rho GTPase-and phosphatidylinositol 3-kinase/Akt-dependent cell invasion. *Infect. Immun.* **83,** 769–779 (2015).

268. Cano, V., Moranta, D., Llobet-Brossa, E., Bengoechea, J. & Garmendia, J. Klebsiella pneumoniae triggers a cytotoxic effect on airway epithelial cells. *Bmc Microbiol* **9,** 1–9 (2009).

269. Pan, Y.-J. *et al.* Genetic analysis of capsular polysaccharide synthesis gene clusters in 79 capsular types of Klebsiella spp. *Sci Reports* **5,** srep15573 (2015).

270. Lin, J.-C. *et al.* High prevalence of phagocytic-resistant capsular serotypes of Klebsiella pneumoniae in liver abscess. *Microbes Infect.* **6,** 1191–1198 (2004).

271. Fung, C.-P. *et al.* A global emerging disease of Klebsiella pneumoniae liver abscess: is serotype K1 an important factor for complicated endophthalmitis? *Gut* **50,** 420–4 (2002).

272. De Majumdar, S. *et al.* Elucidation of the RamA regulon in Klebsiella pneumoniae

reveals a role in LPS regulation. *PLoS Pathog.* **11,** e1004627 (2015).

273. Tsai, Y. K. *et al.* Klebsiella pneumoniae Outer membrane porins OmpK35 and OmpK36 play roles in both antimicrobial resistance and virulence. *Antimicrob. Agents Chemother.* **55,** 1485–1493 (2011).

274. Tomás, A. *et al.* Functional Genomic Screen Identifies Klebsiella pneumoniae Factors Implicated in Blocking Nuclear Factor κB (NF-κB) Signaling. *J. Biol. Chem.* **290,** 16678–97 (2015).

275. Brinkworth, A. J. *et al.* Identification of Outer Membrane and Exoproteins of Carbapenem-Resistant Multilocus Sequence Type 258 Klebsiella pneumoniae. *PLoS One* **10,** e0123219 (2015).

276. Munoz-Price, S. L. *et al.* Clinical epidemiology of the global expansion of Klebsiella pneumoniae carbapenemases. *Lancet Infect Dis* **13,** 785–796 (2013).

277. Murray, T. S. & Peaper, D. R. The contribution of extended-spectrum β-lactamases to multidrug-resistant infections in children. *Curr Opin Pediatr* **27,** 124 (2015).

278. Antoniadou, A. *et al.* Colistin-resistant isolates of Klebsiella pneumoniae emerging in intensive care unit patients: first report of a multiclonal cluster. *J Antimicrob Chemoth* **59,** 786–790 (2007).

279. Coles, C. H. & Bradke, F. Coordinating Neuronal Actin–Microtubule Dynamics. *Curr. Biol.* **25,** R677–R691 (2015).

280. Wenzel, D. M., Stoll, K. E. & Klevit, R. E. E2s: structurally economical and functionally replete. *Biochem J* **433,** 31–42 (2011).

281. Matsuzawa, T., Kuwae, A., Yoshida, S., Sasakawa, C. & Abe, A. Enteropathogenic Escherichia coli activates the RhoA signaling pathway via the stimulation of GEF-H1. *EMBO J.* **23,** 3570–3582 (2004).

282. Travier, L. & Lecuit, M. Listeria monocytogenes ActA: a new function for a 'classic' virulence factor. *Curr. Opin. Microbiol.* **17,** 53–60 (2014).

283. Podschun, R. & Ullmann, U. Klebsiella spp. as nosocomial pathogens: epidemiology, taxonomy, typing methods, and pathogenicity factors. *Clin. Microbiol. Rev.* **11,** 589–603 (1998).

284. Anderson, C. J. & Kendall, M. M. Salmonella enterica Serovar Typhimurium Strategies for Host Adaptation. *Front. Microbiol* **8,** 1983 (2017).

285. Swaminathan, B. & Gerner-Smidt, P. The epidemiology of human listeriosis. *Microbes Infect* **9,** 1236–1243 (2007).

286. Wotzka, S. Y., Nguyen, B. D. & Hardt, W.-D. Salmonella Typhimurium Diarrhea Reveals Basic Principles of Enteropathogen Infection and Disease-Promoted DNA Exchange. *Cell Host Microbe* **21,** 443–454 (2017).

287. Lai, Y., Rosenshine, I., Leong, J. & Frankel, G. Intimate host attachment: enteropathogenic and enterohaemorrhagic Escherichia coli. *Cell Microbiol* **15,** 1796–1808 (2013).

288. Lamason, R. L. & Welch, M. D. Actin-based motility and cell-to-cell spread of bacterial pathogens. *Curr Opin Microbiol* **35,** 48–57 (2017).

289. F., N.-G. *et al.* Actin cytoskeleton manipulation by effector proteins secreted by diarrheagenic Escherichia coli pathotypes. *Biomed Res. Int.* **2013,** 374395 (2013).

290. Shifrin, D. A., Crawley, S. W., Grega-Larson, N. E. & Tyska, M. J. Dynamics of brush border remodeling induced by enteropathogenic E. coli. *Gut Microbes* **5,** 504–516 (2014).

291. Crepin, V. F. F. *et al.* Dissecting the role of the Tir:Nck and Tir:IRTKS/IRSp53 signalling pathways in vivo. *Mol. Microbiol.* **75,** 308–323 (2010).

292. Frankel, G. & Phillips, A. D. Attaching effacing Escherichia coli and paradigms of Tir-triggered actin polymerization: Getting off the pedestal. *Cell. Microbiol.* **10,** 549–556 (2008).

293. Kalman, D. *et al.* Enteropathogenic E. coli acts through WASP and Arp2/3 complex to form actin pedestals. *Nat Cell Biol* **1,** ncb1099_389 (1999).

294. Mengaud, J., Ohayon, H., Gounon, P., Mège, R.-M. & Cossart, P. E-Cadherin Is the Receptor for Internalin, a Surface Protein Required for Entry of L. monocytogenes into Epithelial Cells. *Cell* **84,** 923–932 (1996).

295. Sechi, A. S., Wehland, J. & Small, J. V. The Isolated Comet Tail Pseudopodium of. **137,** (1997).

296. Cossart, P. & Kocks, C. The actin-based motility of the facultative intracellular pathogen Listeria monocytogenes. *Mol Microbiol* **13,** 395–402 (1994).

297. Pust, S., Morrison, H., Wehland, J., Sechi, A. S. & Herrlich, P. Listeria monocytogenes exploits ERM protein functions to efficiently spread from cell to cell. *EMBO J.* **24,** 1287–1300 (2005).

298. Truong, D. *et al.* Formin-mediated actin polymerization promotes Salmonella invasion. *Cell Microbiol* **15,** 2051–2063 (2013).

299. Law, H. T., Chua, M., Moon, K.-M. M., Foster, L. J. & Guttman, J. A. Mass Spectrometry-Based Proteomics Identification of Enteropathogenic Escherichia coli Pedestal Constituents. *J. Proteome Res.* **14,** 2520–2527 (2015).

300. Liu, R. & Jin, J.-P. Deletion of calponin 2 in macrophages alters cytoskeleton-based functions and attenuates the development of atherosclerosis. *J Mol Cell Cardiol* **99,** 87–99 (2016).

301. Hoiseth, S. K. & Stocker, B. A. D. Aromatic-dependent Salmonella typhimurium are non-virulent and effective as live vaccines. *Nature* **291,** 238–239 (1981).

302. Steele-Mortimer, O. *et al.* Activation of Akt/Protein Kinase B in Epithelial Cells by theSalmonella typhimurium Effector SigD. *J Biol Chem* **275,** 37718–37724 (2000).

303. Levraud, J.-P. *et al.* Real-Time Observation of Listeria monocytogenes-Phagocyte Interactions in Living Zebrafish Larvae. *Infect Immun* **77,** 3651–3660 (2009).

304. Mengaud, J., Geoffroy, C. & Cossart, P. Identification of a new operon involved in Listeria monocytogenes virulence: its first gene encodes a protein homologous to bacterial metalloproteases. *Infect Immun* **59,** 1043–1049 (1991).

305. Nigam, R., Jin, J.-P. & Triggle, C. R. h1- and h2-calponins are not essential for norepinephrine- or sodium fluoride-induced contraction of rat aortic smooth muscle. *J Muscle Res Cell Motil* **19,** 695–703 (1998).

306. Hossain, M. M. *et al.* Developmentally regulated expression of calponin isoforms and the effect of h2-calponin on cell proliferation. **4970,** 156–167 (2003).

307. Paluch, E., van der Gucht, J., Joanny, J.-F. & Sykes, C. Deformations in Actin Comets from Rocketing Beads. *Biophys J* **91,** 3113–3122 (2006).

308. Hossain, M. M., Crish, J. F., Eckert, R. L., Lin, J. & Jin, J.-P. h2-calponin Is Regulated by Mechanical Tension and Modifies the Function of Actin Cytoskeleton. *J Biol Chem* **280,** 42442–42453 (2005).

309. Bhavsar, A. P., Guttman, J. A. & Finlay, B. B. Manipulation of host-cell pathways by bacterial pathogens. *Nature* **449,** 827–834 (2007).

310. Welch, M. D. & Way, M. Arp2/3-mediated actin-based motility: a tail of pathogen abuse. *Cell Host Microbe* **14,** 242–255 (2013).

311. Schüller, S. *et al.* Tir phosphorylation and Nck/N-WASP recruitment by enteropathogenic and enterohaemorrhagic Escherichia coli during ex vivo colonization of human intestinal mucosa is different to cell culture models. *Cell. Microbiol.* **9,** 1352–1364 (2007).

312. Lommel, S. *et al.* Actin pedestal formation by enteropathogenic Escherichia coli and intracellular motility of Shigella flexneri are abolished in N-WASP-defective cells. *EMBO Rep.* **2,** 850–857 (2001).

313. Bonazzi, M. *et al.* Clathrin phosphorylation is required for actin recruitment at sites of bacterial adhesion and internalization. *J. Cell Biol.* **195,** 525–536 (2011).

314. Tilney, L. G., Connelly, P. S. & Portnoy, D. A. Actin filament nucleation by the bacterial pathogen, Listeria monocytogenes. *J. Cell Biol.* **111,** 2979–2988 (1990).

315. May, R. C. *et al.* The Arp2/3 complex is essential for the actin-based motility of Listeria monocytogenes. *Curr. Biol.* **9,** 759–762 (1999).

316. Van Troys, M. *et al.* The actin propulsive machinery: the proteome of Listeria monocytogenes tails. *Biochem. Biophys. Res. Commun.* **375,** 194–199 (2008).

317. Travier, L. *et al.* ActA Promotes Listeria monocytogenes Aggregation, Intestinal Colonization and Carriage. *PLoS Pathog.* **9,** (2013).

318. Nair, R. R., Solway, J. & Boyd, D. D. Expression cloning identifies transgelin (SM22) as a novel repressor of 92-kDa type IV collagenase (MMP-9) expression. *J. Biol. Chem.* **281,** 26424–26436 (2006).

319. Schindelin, J., Rueden, C. T., Hiner, M. C. & Eliceiri, K. W. The ImageJ ecosystem: An open platform for biomedical image analysis. *Mol. Reprod. Dev.* **82,** 518–529 (2015).

320. Fu, Y. *et al.* Mutagenesis analysis of human SM22: characterization of actin binding. *J. Appl. Physiol.* **89,** 1985–1990 (2000).

321. Palasca, O., Santos, A., Stolte, C., Gorodkin, J. & Jensen, L. TISSUES 2.0: an integrative web resource on mammalian tissue expression. *Database* **2018,** bay003 (2018).

322. Schmidt, T. *et al.* ProteomicsDB. *Nucleic Acids Res* gkx1029-doi:10.1093/nar/gkx1029

323. Kim, H.-R. *et al.* TAGLN2 polymerizes G-actin in a low ionic state but blocks Arp2/3-nucleated actin branching in physiological conditions. *Sci Reports* **8,** 5503 (2018).

324. Bartegi, A., Roustan, C., Kassab, R. & Fattoum, A. Fluorescence studies of the carboxyl-terminal domain of smooth muscle calponin effects of F-actin and salts. *Eur. J. Biochem.* **262,** 335–341 (1999).

325. Carlier, M.-F. F., Le Clainche, C., Wiesner, S. & Pantaloni, D. Actin-based motility: from molecules to movement. *Bioessays* **25,** 336–345 (2003).

326. Yarar, D., To, W., Abo, A. & Welch, M. D. The Wiskott-Aldrich syndrome protein directs actin-based motility by stimulating actin nucleation with the Arp2/3 complex. *Curr. Biol.* **9,** 555–558 (1999).

327. Ishihama, Y., Rappsilber, J., Andersen, J. S. & Mann, M. Microcolumns with self-assembled particle frits for proteomics. *J Chromatogr A* **979,** 233–239 (2002).

328. Gibbs, M. R. *et al.* Conserved GTPase LepA (Elongation Factor 4) functions in biogenesis of the 30S subunit of the 70S ribosome. *Proc. Natl. Acad. Sci. U.S.A.* **114,** 980–985 (2017).

329. Cox, J. & Mann, M. MaxQuant enables high peptide identification rates, individualized p.p.b.-range mass accuracies and proteome-wide protein quantification. *Nat. Biotechnol.* **26,** 1367–1372 (2008).

330. Wu, Y., Li, Q. & Chen, X.-Z. Z. Detecting protein-protein interactions by Far western blotting. *Nat Protoc* **2,** 3278–3284 (2007).

331. Meijering, E., Dzyubachyk, O. & Smal, I. Methods for cell and particle tracking. *Meth. Enzym.* **504,** 183–200 (2012).

332. Pulvino, M. *et al.* Inhibition of proliferation and survival of diffuse large B-cell lymphoma cells by a small-molecule inhibitor of the ubiquitin-conjugating enzyme Ubc13-Uev1A. *Blood* **120,** 1668–1677 (2012).

333. Hodge, C. D. *et al.* Covalent Inhibition of Ubc13 Affects Ubiquitin Signaling and Reveals Active Site Elements Important for Targeting. *ACS Chem. Biol.* **10,** 1718–28 (2015).

334. Biswas, R. & Bagchi, A. Inhibition of TRAF6-Ubc13 interaction in NFkB inflammatory pathway by analyzing the hotspot amino acid residues and protein-protein interactions using molecular docking simulations. *Comput Biol Chem* **70,** 116–124 (2017).

335. Strauss, C., Halevy, T., Macarov, M., Argaman, L. & Goldberg, M. MDC1 is ubiquitylated on its tandem BRCT domain and directly binds RAP80 in a UBC13-dependent manner. *DNA Repair* **10,** 806–814 (2011).

336. Lee, B. L., Singh, A., Mark Glover, J. N., Hendzel, M. J. & Spyracopoulos, L. Molecular Basis for K63-Linked Ubiquitination Processes in Double-Strand DNA Break Repair: A Focus on Kinetics and Dynamics. *J. Mol. Biol.* (2017). doi:10.1016/j.jmb.2017.05.029

337. Wu, Z., Shen, S., Zhang, Z., Zhang, W. & Xiao, W. Ubiquitin-conjugating enzyme complex Uev1A-Ubc13 promotes breast cancer metastasis through nuclear factor-κB mediated matrix metalloproteinase-1 gene regulation. *Breast Cancer Res.* **16,** R75 (2014).

338. Wu, X. *et al.* Ubiquitin-conjugating enzyme Ubc13 controls breast cancer metastasis through a TAK1-p38 MAP kinase cascade. *Proc. Natl. Acad. Sci. U. S. A.* **111,** 13870–5 (2014).

339. Eddins, M. J., Carlile, C. M., Gomez, K. M., Pickart, C. M. & Wolberger, C. Mms2-Ubc13 covalently bound to ubiquitin reveals the structural basis of linkage-specific polyubiquitin chain formation. *Nat. Struct. Mol. Biol.* **13,** 915–920 (2006).

340. Hodge, C. D., Spyracopoulos, L. & Glover, J. N. Ubc13: the Lys63 ubiquitin chain building machine. *Oncotarget* **7,** 64471–64504 (2016).

341. Mohiuddin *et al.* The role of HERC2 and RNF8 ubiquitin E3 ligases in the promotion of translesion DNA synthesis in the chicken DT40 cell line. *DNA Repair* **40,** 67–76 (2016).

342. Zhang, W. *et al.* Uev1A facilitates osteosarcoma differentiation by promoting Smurf1-mediated Smad1 ubiquitination and degradation. *Cell Death Dis* **8,** e2974 (2017).

343. Polge, C., Attaix, D. & Taillandier, D. Role of E2-Ub-conjugating enzymes during skeletal muscle atrophy. *Front Physiol* **6,** 59 (2015).

344. Stewart, M. D., Ritterhoff, T., Klevit, R. E. & Brzovic, P. S. E2 enzymes: more than just middle men. *Cell Res.* **26,** 423–440 (2016).

345. Fung, C.-P. *et al.* Klebsiella pneumoniae in gastrointestinal tract and pyogenic liver abscess. *Emerg. Infect. Dis.* **18,** 1322–5 (2012).

346. Martino, D. P. *et al.* Molecular characterization and adhesive properties of CF29K, an adhesin of Klebsiella pneumoniae strains involved in nosocomial infections. *Infect Immun* **63,** 4336–4344 (1995).

347. Rosen, D. A. *et al.* Molecular variations in Klebsiella pneumoniae and Escherichia coli FimH affect function and pathogenesis in the urinary tract. **76,** 3346–3356 (2008).

348. March, C. *et al.* Klebsiella pneumoniae Outer Membrane Protein A Is Required to Prevent the Activation of Airway Epithelial Cells. *J Biol Chem* **286,** 9956–9967 (2011).

349. Fung, C.-P. P. *et al.* Klebsiella pneumoniae in gastrointestinal tract and pyogenic liver abscess. **18,** 1322–1325 (2012).

350. Paterson, D. L. *et al.* International prospective study of Klebsiella pneumoniae bacteremia: implications of extended-spectrum beta-lactamase production in nosocomial Infections. *Ann Intern Med* **140,** 26–32 (2004).

351. Noskin, G. A. Tigecycline: A New Glycylcycline for Treatment of Serious Infections. *Clin Infect Dis* **41,** S303–S314 (2005).

352. Nogales, E. & Wang, H.-W. Structural intermediates in microtubule assembly and disassembly: how and why? *Curr Opin Cell Biol* **18,** 179–184 (2006).

353. Radhakrishnan, G. K. & Splitter, G. A. Modulation of host microtubule dynamics by pathogenic bacteria. *Biomol. Concepts* **3,** 571–580 (2012).

354. Mostowy, S. Multiple Roles of the Cytoskeleton in Bacterial Autophagy. *Plos Pathog* **10,** e1004409 (2014).

355. Cortés, G. *et al.* Molecular Analysis of the Contribution of the Capsular Polysaccharide and the Lipopolysaccharide O Side Chain to the Virulence of Klebsiella pneumoniae in a Murine Model of Pneumonia. *Infect Immun* **70,** 2583–2590 (2002).

356. Kelley, L. A., Mezulis, S., Yates, C. M., Wass, M. N. & Sternberg, M. J. E. The Phyre2 web portal for protein modeling, prediction and analysis. *Nat Protoc* **10,** 845–858 (2015).

357. Krogh, A., Larsson, B., von Heijne, G. & Sonnhammer, E. Predicting transmembrane protein topology with a hidden markov model: application to complete genomes11Edited by F. Cohen. *J Mol Biol* **305,** 567–580 (2001).

358. Yoshida, S. *et al.* Microtubule-Severing Activity of Shigella Is Pivotal for Intercellular Spreading. *Science (80-.).* **314,** 985–989 (2006).

359. Ochoa, C. D., Alexeyev, M., Pastukh, V., Balczon, R. & Stevens, T. Pseudomonas aeruginosa Exotoxin Y Is a Promiscuous Cyclase That Increases Endothelial Tau Phosphorylation and Permeability. *J Biol Chem* **287,** 25407–25418 (2012).

360. Stevens, T. *et al.* The Pseudomonas aeruginosa exoenzyme Y impairs endothelial cell proliferation and vascular repair following lung injury. *Am J Physiol. - Lung Cell Mol Physiol.* **306,** L915–L924 (2014).

361. Zhang, D., Rogers, G. C., Buster, D. W. & Sharp, D. J. Three microtubule severing enzymes contribute to the “Pacman-flux” machinery that moves chromosomes. *J Cell Biol.* **177,** 231–242 (2007).

362. Roll-Mecak, A. & McNally, F. J. Microtubule-severing enzymes. **22,** 96–103 (2010).

363. Sharp, D. J. & Ross, J. L. Microtubule-severing enzymes at the cutting edge. **125,** 2561–2569 (2012).

364. Goosney, D. L. *et al.* Enteropathogenic E. coli translocated intimin receptor, Tir, interacts directly with alpha-actinin. *Curr. Biol.* **10,** 735–8 (2000).

365. Ruetz, T., Vogl, A. & Guttman, J. Detailed Examination of Cytoskeletal Networks Within Enteropathogenic Escherichia coli Pedestals. *Anat. Rec* **295,** 201–207 (2012).

366. Pontrelli, P. *et al.* Lysine 63 ubiquitination is involved in the progression of tubular damage in diabetic nephropathy. *FASEB J.* **31,** 308–319 (2017).

367. Lin, A. & Guttman, J. The Escherichia coli adherence factor plasmid of

enteropathogenic Escherichia coli causes a global decrease in ubiquitylated host cell proteins by decreasing ubiquitin E1 enzyme expression through host aspartyl proteases. *Int J Biochem Cell Biol.* **44,** 2223–2232 (2012).

368. Prasain, N., Alexeyev, M., Balczon, R. & Stevens, T. Soluble adenylyl cyclase-dependent microtubule disassembly reveals a novel mechanism of endothelial cell retraction. *Am J Physiol. - Lung Cell Mol Physiol.* **297,** L73–L83 (2009).

369. Tiwari, S. *et al.* Two-Component Signal Transduction Systems of Pathogenic Bacteria As Targets for Antimicrobial Therapy: An Overview. *Front. Microbiol.* **8,** 1878 (2017).

370. Hartman, J. J. & Vale, R. D. Microtubule Disassembly by ATP-Dependent Oligomerization of the AAA Enzyme Katanin. *Science (80-.).* **286,** 782–785 (1999).

371. Qiang, L., Yu, W., Andreadis, A., Luo, M. & Baas, P. W. Tau Protects Microtubules in the Axon from Severing by Katanin. *J. Neurosci.* **26,** 3120–3129 (2006).

372. Kuo, T.-C. *et al.* Purine-Type Compounds Induce Microtubule Fragmentation and Lung Cancer Cell Death through Interaction with Katanin. *J. Med. Chem.* **59,** 8521–8534 (2016).

373. Tantama, M., Martínez-François, J. R., Mongeon, R. & Yellen, G. Imaging energy status in live cells with a fluorescent biosensor of the intracellular ATP-to-ADP ratio. *Nat. Commun.* **4,** 2550 (2013).

374. Lee, C.-T., Huang, Y.-W., Yang, C.-H. & Huang, K.-S. Drug delivery systems and combination therapy by using vinca alkaloids. *Curr. Top. Med. Chem.* **15,** 1491–500 (2015).

375. Bates, D. & Eastman, A. Microtubule destabilising agents: far more than just antimitotic anticancer drugs. *Br. J. Clin. Pharmacol.* **83,** 255–268 (2017).

Appendix A.

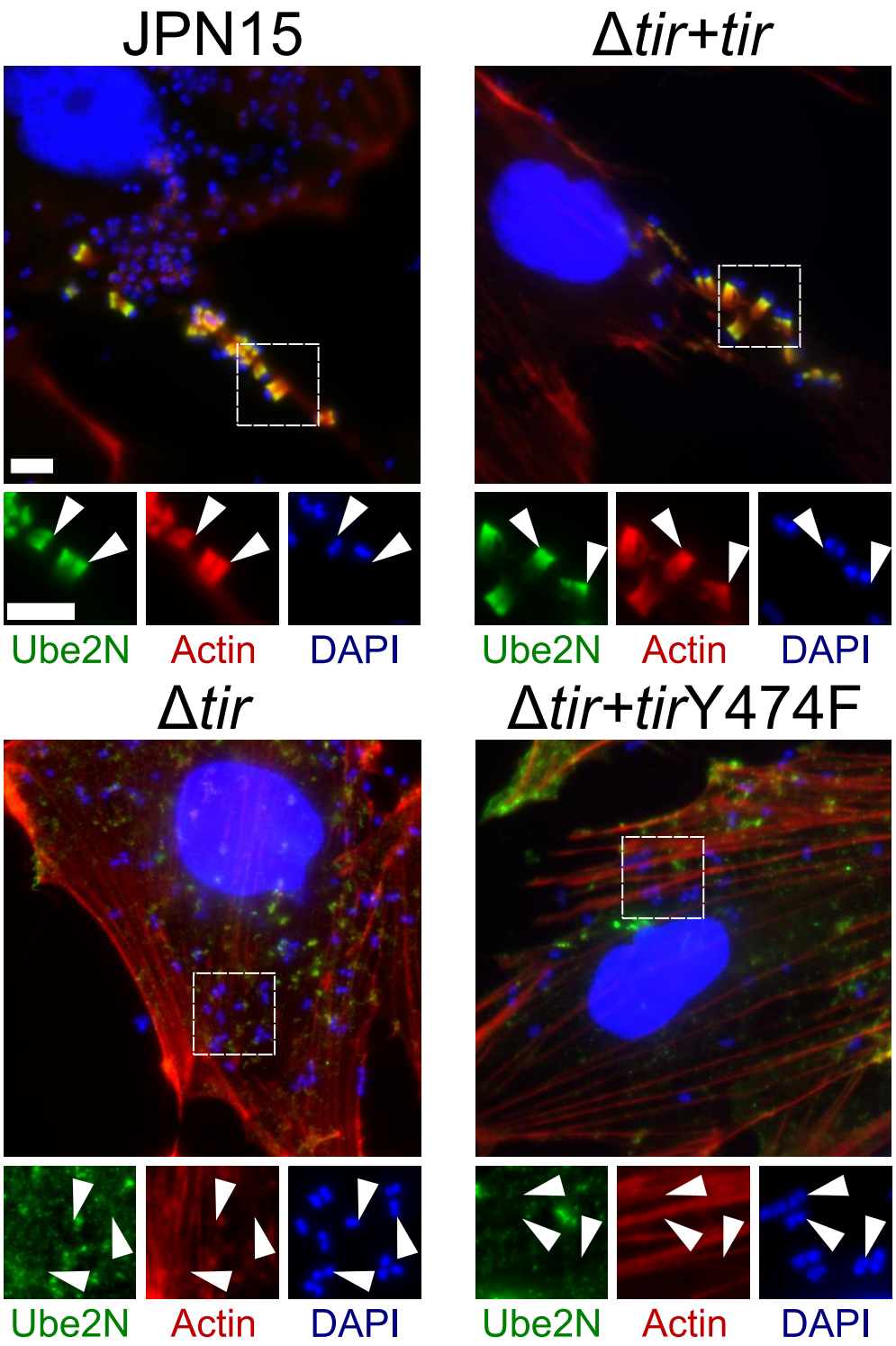

Figure A1. Ube2N immunolocalized to the apical tips of EPEC (JPN15) pedestals. Scale bars = 5 µm. Arrowheads indicate attached bacteria. Only JPN15 and Δ*tir+tir* bacteria can form pedestals and Ube2N only immunolocalized to the tips of those pedestals.